

SUPERCRITICAL WATER OXIDATION: TESTING OF  
AQUEOUS WASTEWATER SOLUTIONS FOR SPACE APPLICATIONS

A Thesis

by

CALEB ANTHONY RIGGINS

Submitted to the Office of Graduate Studies of  
Prairie View A&M University  
in partial fulfillment of the requirements for the degree of

MASTER OF SCIENCE

May 2023

Major Subject: Mechanical Engineering

SUPERCRITICAL WATER OXIDATION: TESTING OF AQUEOUS  
WASTEWATER SOLUTIONS FOR SPACE APPLICATIONS

A Thesis

by

CALEB ANTHONY RIGGINS

Submitted to the Office of Graduate Studies of  
Prairie View A&M University  
in partial fulfillment of the requirements for the degree of

MASTER OF SCIENCE

Approved as to style and content by:

---

Yuhao Xu  
Chair of committee

---

Ziaul Huque  
Member

---

Paul O. Biney  
Member

---

Michael C. Hicks  
Member

---

Jeffrey Streater  
Head of Department

---

Pamela H. Obiomon  
Dean of College

---

Tyrone Tanner  
Dean of Graduate Studies

May 2023

Major Subject: Mechanical Engineering

## ABSTRACT

Supercritical Water Oxidation: Testing of Aqueous Wastewater Solutions for Space Applications

(May 2023)

Caleb Riggins, M.S., Prairie View A&M University; B.S., Prairie View A&M University

Chair of Advisory

Committee: Dr. Yuhao Xu

Abstract: Future extended-duration space missions will only be practicable with effective life support systems that incorporate resource reclamation technologies from bio-waste streams. In the case of water reclamation during these missions, Supercritical Water Oxidation (SCWO) has been proposed as an attractive technology. In SCWO processes, organic waste compounds are oxidized in water above its critical point at 374°C and 22 MPa. This work focuses on the SCWO of ersatz wastewater (EWW) streams that simulate waste streams typically observed during International Space Station (ISS) isolated crew missions. A tubular reactor was designed and built at NASA's Glenn Research Center (NASA-GRC) to allow the oxidation of a continuous flow of ersatz waste at isobaric supercritical conditions. A description of the reactor design and the operational procedures for the heat-up, injection, and establishment of steady-state conditions are presented. The oxidizer in these tests, air (21% O<sub>2</sub> with balanced N<sub>2</sub>) was used and "fuel" (i.e., EWW at different levels of dilution) were independently heated and pressurized as they entered the reactor in a co-flow configuration at supercritical conditions. Experiments were performed at reactor set point temperatures and pressures ranging from 550-610°C and 26-28 MPa

with air flows ranging from 0.75 to 2.5 standard liters per minute (SLPM) and fuel flows ranging from 2.0 to 4.0 mL/min. Qualitative assessments of the extent of conversion (odor, foaming, turbidity) are discussed along with quantitative measurements using Raman spectroscopy and Total Organic Carbon (TOC) analysis. Additional co-fuel experiments using ethanol were conducted to increase internal bulk temperatures for conversion of the dilute EWW stream. The overall results of the EWW tests concluded that with appropriate reaction temperatures, equivalence ratios favoring excess air, and residence time of 55 seconds to 93 seconds, near 100% TOC conversion could be achieved. An additional preliminary study for less complex mixtures using urea-aqueous solutions was conducted. Preliminary results show a similar trend in the EWW results, but with challenges in maintaining sufficient bulk fluid temperatures due to reactor constraints, thus limiting complete conversion of ammonia. Preliminary on-time gas measurements taken presents great potential for future gas analysis from detections of CO<sub>2</sub> and NO.

**Keywords:** supercritical water oxidation, urea, Raman, high pressure, water reclamation

## **DEDICATION**

In loving memory of my grandpa, Dorris Winston Colvin

01/07/1938- 3/25/2020

This thesis is dedicated to him and my family for their endless love and support.

## ACKNOWLEDGMENTS

Firstly, I give all my thanks and honor to God for all he has done and provided in my life thus far, followed by my family for all their love, encouragement, and faith. Next, Dr. Yuhao Xu for pushing me to strive for greatness through his mentorship, support, and motivation throughout my college career and experiences. I would like to acknowledge and thank my NASA mentors Michael C. Hicks, Rosa E. Padilla, Uday G. Hegde and colleagues Jun Kojima and Daniel J. Gotti for their support and guidance during my internships, research work, professional experiences, and completion of this thesis. Finally, I would like to thank Dr. Yuhao Xu, Michael C. Hicks, Dr. Ziaul Huque, and Dr. Paul O. Biney for serving on this thesis committee. This research was funded in part by the Minority University Research and Education Project (MUREP) Institutional Research Opportunity (MIRO) award #80NSSC19M0195.

## TABLE OF CONTENTS

	Page
ABSTRACT.....	iii
DEDICATION.....	v
ACKNOWLEDGMENTS .....	vi
TABLE OF CONTENTS.....	vii
LIST OF FIGURES .....	ix
LIST OF TABLES.....	xi
Chapter 1: INTRODUCTION.....	1
1.1 Significance .....	<b>Error! Bookmark not defined.</b>
Chapter 2: LITERATURE REVIEW.....	4
2.1 Supercritical Water Oxidation Background and Processes .....	4
2.2 Problems With SCWO Technology.....	9
2.3 Reactor Design Considerations.....	10
2.4 SCWO for Nitrogenous Wastes.....	11
2.5 SCWO Reaction Mechanisms and Kinetics .....	13
2.6 Present Waste Treatment Processes on the ISS .....	14
Chapter 3: METHODOLOGY.....	16
3.1 Research Design .....	16
3.1.1 Test Cell.....	16
3.1.2 Pressure Supply and Collection System .....	18
3.1.3 Air and Fuel Injection Systems.....	23
3.2 Diagnostic Equipment.....	24
3.2.1 Conductivity Meter .....	24
3.3 Benchtop Raman Analyzer .....	25
3.3.1 Total Organic Carbon Analyzer.....	32
3.3.2 Gas Analyzer.....	35
3.4 Experimental Procedure.....	36

3.5 Wastewater Characterization .....	37
3.6 Data Analysis .....	41
3.6.1 Calculated Parameters.....	42
Chapter 4: RESULTS .....	45
4.1 SCWO Conversion of Ersatz Wastewater .....	45
4.1.1 Qualitative Results for EWW: pH, Turbidity and Conductivity.....	46
4.2 EWW Quantitative Results.....	50
4.2.1 EWW TOC Results.....	50
4.2.2 Raman Results for EWW.....	52
4.3 Observation of Residence Time.....	63
4.4 Influence of Operating Temperature.....	64
4.5 Observation of Equivalence Ratio .....	66
4.5.1 EWW Equivalence Ratios: NASA GRC .....	66
4.5.2 EWW Equivalency Ratios: NASA ARC .....	67
4.5.3 EWW Theoretical Equivalency Ratios .....	68
4.6 Preliminary SCWO Tests for Urea-Aqueous Solutions .....	70
4.7 Preliminary Quantitative Results for Urea-Aqueous Solutions .....	72
4.7.1 TOC Results for Urea-Aqueous Solutions.....	73
4.7.2 Preliminary Raman Results for Urea-Aqueous Solutions .....	74
4.8 Observation of Residence Time.....	82
4.9 Influence of Operating Temperatures .....	83
4.10 Urea- Aqueous Solutions Preliminary Equivalence Ratios .....	84
4.11 Preliminary Gas Measurements for Urea-Ethanol Tests .....	85
Chapter 5: CONCLUSION AND DISCUSSION.....	88
5.1 Recommendations for Future Work .....	90
REFERENCES .....	92
APPENDIX A: Raw data.....	98
APPENDIX B: Experimental Apparatus .....	113
APPENDIX C: Additional Supplemental References .....	118
APPENDIX D: Thermophysical Properties and Test Parameters .....	120
CURRICULUM VITAE.....	123

## LIST OF FIGURES

FIGURE	Page
Figure 1: Pressure versus temperature diagram [5].	5
Figure 2: Solubility versus temperature diagram [5].	6
Figure 3: Process for SCWO [4].	7
Figure 4: Schematic of test cell with label descriptions.	17
Figure 5: SCWO Pressure Panel [55].	19
Figure 6: Support infrastructure with description of hardware [4].	21
Figure 7: LabVIEW Control Panel.	23
Figure 8: Raman Analyzer System.	27
Figure 9: Schematic of spectrograph optical layout.	28
Figure 10: Energy process diagram for (a) Rayleigh, (b) Stokes and (c) Anti-stokes	30
Figure 11: Raman Spectrum for pure deionized water using 532 nm, 100 mW laser.	31
Figure 12: TELEDYNE TEKMAR Lotix TOC Analyzer [60].	34
Figure 13: Images of untreated and treated water by SCWO testing.	47
Figure 14: Conductivity measurements for EWW tests	49
Figure 15: Raman shifts after SCWO conversion with comparisons to pure water	53
Figure 16: Normalized Raman shifts after SCWO conversion for Tests 6 and 7.	54
Figure 17: Normalized Raman shifts after SCWO conversion for Test 8 and Test 9.	56
Figure 18: Normalized Raman shifts after SCWO conversion for Test 10 and Test 11.	58
Figure 19: Normalized Raman shift comparisons for EWW for (2:1) + 5% wt. ethanol.	60
Figure 20: Normalized Raman shift comparisons for Test 15.	62
Figure 21: TOC Reduction vs. Residence Time for EWW SCWO Tests	63

Figure 22: Influence of operating temperatures on residence time for EWW TOC.....	65
Figure 23: TOC vs. equivalence ratios for EWW SCWO tests at NASA GRC. ....	67
Figure 24: TOC vs. equivalence ratios for EWW SCWO tests at NASA ARC. ....	68
Figure 25: Theoretical calculations of TOC vs. equivalence ratios for EWW tests. ....	69
Figure 26: Raman scatter for 90,000 ppm Urea-water (non-normalized). ....	75
Figure 27: Normalized Raman shift comparisons for Urea Test 3. ....	77
Figure 28: Normalized Raman comparisons for 50,000 ppm urea + 5% wt. ethanol . ...	79
Figure 29: Normalized Raman comparisons for 50,000 ppm urea + 10% wt. ethanol. ...	81
Figure 30: Observation of residence times for urea-aqueous solutions.....	83
Figure 31: Influence of operating temperatures on residence time for Urea TOC . ....	84
Figure 32: Equivalency ratios for urea-ethanol-treated tests. ....	85
Figure 33: Preliminary gas measurements for Urea Test 6.....	86
Figure 34: Preliminary gas measurements for Urea Test 7.....	86

## LIST OF TABLES

TABLE	Page
Table 1: Hardware Description [4] .....	22
Table 2: Standard Conductivity Values of Water .....	25
Table 3: Additional Lotix Components [60].....	35
Table 4: Ersatz Wastewater Composition [5]. .....	39
Table 5: EWW Chemical Recipe Composition [5].....	40
Table 6: Test Matrix for EWW Experiments.....	46
Table 7: EWW Results for pH and Turbidity .....	48
Table 8: Overall Results for EWW TOC Analysis.....	51
Table 9: Test Matrix for Urea-Aqueous Solutions .....	71
Table 10: pH Results for Urea-Aqueous Solutions.....	72
Table 11: TOC Results for Urea-Aqueous Solutions .....	73

## INTRODUCTION

Life support systems in extended space missions involve the need for technology that can allow the reclamation of resources from the air, water, and waste stream accumulation. The constant transport of resources and materials during space missions creates an overwhelming amount of waste and inefficient use of time, resources, and money. It has been estimated that it costs 10,000 USD for one pound of water to be sent to the low Earth orbit and will cost up to 40 times more to send the same amount to Mars [1]. The waste produced is typically wet, voluminous, and biologically unstable, with most of the composition being plastics (nearly 30%) and water (also almost 30%). It has also been estimated that for a lunar outpost, each inhabitant produces 6.8 kg to 9.6 kg of waste per day [2,3]. Waste is generated from food residues, hygiene wipes, and leftover liquids from drink consumption. In addition, future space exploration will require regenerative systems for plant and food growth, which will require extensive resource reclamation (e.g., carbon dioxide, water, and plant nutrients) from bio-waste streams. Current efforts for in-space water reclamation are limited to procedures like reverse osmosis for water potability. Supercritical Water Oxidation (SCWO) technology can be used to treat wet waste streams more efficiently without creating additional pollutants like NO<sub>x</sub> or SO<sub>x</sub> that would require further scrubbing. In the SCWO process, organic compounds are oxidized in water above its critical point at 374°C and 22 MPa

High reaction rates are typically observed since gases and organic compounds are highly soluble in water due to the change in polarity of water under these conditions [4].

Carbon dioxide and water are the primary products of organic oxidation, and product streams are microbially inert, benign, and amenable to resource recovery with nearly 100% water recovery. SCWO technology has advanced globally for large-scale commercial use for waste processing of sewage sludge, organic wastewater, and solid waste. Past work by Hicks et al. [4] at Glenn Research Center involved designing and fabricating a tubular SCWO reactor to oxidize aqueous waste solutions. Additionally, two experimental tests and conversions of ethanol and ersatz wastewater (EWW) as the two fuel constituents at various concentrations were performed. NASA Ames Research Center (NASA ARC) provided EWW to represent typical International Space Station (ISS) waste streams. A numerical study was also conducted to simulate the extent of oxidation for ethanol through observations of temperature, species mass fraction, and residence time.

The primary objectives of this work were to (i) optimize the performance for SCWO of ersatz wastewater through reactor reconfiguration, (ii) perform qualitative analysis for treated and untreated ersatz waste, and (iii) perform Raman spectroscopy, Total Organic Carbon (TOC), and gas diagnostics to understand the extent of conversion and (iv) perform experiments and diagnostics for urea-aqueous solutions. Results from this research will further guide an understanding of the capabilities of SCWO technology for future space exploration.

## **1.1 Significance**

The development of SCWO technology is a crucial area of research and development for both terrestrial and extraterrestrial applications. SCWO technology exists

as a more abstract counterpart to traditional combustion research, with great potential for major advances and can serve as a key link in the future development of waste treatment processes. Proper waste management for extended space administration has been a technical challenge for mission management due to the increasing emphasis on resource recovery and the accumulation of large amounts of waste during these extended space missions.

Owing to the SCWO technique and the lack of experiments performed with reactor setups using other organic and inorganic solid and liquid chemical fuels, further development of the oxidation mechanisms is required. Under the guidance and research of SCWO of EWW, the development of urea within similar test parameters should also be considered. As a waste product of all mammals, not only would the supercritical water oxidation technique results deemed significant to space applications but also for terrestrial applications as our world continues to battle the effects of waste processing. Unknown parameters for urea processing include determining the temperature, pressure and amount of oxygen required for rapid oxidation. The applications would also allow for further SCWO design improvements and increase relevance to NASA's efforts to near-future space exploration missions.

## LITERATURE REVIEW

Chapter 2 discusses relevant published research involving the use of SCWO methods and used in relevant research in the past and present. The study will serve to evaluate the most recent efforts in SCWO technology and current waste recovery systems utilized for low-orbit earth missions. Additionally, this chapter will guide reasoning for the conducting of the work presented in this project.

### 1.2 Supercritical Water Oxidation Background and Processes

Supercritical Water Oxidation (SCWO), also called hydrothermal oxidation (HTO), and supercritical water gasification (SCWG), is a process that consists of homogeneous oxidation of chemical compounds with an aqueous medium using an oxidizing agent such as oxygen or hydrogen peroxide at temperatures and pressures above water's critical point (374°C and 22 MPa). Reactions may be heterogenous if the presented organic material is a solid or involves a catalyst. SCWO was first proposed in the mid-1980s by American Scholar Michael Modell at MIT. In his patent (4,338,199), Modell describes SCWO as a useful method that permits using a vast range of organic materials as a fuel in desalinating seawater and brine or for removing specific inorganic salts from water [5-7]. Under normal conditions, water can exist as a solid, liquid, or gas. However, if water is within a supercritical point, a new phase that is neither a solid, liquid, nor a gas will appear. This additional phase only exists above the supercritical point [8]. This state of water is known as supercritical water (SCW) [6]. Figure 1 presents a pressure and temperature diagram for the different water phases at their critical points [5]. At supercritical conditions, water possesses many special characteristics like high diffusivity, low viscosity, low thermal

conductivity, zero surface tension, reduced hydrogen bonding, controllable dissociation constant a small dielectric constant, and favorable transport properties [5,9,10,13].

Additionally, at this stage, water has a low polarity, allowing it to act more like an organic molecule, making it a nonpolar solvent that is miscible for gases, organics, and other ionically attracted molecules. Furthermore, salts become nonpolar at SCW conditions and are extracted from the solution [10-12]. Figure 2 presents a solubility versus temperature diagram for salts observed in supercritical conditions [5].

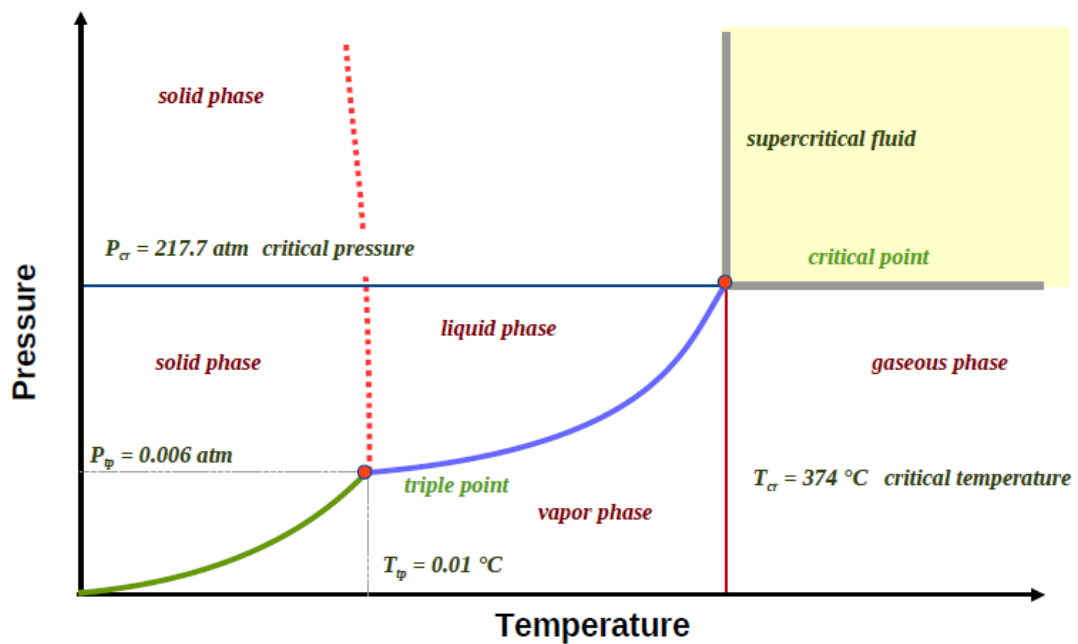


Figure 1: Pressure versus temperature diagram [5].

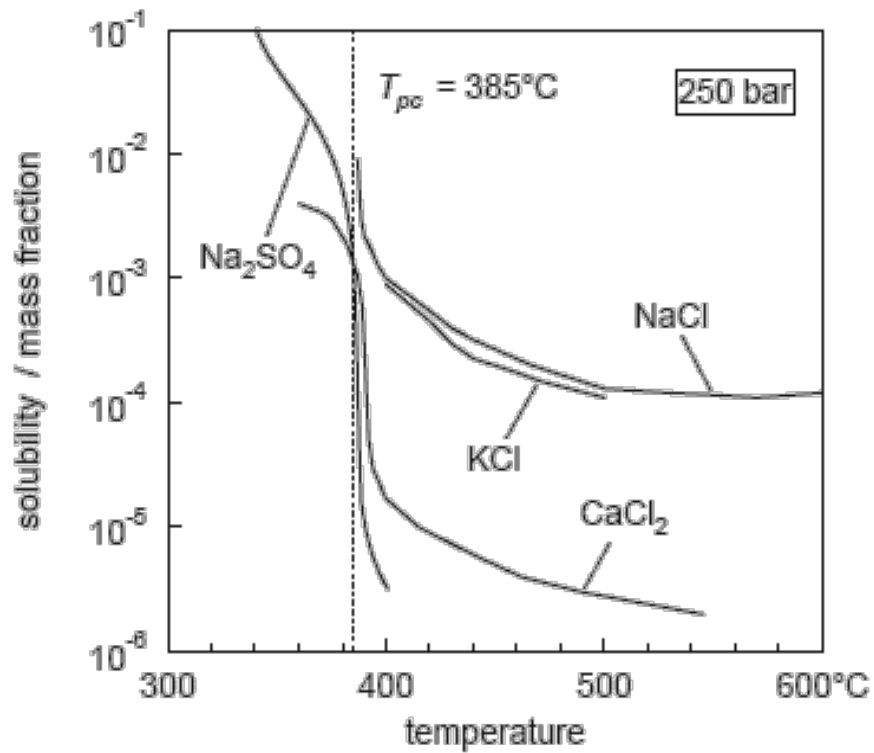


Figure 2: Solubility versus temperature diagram [5].

Various advanced oxidation processes (AOPs) have been used to destroy organic materials, including wet air oxidation, incineration, biological treatment, and SCWO. The choice of a method depends upon the wastewater's organic content. For contents up to 1%, biological and AOP methods are suitable. For the case of highly concentrated wastes (1%-20% organic matter) [13], incineration is favored, but SCWO is the better option due to the high costs and production of toxic gases by incineration. Figure 3 presents a diagram for the SCWO process.

Bermejo and Cocero described the SCWO process in four main steps. These steps are feed preparation and pressurization, reaction, salt separation, heat recovery, and depressurization. The steps are described below [5,15].

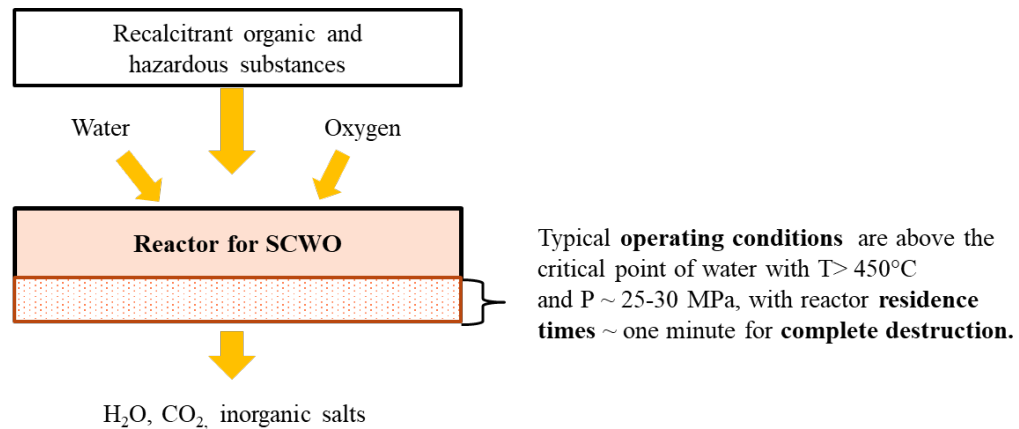


Figure 3: Process for SCWO [4].

1. Feed preparation and pressurization: The feed subjects are the oxidant, wastewater, and sometimes solids. Oxygen or hydrogen peroxide is typically used, so the process efficiency is independent of the oxidant. The choice of oxidant is determined by economics. Wastewater and oxidant are pressurized separately above 22.1 MPa. In some cases of high amounts of feed, a third input for pure water, pressurized separately, may be used to control reactor temperature. Heating values are determined by the temperature limits of the oxidizer (700- 750°C).
2. Reaction: Waste stream and oxidizer mix and react exothermally at supercritical conditions. Oxidation reactions are driven quickly due to the high solubility and the high temperatures. The insolubility of inorganics results in precipitation into a solid phase.
3. Salt separation: Salts are produced within the reactor as either sticky or non-sticky since they are insoluble. These particles can lead to adverse effects such as corrosion, fouling, plugging, etc... These salts are typically precipitated and can be removed using filtration systems or hydro-cyclones. For sticky salts, impingement canisters are typically

used. Suppose the salts are not removed through these processes. In that case, they can eventually redissolve once the product is no longer in SCW conditions and can be removed through reverse osmosis (RO) or other desalination methods.

4. Heat recovery and depressurization: Product streams and gaseous products must be cooled, depressurized to room conditions, and separated into two phases. Preheating the feed can cool products with a heat exchanger [23]. For more extensive scaled operations, electrical energy recovery is possible if the organic content of the feed is sufficient. A steam turbine may recover the energy not consumed during the process.

At appropriate temperatures, reaction temperatures, pressures, and residence times at SCW conditions, pollutants can be wholly eradicated (99%) in a few minutes or within times < 1 minute [14,15]. Primary products for SCWO processes include H<sub>2</sub>O, CO<sub>2</sub>, and inorganic salts. Other oxidized hetero atoms, like chlorine, phosphorus, and sulfur, are converted to inorganic acids [17,18]. The main operating parameters for the reaction process are the reaction temperature, oxidant concentration, residence time, and pressure. Reaction efficiency increases with increasing temperature, especially for nitrogenous waste, which requires higher temperature limits for complete conversion.[4]. With residence time, reaction temperatures around 650°C require residence times of <50 s for complete conversion [15]. Additionally, residence time, in general, may vary from an order of seconds to many minutes depending on the temperature and characteristics of the wastewater [16]. The oxidant concentration commands the reaction in which excess oxidant over stoichiometric requirement favors the complete oxidation of organics [4,19,20]. The role of operation pressure only serves to function as water's ability to be supercritical. When the pressure is above the critical pressure of water (22.1 MPa), reaction

conversion and kinetics do not noticeably improve [21,22]. The conversion efficiency only depreciates at lower sub-critical pressures, but this can be compensated if the reaction temperatures are high enough. The most promising benefit is that in comparison to other organic solvents, supercritical water is environmentally friendly, and the process eliminates oxidizable constituents completely. SCWO can be used and has been widely studied across biomass processing, synthetic fuel production, and material synthesis [11].

### **1.3 Problems With SCWO Technology**

Although SCWO technology has advanced throughout the years and is commercially available, many problems involve corrosion and salt precipitation. A variety of characteristics make SCWO an attractive process for corrosion tendencies. In-situ measurements have been performed for various factors affecting the corrosion rate for subcritical/supercritical environments [24]. Elevated temperatures and high concentrations of dissolved oxygen, extreme pH values, sharp pressure changes, and high concentrations of ionic species (during subcritical conditions) are all factors that make SCWO vulnerable to corrosion [15,25]. The four dominant types of corrosion for these applications are general corrosion, stress corrosion cracking, pitting corrosion, and intergranular corrosion [15]. Corrosion mitigation techniques have been examined and described by Marrone et al... These include (i) preventing corrosive species from interacting with the reactor surface, (ii) forming a corrosion-resistant barrier, (iii) selecting materials resistant to corrosion, and (iv) tuning operating conditions to avoid severe corrosion conditions [26,27]. In addition, it has been identified that reactors' most severe corrosion develops at conditions just below the supercritical threshold, and soluble ionic species are present [27,28]. This is mainly observed within piping used for heat exchanging before entrance

into the SCWO reactor inlet [5]. Another problem endured by SCWO reactors due to the insolubility of salts in supercritical water is salt precipitation. Inorganic salts are readily soluble in water at room conditions. Near the critical point of water, the solubility of inorganic salts decreases dramatically. Hence, at supercritical conditions, precipitated salts can cause problems such as erosion of equipment, plugging, and fouling. Long-term agglomeration of these precipitated salts can lead to issues like system failure and over-pressurization, resulting in safety concerns. These problems and solutions will need to be considered for in-space applications, especially with additional parameters such as reduced gravity and a vacuumed environment.

#### **1.4 Reactor Design Considerations**

Multiple SCWO reactor designs have been developed over the years. Schmeider et al. [18] conducted a study to characterize and group different reactor types. The most popular and commonly used reactor types are tubular (plug-flow), transpiring wall reactors (TWR), and tank reactors. The reactor type for this project was a tubular reactor, the most widely used reactor. Although tubular reactors have been utilized for industrial use in SCWO facilities for large-scale treatment [32], like this work, tubular reactors are also present in small laboratories for studying new advances in SCWO applications [4,29,30,67]. Since SCWO kinetics operate in a pseudo-first-order process for waste concentration, plug flow reactors can achieve the highest conversions within a particular residence time [15]. There are some disadvantages to plug flow reactors to take into consideration. Due to the salt precipitation, the reactors tend to plug. Also, high-rate exothermal reactions can cause localized and uncontrollable pockets of high temperatures within the reactor. Another area for improvement with this reactor design is the inability to

separate the pressure and temperature effects on the inner reactor walls. Coating the inner wall with temperature-resistant material will need to be paired with thicker walls to withstand high pressures, which can be expensive [10,15]. The extreme conditions of SCWO can make the choice of material difficult, so it is necessary to choose the material as a function of desired operation conditions [33]. For reactor material, Vadillo et al. [17] suggested that Inconel 625 is a good material for avoiding the effects of extreme reactor conditions due to its high corrosion resistance. An additional study by Tang et al. observed corrosion behavior for Inconel 625 and other similar Ni-based alloys in SCWO conditions. Results showed that the material exhibited good corrosion resistance in the presence of oxygen and salts [34]. Additional design considerations for counteracting SCWO destructive tendencies include the use of cold (ambient temperature) feed injection, optimization of operating conditions [35], avoiding corrosive feeds [36], and using smaller inlet diameters to increase the velocity of fluids to prevent salt precipitation. These design considerations have been utilized to develop the reactor used in this project.

### **1.5 SCWO for Nitrogenous Wastes**

The degradation of organic pollutants in SCWO can be complex due to many factors. Jiang et al. [11] reviewed mechanisms and kinetics for SCWO processes. Although oxidation is the primary reaction, many other reactions, such as pyrolysis, hydrolysis, polymerization, and catalysis, may also occur. As a representative of International Space Station (ISS) produced wastewater, the ersatz solution used in this project was produced with concentrations of ethanol (highest concentration), acetic acid, formic acid, acetone, urea, and ammonium bicarbonate. Reaction pathways for organics containing only C, H, and O have a simple conversion path that usually leads to CO<sub>2</sub> and H<sub>2</sub>O. With the addition

of organics like N, S, and Cl, the production of intermediate species occurs, which can cause the reaction pathway to change. The degradation of hydrocarbons also leads to the intermediate production of acetic acid during the oxidation of alcohols [35].

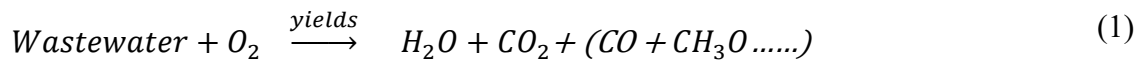
Additionally, Urea, which is subject to hydrolysis, can break down into ammonia, bicarbonate, and eventually nitrogen compounds. Treatment of nitrogenous wastes is relatively tricky due to the stubborn intermediate acids and salts that can be produced that can lead to corrosion [38]. An earlier study conducted in 1982 by Timberlake et al. [39] concluded that above 650°C, urea breaks down into nitrogen gas, water, and carbon dioxide without using a catalyst. A more recent study, performed by Okazaki and Funaukuri [40], observed the effects with/without the addition of hydrogen peroxide in urea-water at sub- and supercritical conditions in the presence of additives. Results obtained from conditions of sub- and supercritical (265-376°C) showed that the addition of acids did not increase conversion rates, but the addition of NaOH did remarkably. The roles of alcohols as co-fuels have also been examined as suitable treatment techniques for other heterocyclic and ammonia-based wastes [41-44,67]. Other than molecular nitrogen, for the oxidation of similar nitrogenous wastes like urea and ersatz, additional compounds produced include ammonia (NH<sub>3</sub>), nitrate (NO<sub>2</sub>-), and nitrite (NO<sub>3</sub>-). Ammonia is the most refractory of the intermediate species produced from these nitrogenous waste streams. As a toxic pollutant to the human body and aquatic life at moderate levels, it is of high interest to SCWO technology, especially for future human space exploration efforts [47]. Complete oxidation of ammonia requires extreme temperatures (<650°C) and longer residence times (~ 1 min.) with the absence of a catalyst. This was especially true for industrial waste streams with high ammonia concentrations. Helling and Tester [45] observed that ammonia would not

oxidize at a measurable rate below 540°C with only 5% conversion at 6-13s residence time. Additionally, their results suggest that reactor type and material were also observed as a factor of conversion. Results showed that ammonia was partially catalyzed by the reactor wall material (Inconel 625) within a tubular and packed bed reactor at temperatures between 640-700°C. But, the packed bed reactor, with 30 times more surface area than the tubular, showed 4 times higher reactor rates. Using co-fuels is an effective way to counteract the stubborn conversion tendencies of ammonia and other nitrogenous wastes. A key advantage of using a co-fuel is that they can improve the production of free radicals during their conversions which can further enhance the conversion of the treated subject [16,45,46]. Additionally, co-fuels can oxidize more rapidly within the reactor when mixed with oxidants, accelerating the oxidation of the treated solution [16,41,45]. The general use of co-fuels helps decrease the activation energy needed for these high-energy reactions, minimizes the need for high operating temperatures, and conserves energy [16,45,46].

## **1.6 SCWO Reaction Mechanisms and Kinetics**

SCWO reaction mechanisms and pathways are important for effective wastewater treatment and successful engineering design. Several studies have developed kinetic modeling for SCWO reactions of organics focusing on the influence of water properties. Computational calculations for fluid properties have also been conducted in the past. The simple mechanism for SCWO involves an organic compound and oxygen dissolving in water as a homogeneous phase. Li et al. [37] determined that the production and destruction of rate-controlling intermediates influence the rates of these reactions. Additionally, the type and amount of these intermediates can also affect these rates. The SCWO mechanism can also be influenced by oxidant type. As mentioned, oxygen, air, and hydrogen peroxide

are the most used oxidants. Depending on the oxidant, forming radicals can lead to different reaction pathways based on their behaviors. Due to the complexity of the waste used in this research, numerical simulation of reaction intermediate kinetics is difficult to predict and model. As a pseudo-first-order reaction, the simplest mechanism for this project can be observed in equation 1 [4].



Studies relating to reaction kinetics for SCWO have determined that the reaction order for the organic is found to favor excess use of the oxidant [47]. Martino and Savage [49] developed an equation for plug-flow (tubular) reactors that related the rate of TOC decrease to residence time  $\tau$ , to oxygen concentration  $[O_2]$  and  $k$ , the Arrhenius rate constant, which is a function of absolute temperature  $T$  (K) and activation energy [46]. For a complex solution like ersatz, the rate for degradation of TOC is expressed as shown in equation (2).

$$-\frac{d[TOC]}{dT} = k \cdot [TOC]^a \cdot [O_2]^b \quad (2)$$

### 1.7 Present Waste Treatment Processes on the ISS

The Water Recovery System (WRS) currently used on the ISS can provide clean water for crew members through recycling urine, respiration, cabin humidity condensate from crew sweat, and hygiene. A Urine Processor Assembly (UPA) chemically pretreats urine recovered through distillation for a significant 87% water recovery. This process, combined with an additional Water Processing Assembly (WPA) allows for an overall 93.5% water recovery [50]. For long-term space exploration and habitation outside of the low Earth orbit, sustainable life support systems will require water recovery near 98% of

the original water supply [50,51]. Prior to desalination, chemical pretreatment for urine is performed to prevent urea hydrolysis which increases pH levels and influences salt precipitation and production of ammonia. The brine created from this pretreated process is then subjected to a Vapor Compression Distillation (VCD) process, which is restricted by a solubility limit [52]. Since only a portion of this urine brine (15%) is converted, the remaining chemicals, strong acids, and oxidants prevent ammonia from evaporating with the water vapor. Therefore, this hazardous brine cannot be further distilled, leading to water loss [53,54]. For this reason, substitutions for the current chemical pretreatment and distillation processes can be achieved through a WRS using SCWO technology to avoid hazardous products.

## METHODOLOGY

### 1.8 Research Design

The experimental work involved the use of the Advanced Exploration Systems (AES) reactor that was designed and fabricated at NASA GRC). Various components of the experimental system include an oxidant supply system, a fuel injection system, a reaction chamber, and a collection sub-system. Supporting components include a booster pump for oxidizer supply, side ports for entrances for the reactor stream, and a thermocouple system. Each aspect of the system is described below.

#### 1.8.1 Test Cell

Figure 4 presents the schematic of the test cell used for experimentation with significant dimensions. The test cell is the portion of the system that is heated. The maximum operating pressure is 5000 psi (28.3 MPa) at a temperature of 630° C (1166° F). Material specifications for the test cell are 1.50" OD Rod, Inconel 625 Grade 1, ASME SB-446/ASTM B-446. This material provides corrosion resistance and adequate strength at high operating temperatures. The maximum design temperature is 630° C with an unspecified maximum allowable design pressure, but testing parameters should not exceed 5000 psi. The SCWO test cell is a *tubular or plug-flow reactor* with a volume of 62 mL. A thermocouple extends through an adapted fitting at the top of the reactor and registers temperatures in the reaction zone. This thermocouple provides the best real-time indication of the presence and extent of the oxidative reactions. Two inlet ports exist at the side for the oxidizer stream (air) and at the bottom for the fuel (wastewater). The fuel enters the reactor core at ~2.22 cm above the bottom of the reactor. The previous design of the AES reactor had a fuel entrance ~7.62 cm above the base of the reactor. Optimization of this

configuration was performed to allow an earlier entrance of the fuel to enable a faster reaction ignition at the inlets. Relative to the position of the inlet ports, an annular and axisymmetric flow is established at the fuel line's exit point. The test cell is heated using embedded heating tape and a power supply. The inlet ports are heated separately using a line heater supply and heater tape. Heating capabilities are controlled using a LabView Heat Control Program.

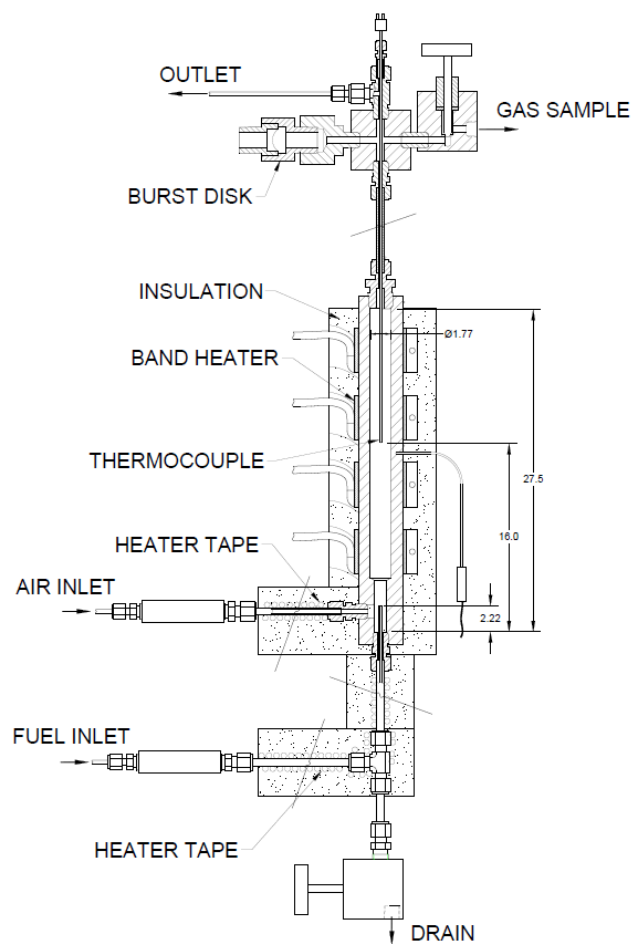


Figure 4: Schematic of test cell with label descriptions.

## 1.8.2 Pressure Supply and Collection System

A panel was designed to control the flow and pressure of the test cell during experimentation. Figure 5 presents the SCWO panel configuration. Panel operating procedures were created at NASA Glenn [55]. The panel is divided into three portions:

- the system that introduces the liquid into the system (left)
- the injection air system (along the top portion)
- the portion that controls the booster pump (lower right)

The system consists of two controls to introduce liquid into the test cell. One set is for fuel, and the other is for the oxidizer. Several controls across the top of the panel are used for air injection. Controls include a gauge that displays the pressure in the storage cylinders and a regulator to control the pressure entering the system (O107). There are also two valves to stop the flow into the system (O109) and vent the cylinders (O102). For the test cell, there is a valve to vent pressure (SH109). This valve bypasses the line that goes through the backpressure regulator. The pressure supply also contains a booster pump supplied by shop air. Shop air is supplied by manually opening a valve on the right side of the system. Booster pump controls feature a shop air regulator (A101) and shop air gauge. The booster pump air flow is controlled by a needle valve (A103). A K bottle containing the air that will be pressurized is located on the wall left of the system. This bottle has a shutoff valve and regulator. Flows from these are introduced to the pump by valve N103.

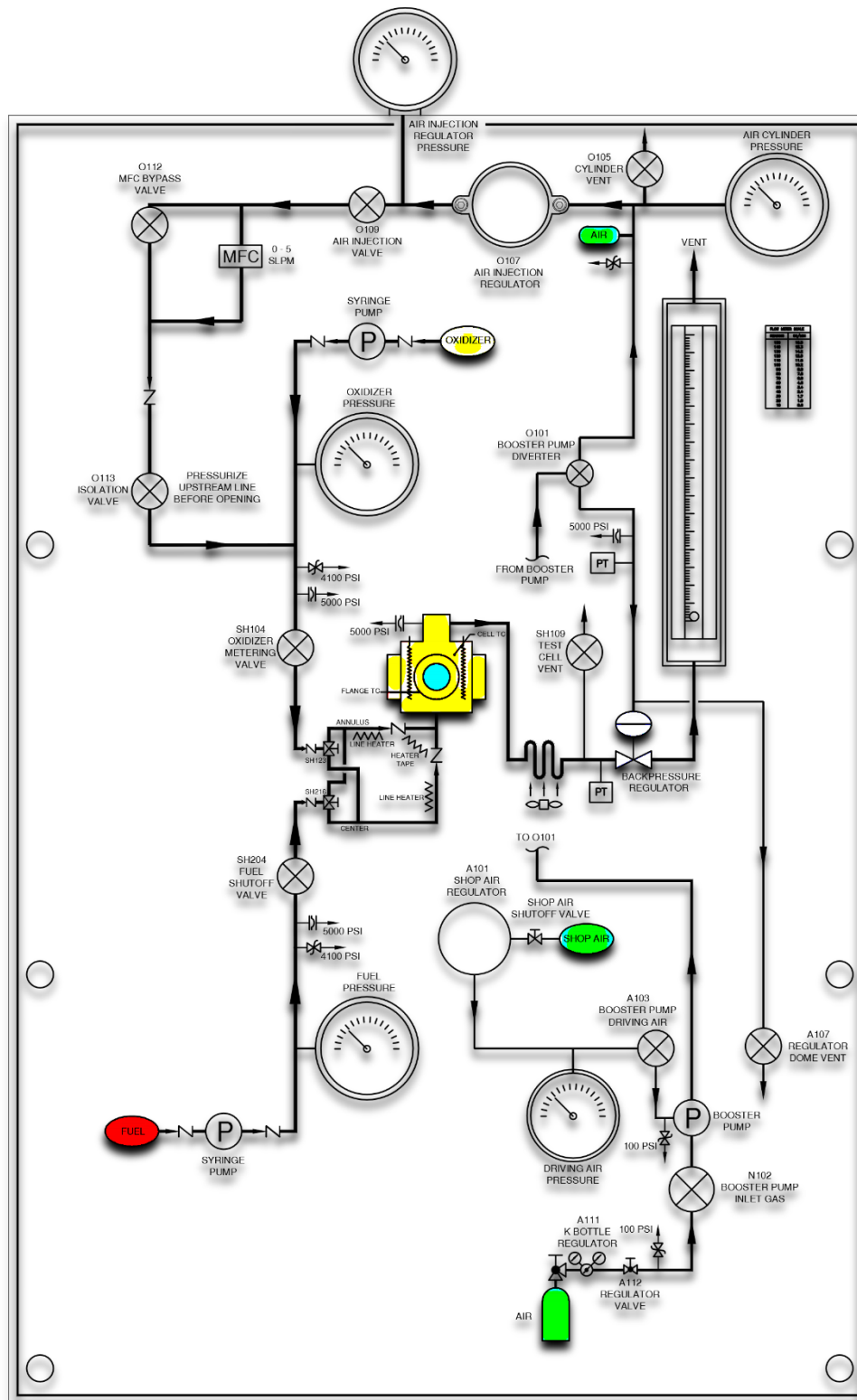


Figure 5: SCWO Pressure Panel [55].

The booster pump flow can be redirected to either the storage cylinders or the backpressure regulator using valve O101. Finally, pressure in the dome of the backpressure regulator can be vented through valve A107.

An important note is that this valve should not be opened if the test cell is pressurized at a temperature above 100° C. If this happens, the hot liquid from the test cell will pass through the heat exchanger at an imposing rate before adequate cooling. Furthermore, the hot fluid would contact the backpressure regulator causing potential damage. For the collection of the effluent after testing and the sample, the collection subsystem uses two methods of sample collection depending on if the sample is vapor or liquid. Liquid samples are collected after the product stream is depressurized and cooled to ambient temperatures through a coiled heat exchanger and flow back up the pressure regulator. The condensed matter is then collected in a dump tank. Once cooled through the same process, the gas sample is collected by attaching a 50 ml sample cylinder to the outlet valve of the back pressure regulator.

Figure 6 presents a schematic for the supporting infrastructure with hardware descriptions described in Table 1. As of now, there has been no buildup of salt precipitate in the reactor. The concentration of salt in the diluted wastewater is small (<0.5% total). Therefore, salt precipitating in the supercritical fluid region is not agglomerating. Most salt presumably exists with the fluid stream and redissolves downstream of the depressurization point [2].

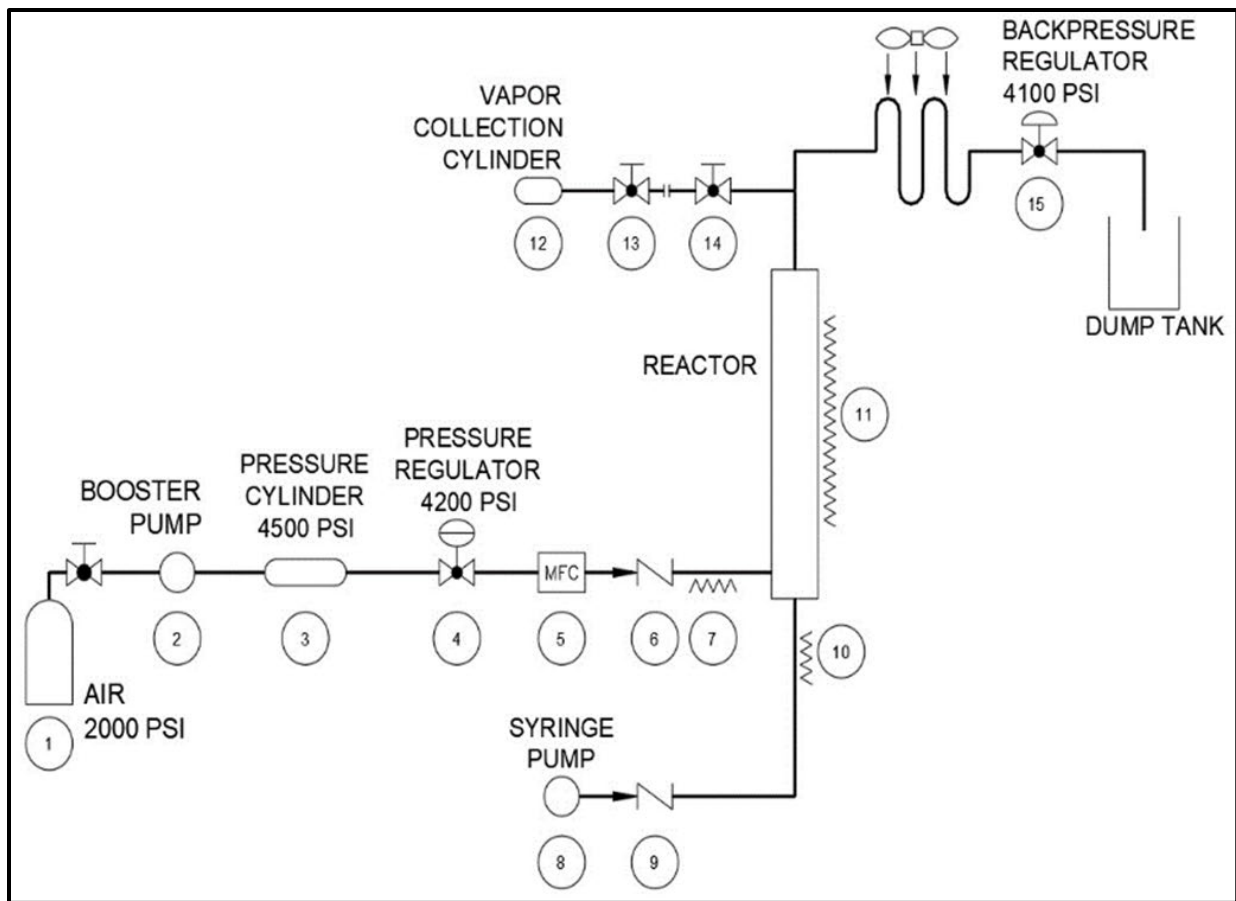


Figure 6: Support infrastructure with description of hardware [4].

Table 1: Hardware Description [4]

Hardware	Description
K bottle	Compressed air supply
Booster pump	3/8" NPT inlet, 1/4" NPT outlet, 55.1 MPa (8000 psi) rating
Storage Cylinder	1/4" NPT inlet and outlet, 34.5 MPa (5000 psi) 5000 psi rating
Pressure regulator	1/4" NPT inlet and outlet, 0-41.3 MPa (0-6000 psi) range
Mass flow controller	1/4" tube inlet and outlet, 34.5 MPa (5000 psi) rating, 0.5 to 5.0 SLPM range
Check valve	NPT inlet and outlet, 96.2 MPa (13950 psi) rating
Heater rope (2)	3 ft. long, 125 W, 120 VAC, 482 °C (900 °F) rating
Syringe pump	500 HP, 1/8" tube outlet, 507 mL capacity, 34.5 MPa (5000 psi) rating
Check valve	NPT inlet and outlet, 96.2 MPa (13950 psi) rating
Heater tape	8 ft. long, 624 W, 120 VAC, 760 °C (1400°F) rating
Sample cylinder	NPT inlet, 50 cc capacity, 12.4 MPa (1800 psi) rating
Needle valve	NPT inlet and outlet, 20.7 MPa (3000 psi) rating
Needle valve	NPT inlet and outlet, 51.5 MPa (7465 psi) rating
Back pressure regulator	1/8" NPT inlet and outlet, 0 to 5000 psi range

### 1.8.3 Air and Fuel Injection Systems

Two separate control mechanisms introduce air, and fuel flows into the system. Mass flow controllers are used for the air supply operates under narrow inlet and outlet pressures. These pressures are 4100 psi for the inlet and 3900 psi for the outlet. Proper outlet pressure must utilize a mass flow controller bypass valve (O112) due to a check valve downstream. Figure 7 presents the LabVIEW program display used for operating parameters such as airflow, set temperatures, and on-time heating settings. Flow rates for air are set using a LabVIEW controller program.

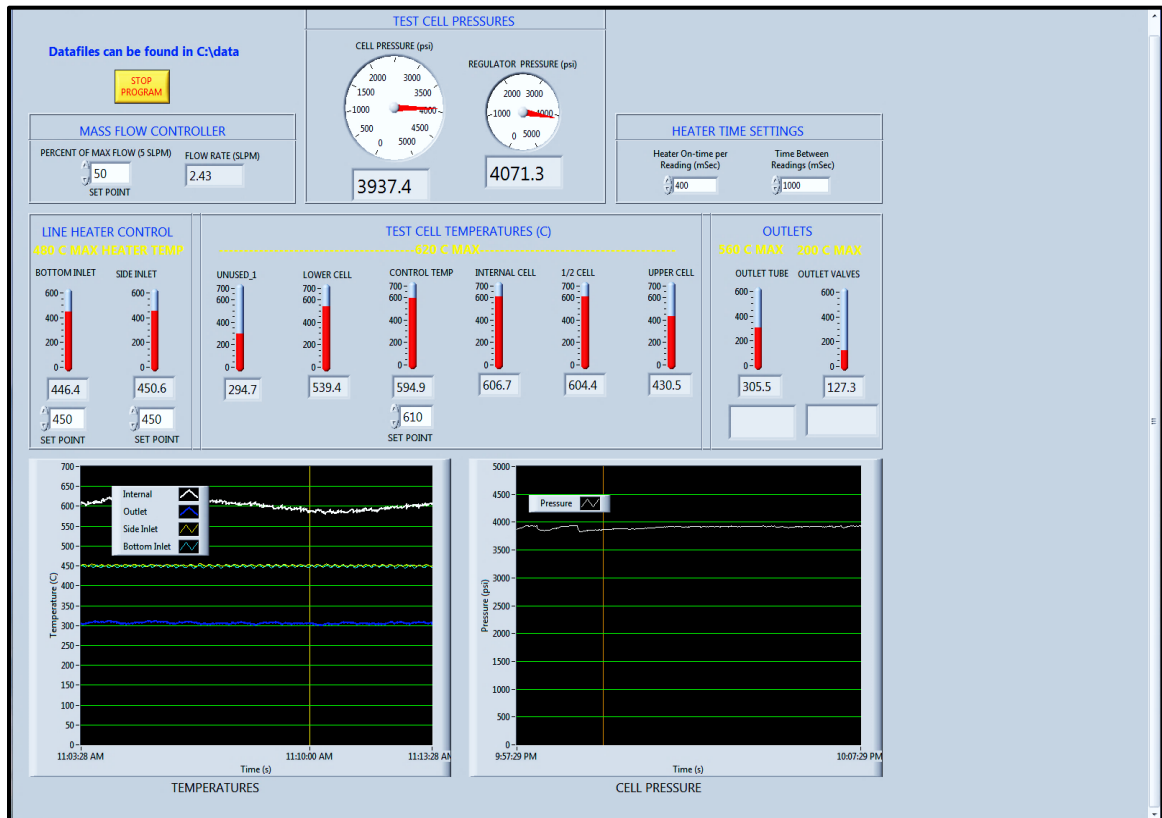


Figure 7: LabVIEW Control Panel.

Additional vital elements for the program allow for real-time display of temperatures for the test cell, inlets, and outlets. The desired airflow can be entered in the "Mass Flow Controller" panel in the top left. The value entered is a percentage of the maximum allowed flow rate of 5 SLPM.

A 507 ml TELEDYNE D-Series syringe pump controller is utilized for fuel injections [Appendix B]. A 2L reservoir is used for the fuel supply to the syringe pump. The system includes two separate pumps that can be operated simultaneously or separately. For these tests, only one pump is used during testing. Once the reservoirs are connected to the syringe pump with quick connections, the system can be filled for testing. Fuel rates can be manipulated manually using standard inputs at 0.10-10.0 mL/min ranges.

## **1.9 Diagnostic Equipment**

Several qualitative and quantitative diagnostic techniques are discussed in the following sections 3.2-3.3. These diagnostics were used for examining the extent of SCWO conversion.

### **1.9.1 Conductivity Meter**

Measurements of conductivity were taken for untreated and treated samples to relate conversion efficiency with the likeness of drinkable water. An Oakton pH/CON 510 Benchtop Meter was used to perform this analysis [Appendix B]. The capabilities of this instrument allow it to measure pH, mV, Conductivity, Total Dissolved Solids (TDS), and temperature (°C, °F). Conductivity and pH measurements were the leading interest for this work. Conductivity is measured in units of micro-Siemens ( $\mu\text{S}/\text{cm}$ ). Ranges of conductivity for this instrumentation include 0 to 199.9  $\mu\text{S}$  and 0 to 199.9 mS. Conductivity measurements were performed by immersing a probe into the sample. Table 2 presents

typical conductivity values for a variety of types of water. The conductivity measurements were conducted to determine if the post-treated solution was ingestible due to safety reasons. Additionally, values of conductivity can be easily related to modes of pH levels which is another valid indicator for determining if water is potentially drinkable.

Table 2: Standard Conductivity Values of Water

<b>Sample Type</b>	<b>Conductivity Range</b>
<b>Distilled Water</b>	<b>0.5 <math>\mu\text{S/cm}</math> to 3 <math>\mu\text{S/cm}</math></b>
<b>Drinking Water</b>	<b>100 <math>\mu\text{S/cm}</math> to 1000 <math>\mu\text{S/cm}</math></b>
<b>Tap Water</b>	<b>50 <math>\mu\text{S/cm}</math> to 800 <math>\mu\text{S/cm}</math></b>
<b>Potable Water in the U.S.</b>	<b>30 <math>\mu\text{S/cm}</math> to 1500 <math>\mu\text{S/cm}</math></b>
<b>Freshwater Streams</b>	<b>100 <math>\mu\text{S/cm}</math> to 2000 <math>\mu\text{S/cm}</math></b>
<b>Wastewater</b>	<b>85 <math>\mu\text{S/cm}</math> to 9000 <math>\mu\text{S/cm}</math></b>
<b>Seawater</b>	<b>55000 <math>\mu\text{S/cm}</math></b>

### 1.10 Benchtop Raman Analyzer

Raman Spectroscopy is a technique used to determine the vibrational modes of molecules and chemical species analysis. For quantitative measurements of the sampled solutions after the SCWO conversion, a laser Raman spectrometer was utilized. A type of Raman spectroscopy used in the present research was a linear spectroscopic diagnostic that

can determine vibrational modes of chemical constituents—primarily liquid-phase—and identify chemical compounds within the aqueous solutions. This Raman chemical analyzer employed an aberration-free spectrograph with a built-in deep-cooled ( $-55^{\circ}\text{C}$ ) couple-charged device (CCD) camera (Princeton Instruments Fergie/IsoPlane 81). It features a broad spectral range from 200 to 1100 nm with up to 0.05 nm spectral resolution. For Raman scattering excitation, a continuous-wave (CW) fiber-optic Nd: YAG laser (532 nm, 100 mW) was coupled to Raman filter cube-optics, collating, and directing the excitation beam to a 10-mm quartz sample cuvette. Raman-shifted spontaneous backscattering from the sample was re-focused by a collimated lens into the spectrograph equipped with a 25- $\mu\text{m}$  entrance slit. An internal optical "edge" filter (Optical Density  $\sim 7.0$ ) attenuated the excitation laser line below the typical Raman band intensity. The typical CCD exposure time of the Raman scan for each sample solution was 5-10 seconds. A laptop was used to run the software needed for the spectrometer and for the calibration and use of the laser. The laser apparatus is considered a class 3, and proper safety training and requirements were performed before using the system. Figure 8 shows the Raman analyzer setup used for these diagnostics. The three main components from left to right present the fiber-optic Nd: YAG laser (with a power supply/controller), Raman-sampling cube-optics assembly, and the CCD imaging spectrograph. Additionally, Figure 9 represents a schematic of the system with descriptions of major components. Samples are prepared in a quartz cuvette and are cleaned with methanol to remove any unwanted residue (i.e., fingerprints, smudges) that may affect the light scattering process.

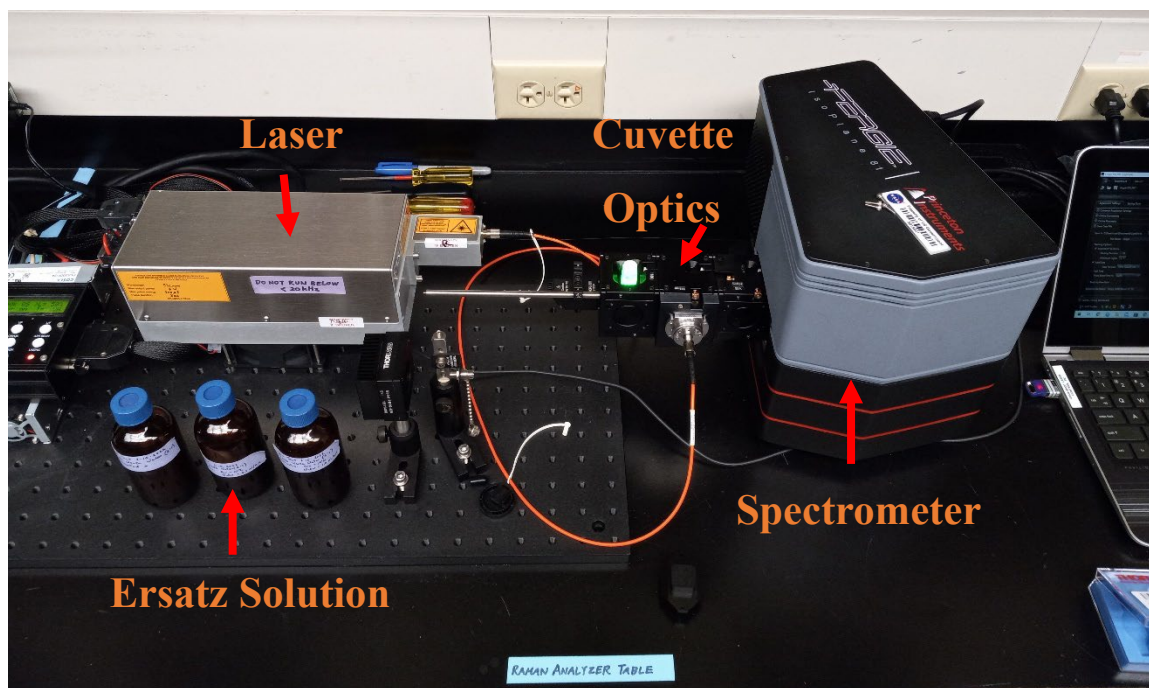


Figure 8: Raman Analyzer System.

After sample preparation, Raman procedure preparations begin. The functionalities of spectroscopy are heavily dependent upon the use of light. For this reason, the lab environment for the Raman procedure requires minimal to no light. Although the Raman sample filter cube includes a cover for light reduction, all lights are turned off for maximum results optimization. Once the system's spectrometer portion (FERGIE) is powered on, the laptop is used to open the software. Safety goggles are put on, and the laser is additionally powered on. Laser restriction protocol for personnel outside of the lab during operation is also initiated during this time. Two people were always present for the operation of the Raman system. This step is critical for laser safety and assurance of proper procedure performance. A detailed schematic of the Raman system configuration can be observed in Figure 9 as well.

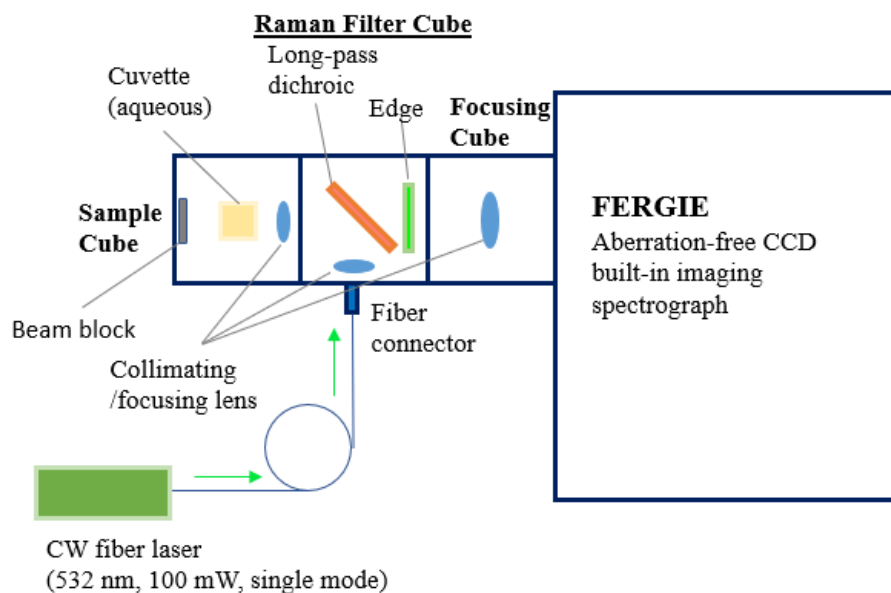


Figure 9: Schematic of spectrograph optical layout.

Raman processes work by exciting molecules into molecular vibrational states and subsequently accounting for this interaction. Molecule excitation is accomplished by emitting a laser, in this case, a 532 nm fiber laser, through a sample that causes two forms of light scattering: an elastic process and an inelastic one [56,57]. Electrons become excited when they interact with photons from the laser beam. At this point, the electrons are in a "virtual state," unstable, causing them to fall to a ground state. As the electrons fall, they emit photons in three different forms. The most abundant form of scattered light from the laser incident is the elastic form called Rayleigh scattered light. This light scatter occurs when an electron falls to the original ground state without energy change. Hence, the same light wavelength is re-emitted. A tiny percentage (about .000001%) of the remaining light

is the inelastic form, or Raman scattered light, also called "stokes" [56,57]. This scattered light can be re-emitted in two forms. The first form is generated when an electron descends to a vibrational level instead of ground level. This means that a portion of energy has been absorbed and causes light to be re-emitted in a longer wavelength than the incident laser light called "Stokes [56,57]." The other form of Raman scattered light happens when an electron is excited at the vibrational level and reaches a higher virtual level with higher energy. When this electron falls to ground level, there is a higher photon emission than the incident, which causes a shorter wavelength. This Raman scatter is called "Anti-Stokes [56,57]." Figure 10 features a diagram of this process where E represents the electron at its final or initial states for the two types of Raman scatter. The filters within the "Raman filter cube" serve to eliminate the excess Rayleigh light at the given 532 nm laser emission and redirect the "stokes" and "anti-stokes" Raman scatter back through the collimating focusing lens for the CCD camera system. A potential drawback of this method is the possibility of undesired fluorescence capture during measurements. Additionally, this study is unable to determine specific constituents on the Raman spectra due to solution complexity. An approximation of the identification of significant species was observed with a Raman band identification chart. This chart can be observed in Appendix C. For this study, comparisons of the before and after treated samples were sufficient for the purpose of observing the reduction of Raman scatter.

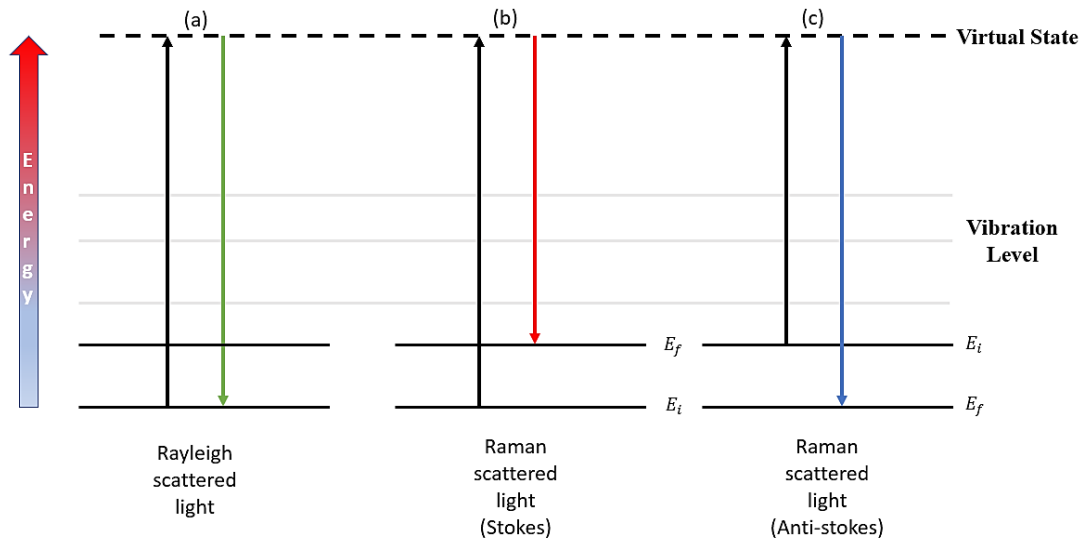


Figure 10: Energy process diagram for (a) Rayleigh, (b) Stokes and (c) Anti-stokes.

The built-in imaging spectrograph captures and detects Raman scattered light using an optical grating to disperse the light onto a CCD detector by deflecting each wavelength at a different angle. Optimization of scatter detection and the spectral range was achieved by adjusting the grating center wavelength within the spectrograph software. Increasing the center wavelength allows for increased resolution and a narrower spectral range. This parameter is the most important for spectrograph grating. Optimal grating and configurations were achieved before the use of the system. Raman scans were captured at two center wavelengths of 575 nm and 650 nm to observe water molecules. The output of the Stokes and Anti-Stokes is called a Raman Spectrum. A visual representation of a Raman spectrum of water for a 532 nm wavelength is presented in Figure 11.

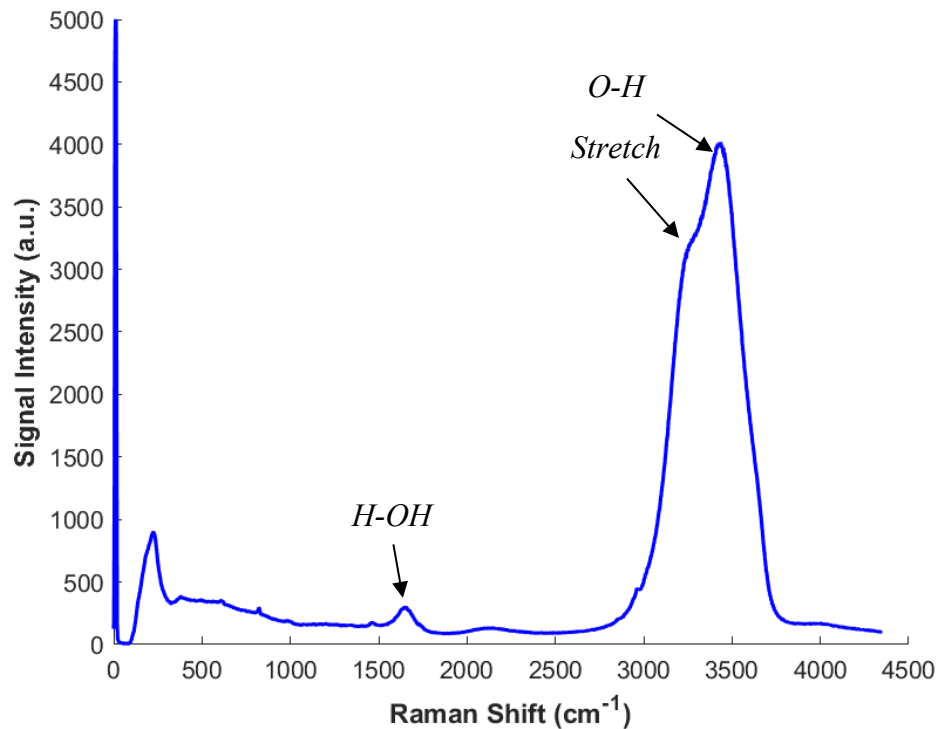


Figure 11: Raman Spectrum for pure deionized water using 532 nm, 100 mW laser.

The Raman spectra was captured at 575 nm and 650 nm and were combined to show the full spectrum of pure deionized water. Initial outputs of the Raman scan are plotted as arbitrary units of intensity vs. wavelength. In Raman spectroscopy, the wavelength,  $\lambda$  (nm), is converted to wavenumber (measured in  $\text{cm}^{-1}$ ) to characterize light. Wavenumber is linearly related to energy and independent of the excitation wavelength, which makes the units convenient for species analysis. Raman shift can be computed using equation 3. Additional interpolation procedures were used to combine the two separate center grating spectrums when applicable. Typically, in Raman processes, every chemical compound has its own characterized wavenumber that can be identifiable. Pure deionized

water is the baseline for these Raman comparisons. Water's O-H stretching vibrations occur at two peaks at approximately  $3400\text{ cm}^{-1}$  and  $3250\text{ cm}^{-1}$ . There is an additional H-OH peak at approximately  $1635\text{ cm}^{-1}$  [58,59]. These criteria were used in the method for the distinction of properties of water.

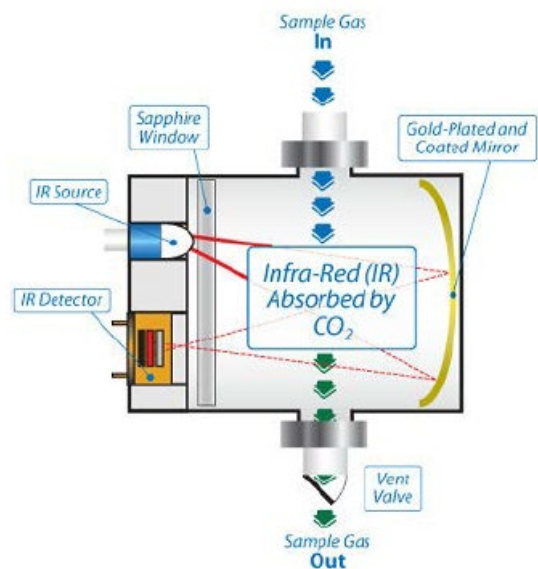
$$\text{Raman Shift } [cm^{-1}] = \frac{10^7}{\lambda_{ex}[nm]} - \frac{10^7}{\lambda[nm]} \quad (3)$$

Pure water was the baseline comparison used for the SCWO tests and serves to quantitatively as well as qualitatively express the extent of conversion for the performed tests. Conversion success is observed by evaluating the change in the Raman profile before and after testing compared to the water, as mentioned above. This diagnostic technique was the most prominent throughout this project.

### **1.10.1 Total Organic Carbon Analyzer**

Analysis of Total Organic Carbon (TOC) is a valued method in many organizations and labs in determining the suitability of treatment and testing processes. TOC is a measure of the total amount of carbon in organic compounds that can be found in pure water and other aqueous solutions. For this work, a TELEDYNE TEKMAR Lotix TOC Analyzer was used [60] and is shown in Fig. 12a. The analyzer uses a non-dispersive infrared (NDIR) detector to measure the carbon content of an aqueous solution at precise levels. TOC analysis is achieved by this system using a combustion catalytic oxidation procedure. The Lotix features a quartz combustion tube packed with a platinum catalyst and quartz beads subject to a continuous air flow at  $200\text{ mL/min}$ . The furnace used for the system is maintained at an operating temperature of  $680^\circ\text{C}$ . A sample loop sampling system automatically introduces samples containing organic carbon. Using catalytic oxidation, the

sample is oxidized into  $\text{CO}_2$  and  $\text{H}_2\text{O}$ . The moisture removal process is performed as gas flow sweeps the  $\text{CO}_2$ -containing steam into a condenser loop and a mist trap. Final efforts of  $\text{H}_2\text{O}$  removal from the  $\text{CO}_2$  gas are achieved with a permeation dry and a U-shaped halogen scrubber filled with 20 mesh copper and tin granules separated with Pyrex® wool. After scrubbing, the gas passes through the  $\text{CO}_2$ -specific NDIR detector for quantification (as shown in Fig. 12b). The measurements are a function of the absorption of IR energy. TOC measurements were provided as ppm. Concentration values rely on the difference of the IR absorption between a reference and sample signal. The Lotix system also allows quantifying inorganic carbon (IC) using a sparger and a predetermined amount of 21% phosphoric acid to purge the IC out of the solution as  $\text{CO}_2$ . For this study, only measurements of TOC were initially desired. Figure 12 presents an image of the TOC analyzer as well as a schematic of the NDIR detector [60]. Additional internal hardware components of the diagnostic system can be observed in Appendix B.



(a)

(b)

Figure 12: TELEDYNE TEKMAR Lotix TOC Analyzer [60].

Additionally, Table 3 presents supporting components. Configuration and simplicity of this system allowed for multiple sample analysis to be taken without the presence of the user. A PC laptop was used to operate the Lotix system through a software program that allows the user to configure the sampling procedure, perform reagent calibrations, and collect the data. Calibration tests were performed before initial sample analysis to ensure accuracy of measurements to the maximum ability. A note to mention is that a fraction of the TOC tests taken for this study were taken at supporting center NASA ARC. In situ measurements at NASA GRC were not taken until acquisition of the TOC analyzer described in this section. Accuracy of measurements will be taken into consideration due to the inability to confirm procedure of TOC measurements for select tests. More details of this matter will be evaluated within the results section.

Samples for TOC analysis was prepared in 40 mL vials that consist of a septum that can be punctured for injection. The sample vials can be arranged to the desired configuration with the sample conveyor. The conveyor sample layout is coordinated to match the data acquisition panel within the TOC TekLink software. The display for the sample scheduling interface used within the software that allows the user to select and configure the desired position of samples, number of sample replications, analysis method, and data output configuration can be found in Appendix B.

Table 3: Additional Lotix Components [60]

Hardware	Description
K bottle	compressed high purity air up to 70 MPa
Needle assembly	mount that secures pressurized needle and sample needle raised by needle elevator
Needle elevator	raises and lowers needle assembly using a pneumatic air cylinder. When lowered the sample and pressurized needle puncture vial cap. When raised above vial, sample conveyor can move sample out of position for rinse and allow next sample to move in place
Rinse station	Rinse Station: station below the sample position that allows DI water to be passed through the sample pathway loop prior to next sample analysis
10 L DI water reservoir	pressurized reservoir that contains DI water for rinse cycles
Pressure regulators	two used, one for system stabilization to maintain 200 mL/min @ 30-40 psi and the other as a step-down system for the DI reservoir to be maintained at 12 psi
Communication cables	Data transfer from Lotix to PC software

### 1.10.2 Gas Analyzer

Measurement for concentrations of effluent gas products was performed using a Horiba Model PG-250 Gas Analyzer [Appendix B]. The analyzer allows for simultaneous analyses of CO<sub>2</sub>, CO, O<sub>2</sub>, NO<sub>x</sub>, and SO<sub>2</sub> in flue gas samples. As previously mentioned, for SCWO processes, the gases observed are typically CO<sub>2</sub> and some small levels of NO<sub>x</sub> gases. At first, gas measurements for this study were taken by directly connecting the

collected effluent sample cylinder to the analyzer after the experiment. To optimize the gas analysis, the subcollection system was redesigned and reconfigured to allow for real-time measurements of gas effluent while the experiment was in operation. This optimization is beneficial for understanding the SCWO operating parameters' effect on the concentrations and amounts of combustion gases produced. The data collected from these gas samples also helped to relate the effects of gas production on the overall SCWO conversion efficiency.

### **1.11 Experimental Procedure**

The procedures for experiments were performed in a series of steps. These include solution preparation, pre-test configuration checks, experimental operation configuration, and sample collection. Descriptions of each step are presented below.

Solutions for testing were created using the EWW concentrate supplied by NASA Ames Research Center. Urea solutions were made in the lab manually using standard dilution techniques. EWW supply was kept in a refrigerator to keep the contents fresh. Solutions for testing were stored in a 2L reservoir to be supplied to the piston pump. Only 1000 mL solutions were made for test purposes. A keynote to mention is that the 1000 mL solutions were used entirely before a new batch was made. This means that although consecutive tests may have used the same solution, there were variations in sample shelf life between them. The effects of sample life will be discussed in the results section. Before the beginning of each test, the reactor is heated using a LabVIEW logic control mechanism at increments of  $\sim 100^{\circ}\text{C}$ . Heating continues until the "bulk fluid" temperature (TB), measured by a thermocouple aligned at the center of the reactor, reaches the appropriate target temperature. Target test temperatures for ersatz waste are between  $550^{\circ}\text{C}$  and  $610^{\circ}\text{C}$ ,

depending on the dilutions and ethanol additions. Line heaters for the air and "fuel" were activated to reach temperatures near the critical point of water (450°C) for the injection streams. After heating, the cell is filled with air to a nominal target pressure of 27.6 MPa. Once temperatures and pressures reach operating conditions, the airflow is initiated through the side port by entering the desired flow rate between ranges of 0.5 SLPM to 5.0 SLPM. Once the airflow is initiated, the piston pump can introduce the fuel flow. When the fuel flow initiates, the testing has officially begun, and sample collection can be commenced once near steady-state conditions have been achieved. The rates of flow for the reactant streams, as well as the fuel concentration, can affect the state of equilibrium of the reaction. To reach and maintain steady-state conditions, the heating supplied to the reactor can be manually adjusted to reach the target temperature. The sample collection sub-system uses two sample collection methods depending on whether the sample is vapor or liquid. Liquid samples are collected after the product stream is depressurized and cooled to ambient temperatures through a coiled heat exchanger and flow back up the pressure regulator. The condensed matter is then collected in a dump tank. Once cooled through the same process, the gas sample is collected by attaching a 50 ml sample cylinder to the outlet valve of the back pressure regulator. Towards the end of this project, a newly designed sample gas separator was created to filter out condensate from effluent gas as well as allow for an easier sample collected process. This apparatus can be observed in Appendix B.

### **1.12 Wastewater Characterization**

Earth-based and other urban impacts are not representative of the impacts of isolated and confined space crews with restricted human movement, regulated diets, and controlled sanitation product use [61,62]. Therefore, it is appropriate to utilize a synthetic

waste representative less characterized by human population-based wastewater for studies like these. Typical waste streams at these isolated space camps include gray wastewater mainly from toilet flush water and shower/sink water.

The EWW stream is a complex mixture of various organic and inorganic components. Compositions of this waste simulant were developed using similar recipe techniques used by Verostko et al. [62]. In this recipe, organic and inorganic simulants for the ersatz were derived through analysis of data received from an integrated WRS test at the Johnson Space Center for an early planetary base (EBP) stream and transit mission [62,63]. As previously mentioned, ethanol is the organic compound with the highest concentration. Additional contaminants and their concentrations are listed in Table 4. Organics can be attributed to urine and hygiene constituents like shaving cream, toothpaste, and body wash. Solid chemical inorganics are also attributed to hygiene and humidity condensate components. Chemical traces of laundry detergent were also used in the development and can be used to observe surfactants due to their foaming tendencies. Within the listed compounds, alcohols, siloxanes, and urea are of great interest due to their difficulties in being removed using other technologies like reverse osmosis and distillation [5].

Additionally, Table 5 presents the EWW chemical recipe used for the composition. The specific masses per 4 L of solution is presented in units of grams. As mentioned, acetic acid measured at 12.875 g of 4 L, is of most abundance of EWW in comparison to the other subsequent chemicals.

Table 4: Ersatz Wastewater Composition [5].

Liquid Chemicals	Solid Chemicals	
	Organic Concentrate	Inorganic Concentrate
Propylene Glycol	Benzoic Acid	Potassium Chloride
Ethanol	Caprolactam	Ammonium Bicarbonate
Acetone	Urea	Sodium Fluoride
2-(2-butoxyethoxy) Ethanol (DGME)		Potassium Iodide
N,N-Dymethylformide		
2-Ethoxyethanol		
1-Methyl-2-Pyrrolidinone		
2-Propanol		
1-Propanol		
4-Ethylmorpholine		
Formic Acid		
Lactic Acid		

Dimethoxydimethylsilane, an additional liquid concentrate, is a colorless fuming liquid with a fetid odor, and has the next highest amount of mass required for a 4 L solution of EWW. This chemical element along with the other additive liquid siloxanes are key qualitative factors used in determining effective conversion by analysis of odor and foaming tendencies for post-treated solutions.

Table 5: EWW Chemical Recipe Composition [5].

<b>Solid Chemicals</b>	<b>Amt. Req. in 4 L(g)</b>
Zinc (II) Acetate dihydrate	0.57
Nickel (III) Acetate tetrahydrate	0.2114
<b>Liquid Chemicals in Acetate Concentrate</b>	<b>Amt. Req. in 4 L(mL)</b>
Acetic Acid	12.875
<b>Liquid in Direct Addition Concentrate</b>	<b>Amt. Req. in 4 L(mL)</b>
Benzyl Alcohol	0.368
Diethylphthalate	0.121
Trimethyl Silanol	0.038
Benzothiazole	0.013
2-Ethyl-1-Hexanol	0.029
Decamethylcyclopentasiloxane (d5)	0.062
Dodecamethylcyclohexasiloxane (d6)	0.060
Octamethylcyclotetrasiloxane (d4)	0.061
Dimethoxydimethylsilane	2.106
<b>Solid Chemicals in Direct Addition Concentrate</b>	<b>Amt. Req. in 4 L(g)</b>
Calcium Sulfate	0.11551
Dimethyl Sulfone	0.01224
Hexamethylcyclotrisiloxane (d3)	0.06122
<b>Phosphate Addition</b>	<b>Amt. Req. in 60 L tank(g)</b>
Monobasic Potassium phosphate	0.05

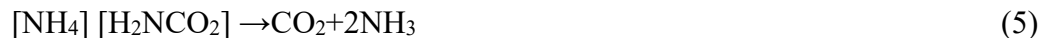
Experiments presented in this study were performed for undiluted concentrate, partially diluted with two parts of distilled water to one part concentrate (i.e., 1 liter of concentrate diluted to 3 liters), and 20 parts distilled water to one part concentrate. An important note is that the undiluted concentration of EWW is a marginal 40 times higher than the concentration typically observed on an ISS mission. The dilution water was pure deionized water with a standard of approximately 17 megaohm resistivity. Additionally,

these presented concentrations still result in much higher concentrations than the expected values aboard the ISS. Variations of concentrations for experiments guide understanding operating procedures for different organic content values and the implication of energy efficiencies based on the reactions they create. Dilutions for urea testing were created using 99.9% pure urea (supplied by Fisher Scientific) at 50,000 ppm of urea in distilled water. Co-fuel experiments performed with ethanol were performed by adding denatured ethanol solution at 5% wt. or 10% wt. of the various EWW and urea dilutions.

Urea, which is a component of the ersatz wastewater undergoes hydrolysis to form ammonium carbamate [4]:



this then undergoes a decomposition reaction to form carbon dioxide and ammonia:



Ammonium bicarbonate, which is a major component of the ersatz wastewater, also produces ammonia according to



As previously discussed, ammonia is the most refractory species associated with the breakdown of nitrogenous wastes, so it was necessary to understand its behaviors for testing of these two constituents.

### 1.13 Data Analysis

Experimental measurements and analysis for both EWW and urea were used to evaluate and assess the destruction efficiency through TOC removal, contaminant destruction, and reaction process. Temperature and pressures were recorded for each experiment to ensure and guarantee operation under supercritical conditions. Temperature

and pressure stability were observed to ensure steady-state isothermal and isobaric conditions for each run. Formulated results were presented at average temperatures and pressures of reaction during the collection phase. Measurements of gas effluents were also performed using the procedure previously described. Desired measurements and results for this work are as follows:

1. Qualitative observation of reaction effluent physical qualities (turbidity/ surfactant)
2. Observe organic contaminants in the product stream (using Raman spectroscopy)
3. TOC removal from reactants (EWW, Urea, Ethanol)
4. Measurements of effluent gas concentration (CO<sub>2</sub>, NO<sub>x</sub>)
5. Volumetric flowrates at desired operating conditions

#### 1.13.1 Calculated Parameters

TOC removal was measured and represents the conversion of the initial concentration in terms of destruction efficiency. In relation to equation 2, equation 7 was used by relating the initial organic concentration ( $TOC_i$ ) and final organic concentration after treatment ( $TOC_f$ ) at any value of residence time.

$$TOC\ Reduction\ \% = \left( \frac{TOC_i - TOC_f}{TOC_i} \right) \times 100\% \quad (7)$$

*Residence time* is the amount of time in which a fluid particle resides within a control volume and is calculated by dividing the amount of material within the reactor by the inflow or outflow of the system. Specifically, the total volumetric flow rates ( $(v_{H_2O}, v_{air})$ ) at the reactor inlet (supercritical conditions) are divided by the total reactor volume (67 mL). Volumetric flow rates for water and air were manually calculated separately using isobaric thermophysical properties gathered from the National Institute of

Standards and Technology (NIST) source at ambient room conditions and supercritical conditions upon entry of the reactor. Thermophysical property values were attained at each test's average bulk temperature and pressure values. The equation for residence time is shown below in equation 8.

$$T_r = \frac{62 \text{ mL}}{v_{EWW} + v_{air}} \quad (8)$$

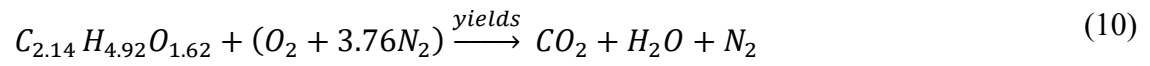
In addition to residence time, another parameter calculated is the stoichiometric equivalence distribution of the amount of oxidant to organic. This can be defined in equation 9 as:

$$\Phi = \frac{(fuel/air)_{actual}}{(fuel/air)_{stoich}} \quad (9)$$

This ratio ( $\Phi$ ) determines if the amount of oxidant supplied is sufficient for the supplied reactants. For standard combustion, if the value is 1, then the amount of oxidant is the exact amount needed. In this study, the observation of the amount of fuel relative to the stoichiometric oxygen is presented. If  $\Phi < 1$ , then the amount of air is more than the amount required per gram of fuel, and if  $\Phi > 1$ , this indicates “excess in fuel relative to stoichiometric air in the system. As mentioned earlier, for the SCWO process, a higher conversion success rate generally favors an excess supply of oxidant.

To calculate the fuel to air ratio in this project, the values of TOC ppm were used to determine the stoichiometric required air required. Chemical formulations for EWW, as in Table 5 but with more extensive detailed parameters, was provided by NASA ARC. A theoretical empirical formula was calculated using the weighted average of all organic material within the simulant. Equation 10 presents the unbalanced stoichiometric equation

with the generated chemical formula for ersatz with molecular counts consisting of mostly carbon, hydrogen, and oxygen.



Equivalence ratios were calculated considering complete combustion of the carbon present at each initial ppm concentration tested.

## RESULTS

Experimental results are presented in mainly two sections, one for EWW and the second for urea aqueous solutions. As previously mentioned, all experiments were performed at NASA GRC and within a span of about 6 months. The results presented will be divided into qualitative and quantitative categories to observe the success of conversion.

### 1.14 SCWO Conversion of Ersatz Wastewater

Major organic contaminants of ersatz waste include mostly ethanol (highest concentration), formic acid, acetone, acetic acid, and urea which is of most interest to NASA Ames Research Center due to its ammonia formation. Siloxanes are also present as surfactants within EWW and are of most interest to NASA Marshall Research Center due to their foaming characteristics. These contaminant compounds are particularly interesting for the SCWO project due to the difficulty of removal with other considerable technologies (i.e., reverse osmosis). For the experimental results described, the wastewater concentrations vary from two parts of deionized water to the one-part ersatz concentrate (2:1), (20:1), and undiluted. A total of 10 experiments were conducted using the EWW solution. A test matrix for the EWW tests is presented below in Table 6. The origin of these tests is documented starting with test 6. This number follows previous testing at NASA GRC. The table features test dates, identities, and desired operating parameters such as flow rates, fuel concentrations, and operating temperatures and pressures. A couple of tests (Test 6 and Test 7) were performed as preliminary experiments for this study and served to ensure proper experimental procedure and overall performance protocol. A critical note regarding this Table is that the oxidizer flow percentage values relate to the maximum allowable 5 SLPM for oxidizer flow. The operating temperatures are the initial set points

for the experiment, but the final temperatures varied during the collection phase. Similarly, the pressure values within the matrix represent the desired nominal initial pressure for isobaric conditions, but actual pressures within the presented results are slightly varied. As previously mentioned, for SCWO processes, pressure does not affect conversion efficiency unless conditions are subcritical, but higher temperatures can compensate.

Table 6: Test Matrix for EWW Experiments

Date	TEST #	Oxidizer flow rate	Fuel (C)/ flow rate (mL/min)	Set Point (°C)	Cell Pressure (psi)
6/23/2022	6	15% (.75 SLPM)	(2:1)/2.5	590	3900
6/30/2022	7	15%. (75 SLPM)	(2:1)/2.5	605	3900
7/5/2022	8	20% (1 SLPM)	(2:1)/3.0	610	3900
7/7/2022	9	20% (1 SLPM)	(2:1)/4.0	550	3900
7/12/2022	10	20% (1 SLPM)	(20:1)/4.0	590	3900
8/2/2022	11	15% (.75 SLPM)	(20:1) + 5% ethanol/4.0	610	3900
8/11/2022	12	25% (1.25 SPM)	(2:1) + 5% ethanol/4.0	550	3900
8/17/2022	13	40% (2 SLPM)	(2:1) + 5% ethanol/2.0	610	3900
8/23/2022	14	50% (2.5SLPM)	(2:1) + 5% ethanol/3.0	610	3900
10/27/2022	15	40% (2 SLPM)	(undiluted)/ 3.0	550	3900

#### 1.14.1 Qualitative Results for EWW: pH, Turbidity and Conductivity

Visual inspection of the treated and untreated water shows a distinct difference in turbidity (clarity), performed after each experiment to compare the before and after treated

samples. Figure 13 (a) presents images of untreated and treated water by SCWO testing to observe the change in turbidity. Additionally, by shaking the vial to induce foaming caused by the siloxanes, a comparison can be made by observing the presence and absence of the surfactants at the water's meniscus in Figure 14 (b).

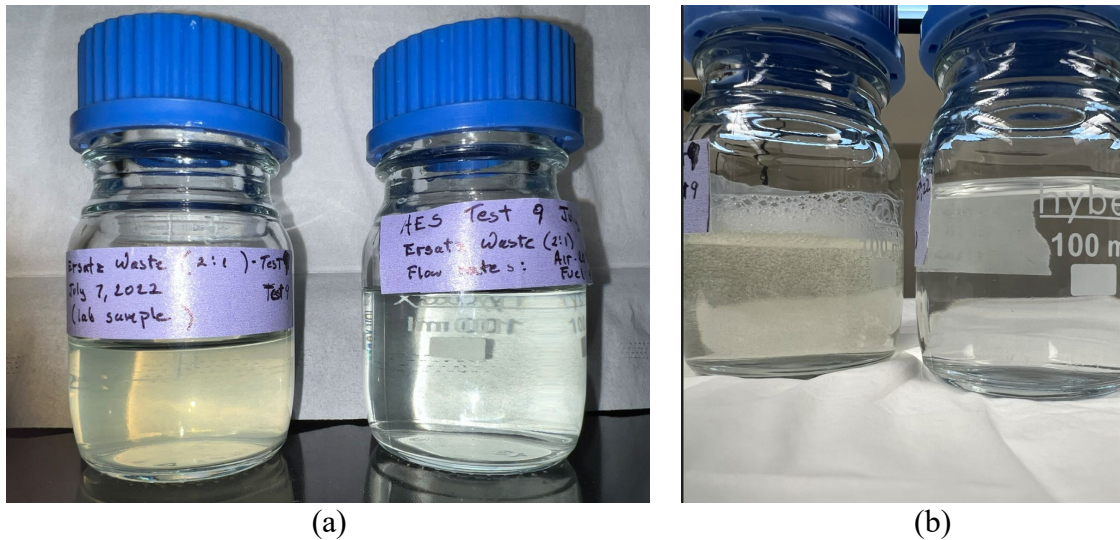


Figure 13: Images of untreated and treated water by SCWO testing.

EWW solution has physical properties comparable to urine, with other sewage like qualities. Along with observing the surfactants, an odor assessment was performed for the untreated and treated solutions. The pre-treatment solution had a distinctly pungent odor and was easily identifiable when evaluated. So, the lack of this odor for the after-treatment samples helped to indicate a level of conversion, at least initial assessment. Table 7 shows the pH and turbidity values for the 10 tests performed on EWW. Note that the tests with an asterisk indicate a freshly made batch. Colors are provided to show varying values of pH. The subscripts "a" and "b" refer to after and before treatment, respectively. This will be the

nomenclature used throughout this section. Additional images of untreated and treated samples can be viewed in Appendix A. Observations of pH changes will be examined.

Table 7: EWW Results for pH and Turbidity

Test #	Turbidity	pH
6b	9.99	9.15
6a	3.55	3.16
7b	13.9	9.14
7a	2	2.85
8b*	9.99	7.67
8a	3.56	7.72
9b	18.3	8.13
9a	5.4	8.13
10b*	3.1	9.05
10a	2.1	8.25
11b	4.14	8.82
11a	26.3	7.2
12b*	3.7	6.91
12a	2.31	4.89
13b	4.67	7.37
13a	4.85	3.24
14b	305	8.12
14a	2.99	2.45
15b*	62.1	9.06
15a	2.22	3.02

To correlate pH measurements and compare post treated samples to the likeness of water, conductivity measurements were also taken. Figure 14 presents the conductivity results for all EWW tests. The data is presented with appropriate test identities, EWW concentrations and their relative acid and base characteristics.

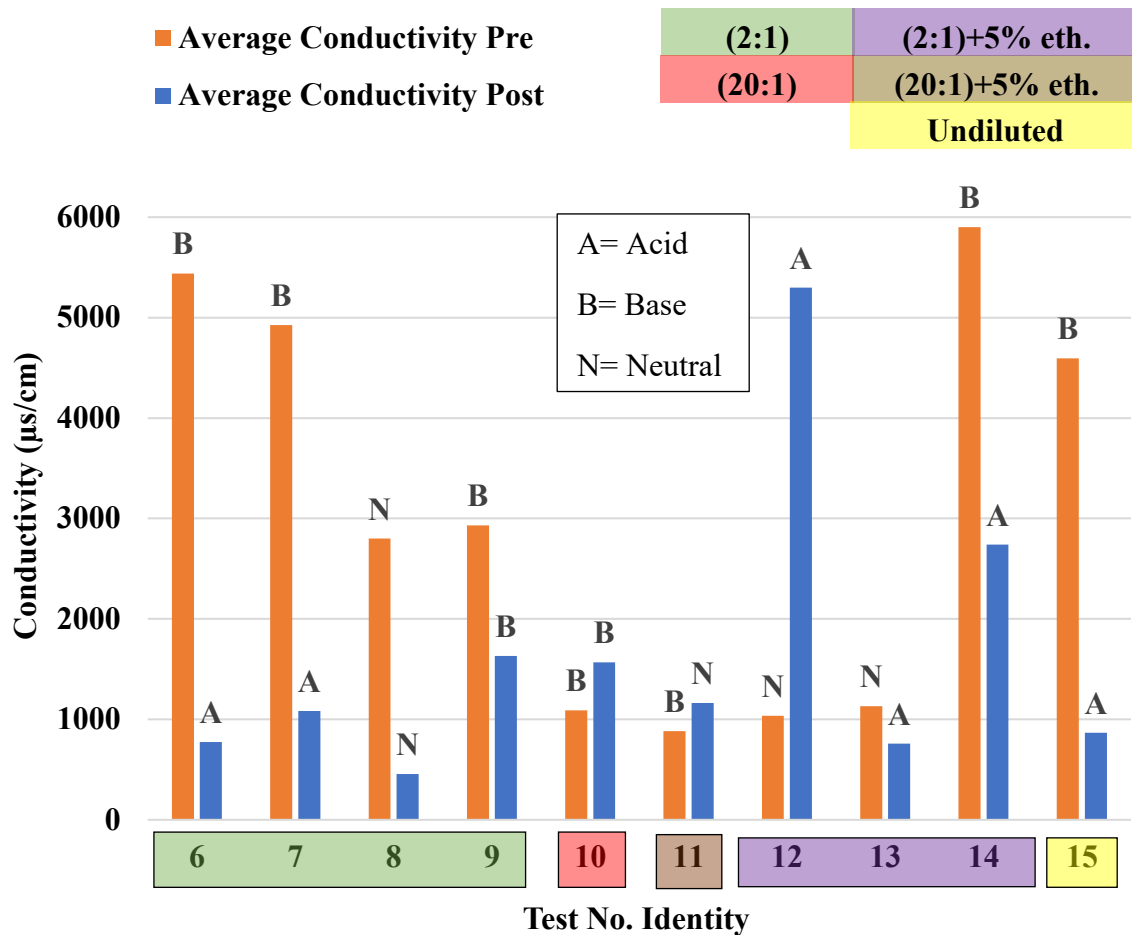


Figure 14: Conductivity measurements for EWW tests

Conductivity results in the study show that 70% of the tests showed a reduction of conductivity from pretreated to post treated solutions. Additionally, 60% of tests resulted in a transition to weak acid aftertreatment. The indication of reduced conductivity with lower pH levels may suggest leftover hydrocarbons as well as presence total dissolved solids (TDS) like urea, salts, and other inorganic materials. The effect of initial dilution concentration also shows a relative trend. Both (20:1) and (20:1) +5 % ethanol conductivity

results show the most resistivity to conductivity and pH change compared to others, most likely due to higher dilutions favoring pure water.

### **1.15 EWW Quantitative Results**

The results presented in this section include measurements for Raman spectroscopy, TOC analysis and effluent gas products. Observations of conversion efficiency will be correlated with patterns of residence time, waste concentration, cell internal temperature and reaction stoichiometry.

#### **1.15.1 EWW TOC Results**

In general, the TOC results of the EWW tests performed are presented first to help guide the understanding of the rest of the presented data, especially the Raman data. As discussed in Chapter 3, analysis of TOC was also performed using an analyzer that uses a catalytic combustion procedure, and a non-dispersive infrared (NDIR) detector to accurately measure the carbon content of aqueous solution down to the level of ppb. For TOC of ISS potable water, the current go/no-go decision on water potability is 3,000  $\mu\text{g/L}$  for WPA-supplied water and 20,000  $\mu\text{g/L}$  for Russian Segment Water as determined by NASA's spacecraft water exposure guidelines and TOC procedures [64, 65]. TOC analyzers primarily convert (oxidize) all organic compounds in the water sample to carbon dioxide gas ( $\text{CO}_2$ ). Afterward, the analyzer separates the  $\text{CO}_2$  and quantifies the amount collected in units of ppm ( $\mu\text{g/L}$ ). Overall, TOC results presented in Table 8 were obtained from two sources, NASA GRC and NASA ARC.

Two analysis modes used at NASA GRC were TC-IC and TOC. Values of IC indicate the presence of precipitated salts and chlorides as well as other inorganics like ammonium bicarbonate. TC-IC results can be found in Appendix A. Part of the TOC

analysis for the EWW test was performed by the supporting center NASA ARC. Overall results of TOC measurements performed at NASA ARC are indicated by samples in red font.

Table 8: Overall Results for EWW TOC Analysis

TOC (ppm)				
C	9	TC	% RD	
(2:1)	6b	56.8	94.54%	
	6a	3.1		
	7b	139.8	99%	
	7a	0		
	8b	270.1	99.60%	
	8a	1.09		
	9b	591	67.50%	
	9a	192.3		
	(20:1)	10b	132	-25.75%
		10a	166	
(20:1) +5% eth.	11b	12575	97.65%	
	11a	295.2		
(2:1) + 5% ethanol	12b	23768.5	82.01%	
	12a	4275.8		
	13b	24310	99.92%	
	13a	17.2		
	14b	22732.9	99.97%	
	14a	6.7		
EWW	15b	1552.7	99.86%	
	15a	2.1		

Measurements at NASA GRC were taken in 3-5 replicates for accuracy, and the average TOC of the replicates is presented in ppm. Outlier tests for conversion of TOC presented are for Test 9 (67.50%) and Test 10 (-25.75%). Due to the inability to confirm the accuracy of measurement for these tests, the TOC value can be neglected. Instead, a comparison of the success of the test was observed through the relationship between the respective fuel/air equivalents and other operating parameters such as solution concentration, bulk temperature, and residence time.

### **1.15.2 Raman Results for EWW**

The bulk of the diagnostic results for this project were obtained with the use of Raman spectrograph analysis methods to observe the characterization of organic material of wastewater solutions. Performances of analysis included the comparisons of Raman scatter profiles for pre-treated and post-treated solutions. Raman results are related to operating conditions such as solution concentration, flow rate and temperature. Additionally, a comparison of percent TOC reduction and pH was done to indicate the overall conversion success of the EWW solution.

#### **1.15.2.1 Raman Results for Preliminary Tests**

Pure water was the baseline comparison used for the SCWO tests and served to quantitatively express the extent of conversion for the performed tests. As previously mentioned, Tests 6 and 7 were preliminary experiments performed to revamp and confirm proper operating procedures for this study. Note that for the Raman results, both spectra in the Raman shift ( $\text{cm}^{-1}$ ) range were compared to the pure water spectrum. Figure 15 shows raw spectral data without normalization, contrasting the relative difference in overall intensity between the treated and untreated water solutions for Tests 6 and 7. Figure 16

shows the normalized spectra of the same recorded signals, contrasting profiles of the Raman spectra in greater detail.

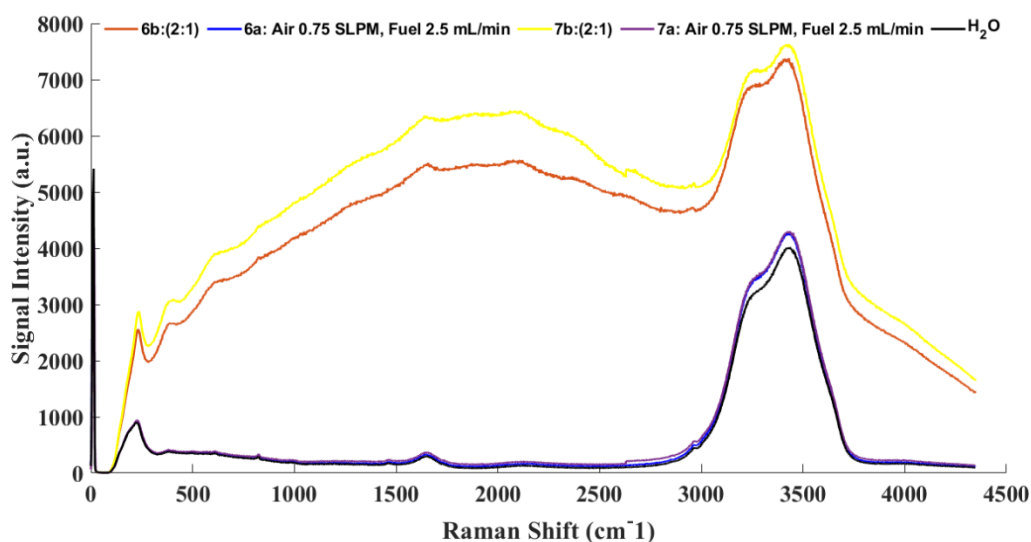


Figure 15: Raman shifts after SCWO conversion with comparisons to pure water

The operating conditions for these tests were identical, with an internal cell temperature of approximately 615°C, a difference of only 7°C. Residence times were similar for both tests, approximately 90 seconds  $\pm$  1 second. Typically, compounds are represented and identified by assigned and designated wavenumbers (characteristic peaks) in the Raman spectrum. Owing to the complex range of the contaminants present in the EWW, individual spectra of specific constituents are largely convoluted into a broadband spectrum over the whole range of measured Raman shift and thus identification of such individual spectra was difficult except for the distinct spectral signature by pure water.

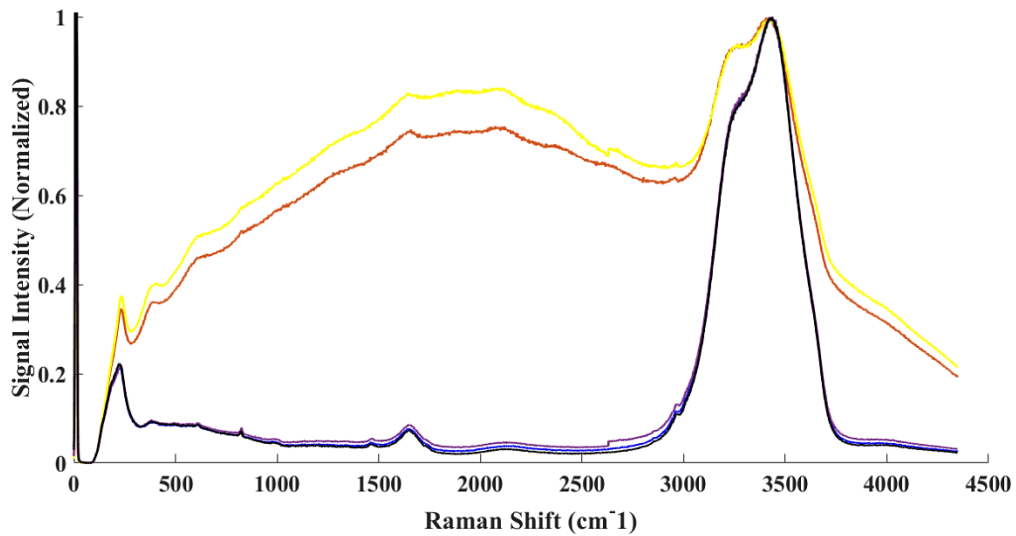


Figure 16: Normalized Raman shifts after SCWO conversion for Tests 6 and 7.

The Raman scan data from these tests guide and express the overall effectiveness of the SCWO conversion by observing changes in the profile. For these preliminary tests, what can be suggested is that conversion success was easily achievable due to the low amount of TOC presented for the pretreated solution (~50 to ~100 ppm). The stoichiometric required air for these tests was only a miniscule .0013 SLPM. Actual air supply for this test was relatively low in terms of maximum allowable flow within the system with a value of 0.75 SLPM. In comparison to the required air, the actual supplied air was ~575 times more than the amount needed. The equivalence ratio of the two preliminary tests was .0017, indicating that the excess fuel is very low. Within the Raman spectra, the reconstruction and elongation of the O-H peak after treatment are caused by stronger vibrational intensities from the addition of hydrogen molecules [65]. Furthermore, these additional hydrogen atoms indicate the formation of water molecules hence suggesting high conversion efficiency under these conditions. The solutions used for these

tests were exposed to lab conditions for approximately 3 months. The overall dip in the broadband spectra of these two tests, and their closeness to the pure water curve, indicates complete conversion of the influent solutions. Most of the spectral broadband before 3000  $\text{cm}^{-1}$  is attributed to excitations from an abundance of weak acids, salts, hydrocarbons, and other nitrogenous species. TOC measurements for the pretreated solution for Test 6 had an approximate 57 ppm and resulted in only about 3 ppm of TOC post treatment. Test 7 was the same test and showed similar results with essentially 99% conversion of all TOC levels. Relating the amount of TC to IC with the sample shelf life and the immense variation in the before and after treated Raman scan suggests that there was probable break down of carbon content over time, thus presenting a very miniscule amount of carbon within the test solution during the SCWO process for these tests. The lower carbon in the fuel further leads to the conclusion that less is needed for a stoichiometric air supply. Turbidity values in the form of suspended solids and additional scattering within Raman are also supported from the observed higher IC values relative to the TC content.

#### **1.15.2.2 Raman Results for Various EWW Solutions**

Figure 17 shows the normalized Raman scans of Test 8 and Test 9, representing the solution concentration (2:1). Test 8 was performed using a freshly made batch solution. Test 9 was performed using the same batch approximately two days later. These tests' average bulk internal temperatures were 632°C and 586°C, respectively. Both tests were subjected to the airflow of 1 SLPM, and fuel flow rates differed by 1 mL/min. Residence times with values of about 67s and 58s, respectively.

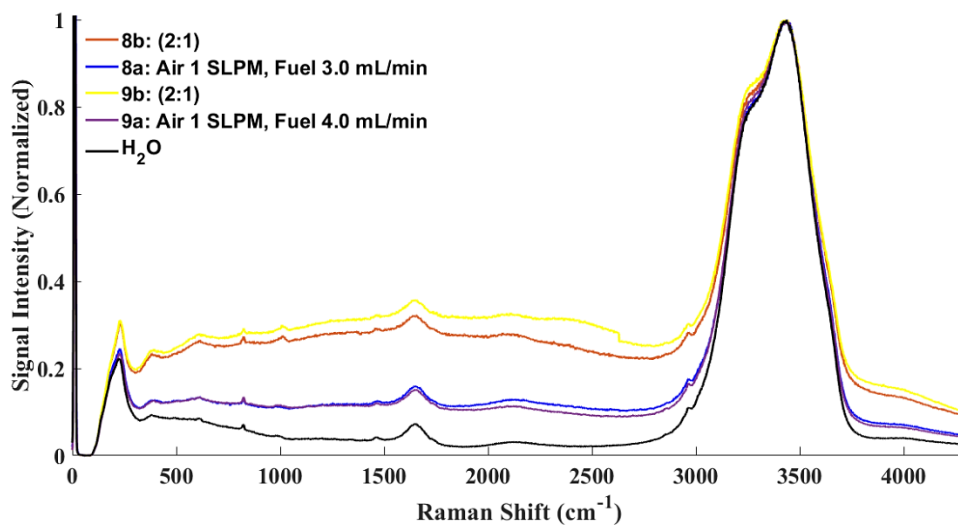


Figure 17: Normalized Raman shift comparisons to pure water and untreated EWW (2:1) for Test 8 and 9.

Raman scattering for these tests had a lower initial spectral background for the pretreatment solution compared to the preliminary tests. TOC content for Test 8 solution was approximately 270 ppm compared to the "stale" solution in the pretests, which featured an approximate 57 ppm of TOC. Note that although Test 8 was performed with a new batch, TOC measurements were not immediately taken post-treatment. In theory, the actual TOC for this test would be closer to 517 ppm (.517 g/l) based on undiluted ppm of ~1550 ppm. Although sample freshness is varying, the overall value of initial TOC is still very small. Hence, the availability of stubborn refractory intermediates can affect conversion rates and efficiency.

At first glance, both tests feature a decrease in spectral background post-treatment. Additionally, within the two days of sample shelf life, there was a measurable increase in scatter intensity between pretreated solutions. The post-treated Raman results suggest that the conversion efficiency for both tests is similar. Test 8 presents 99% carbon conversion,

and although the accuracy of TOC measurement for Test 9 is inconclusive, theoretically the results should also replicate 99% conversion. The theoretical air stoichiometric requirement for Tests 8 and 9 is .014 SLPM and .02 SLPM, respectively. Since the actual supply air for both tests were 1 SLPM, there was overventilation in both tests, indicating nearly 100% carbon conversion. Additional Raman scattering for post-processing is presumed to be residual precipitated salts or hydrocarbons. Another suggestion for remaining scatter could be the presence of urea, due to the need for higher reactor temperatures for complete conversion.

Previous studies conducted by Mylapilli et al. and Oe et al. have suggested that alcohols can increase the generation of free radicals (H, OH, HO, and NO<sub>2</sub>), which can react with organic intermediates that can produce gases of different compositions relying on operating conditions of SCWO [39, 40]. As mentioned, ethanol can also be used to enhance the internal temperature of the reactant while avoiding increasing the temperature of the reactor wall. Maximizing the reaction temperature for the EWW simulant is desired due to its low initial organic content. Additionally, the formation of additional free radicals and oxidative tension from the ethanol also helps to achieve higher reaction rates in a shorter period. For this reason, additional tests with EWW with 5% Wt. ethanol of the total solution were performed. Figure 18 presents a comparison of two different EWW mixtures.

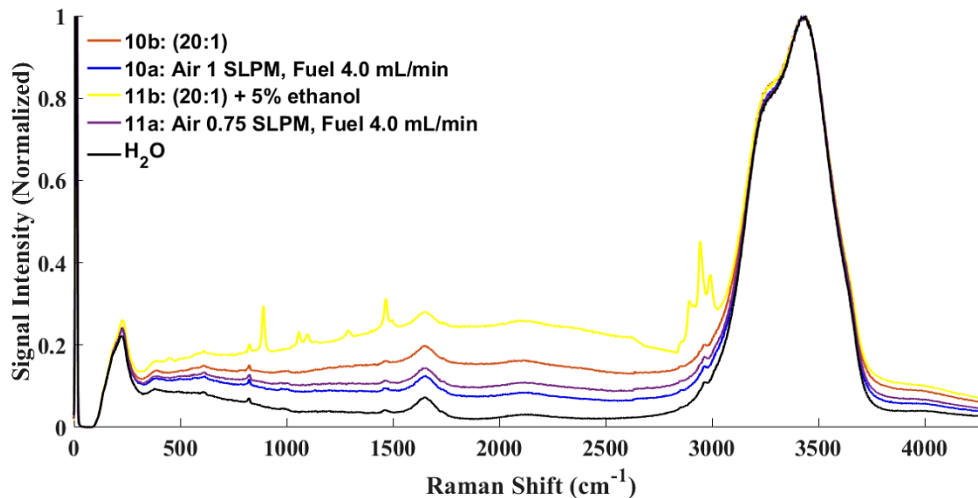


Figure 18: Normalized Raman shift comparisons for Test 10 and Test 11.

First, Test 10 represents a (20:1) diluted EWW solution treated with conditions of 1 SLPM air and 4.0 mL/min "fuel." As an introduction for EWW solutions with 5% ethanol, Test 11 was performed using a (20:1) dilution with 5% Wt. ethanol at operating conditions of 0.75 SLPM air with 4.0 mL/min "fuel." These two tests also serve to present a wastewater dilution that is closer to what one would expect to observe on an ISS mission.

Test 10 had a very small pretreatment TOC level of about 132 ppm or 0.132 g/L. When adding ethanol as a co-fuel, TOC values increase exponentially. For test 11, at (20:1) + 5% Wt. ethanol, its initial TOC count was 12575 ppm. Increasing the carbon content within the influent helps to drive the reaction process more efficiently, especially for higher dilutions. For reference, the solution for Test 11 was created using the leftover solution from Test 10 by adding approximately 40 mL of denatured ethanol to 750 mL. Ethanol's Raman scattering is identifiable around 2900  $\text{cm}^{-1}$ , shown above as mountain peaks representing symmetric and asymmetric stretching of methyl groups ( $\text{CH}_2$ ,  $\text{CH}_3$ ) [66].

Additional methyl stretching can occur around  $1500\text{ cm}^{-1}$ , and C-O and C-C bond stretching modes appear at lower frequencies. The average internal bulk temperature for Test 11 was about  $20^{\circ}\text{C}$  higher than for Test 10. This variance may result from adding ethanol, but these tests' initial set point temperatures were also  $20^{\circ}\text{C}$  apart, so this idea is a speculation. The calculated residence time for these tests was the same, approximately 54 seconds. Although Test 11 was subjected to a lower oxidizer input, due to the higher bulk temperature during mixing, the difference in thermophysical properties (density) at the higher temperature overcompensated the air supply, thus allowing identical residence times. Using an additional co-fuel or catalyst requires operating conditions that allow for the conversion of the additive and the substrate accompanying it. In (20:1) + 5% ethanol solution, most of the carbon content is expressed as ethanol.

Observing the TOC results, Test 10's results, obtained at NASA ARC, are not what was to be predicted which observed 25% more TOC post treatment. Reasoning for this is that the initial TOC including inorganics was too small to be accurately detected. Raman scattering for test 10 supports efficient conversion with reduced spectral background and an equivalence ratio of 0.003. Test 11, also run with excess air, had a 98% reduction in TOC at an equivalence ratio of 0.87. Test 11 could have achieved closer to near 100% conversion if the amount of excess fuel to air was a little less. Results from Tests 10 and 11 show that near complete conversion can be achieved with even the lowest of initial carbon concentrations.

To observe the effects of using ethanol as a co-fuel for higher initial carbon solutions, additional SCWO tests were performed using (2:1) + 5% Wt. ethanol solutions. Figure 19 presents Raman results from Tests 12,13 and 14 performed at (2:1) dilution and

5% Wt. ethanol. All three tests had an average internal cell temperature of about 610°C with residence times of 54s, 73s, and 54s, respectively. Test 12 was performed using a freshly made batch solution, and the progression of these tests was performed six days apart using the same batch supply. An interesting observation was made between the values of TOC between the three tests. Initial TOC was measured for the fresh batch at approximately 24,000 ppm. TOC for Test 13 featured a measurable increase in TOC within six days of subjection to lab conditions. Also, the measured TOC for Test 14 was lower than Test 12 at approximately 23,000 ppm. This suggests that within the 12 days of these tests, there was a slight decrease in TOC across the 12 days of using this batch solution.

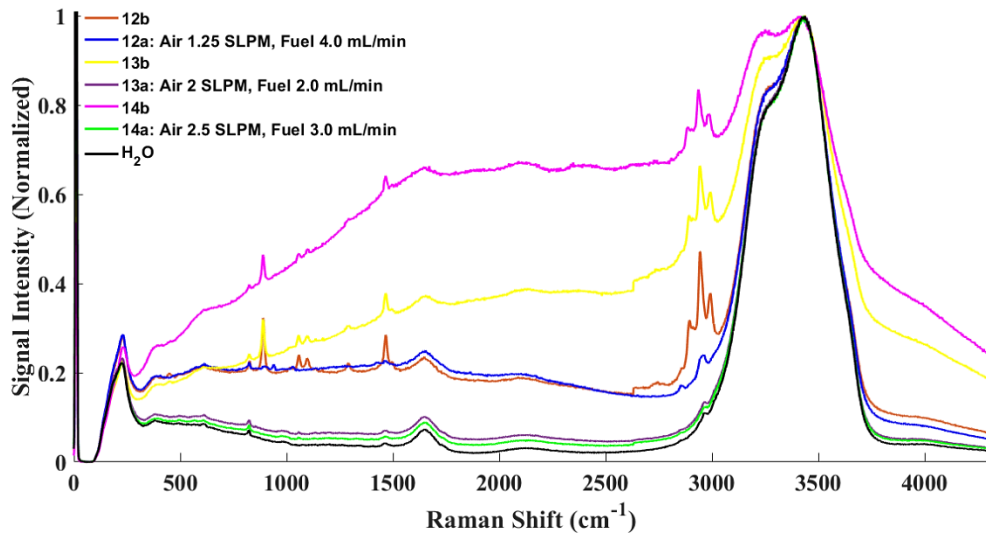


Figure 19: Normalized Raman shift comparisons to pure water and untreated EWW for (2:1) + 5% wt. ethanol.

The pH transitions were from weak bases to weak acids, just like the pH trends from the first two preliminary tests. Sample shelf life is characterized by observing the

increase in Raman intensity between these test runs. Characteristics of sample shelf-life are expressed through observation of increasing Raman intensity between the progression of these tests. The increase in the spectral broadband for the pretreated solutions suggests further breakdown and generation of organic material-like characteristics of the pretreated solutions for the preliminary tests 6 and 7. Each of these tests successfully reduced the presence of ethanol, but the overall difference is observed in the conversion of EWW. Test 12, at a lower oxidizer flow of 1.25 SLPM and a higher fuel flow rate (4 mL/min), experienced a reaction quenched through an inadequate equivalence ratio of excess fuel at an approximate value of 1. This equivalence ratio shows complete combustion of ethanol, which can be compared directly within the Raman scan and TOC results of only 82% of all TOC. The proceeding tests, Tests 13 and 14, operated at higher oxidizer flows of 2 SLPM and 2.5 SLPM air and lower fuel flow at 2 mL/min and 3 mL/min fuel, were able to successfully sustain good energetics for effective conversion from a more significant presence of air in excess. The equivalence ratios for these two tests were .39 and .32, respectively. The importance of these ratios further supports the stoichiometric conditions favoring air excess in the SCWO process.

The final EWW test, Test 15, was performed using a fresh batch of undiluted concentrate. As previously mentioned, the undiluted solution is approximately 40 times the typical waste concentrate observed on an ISS mission. This test was performed without the use of a co-fuel additive. Figure 20 shows a comparison of the normalized Raman scans for Test 15, and the undiluted untreated solution compared to post-treated and pure water spectra. The average bulk temperature for this test was 612°C with flow rates of 40% air (2 SLPM) and fuel at 3.0 mL/min. Although this was the only representative test for an

undiluted EWW solution, the Raman results favored similar trends to the ethanol tests. The higher concentration of TOC presented in the pretreated solution helped to improve reaction initiation in the presence of a sufficient oxidizer supply and temperature. The equivalence ratio for this test was .02, indicating extreme excess in air per gram of fuel.

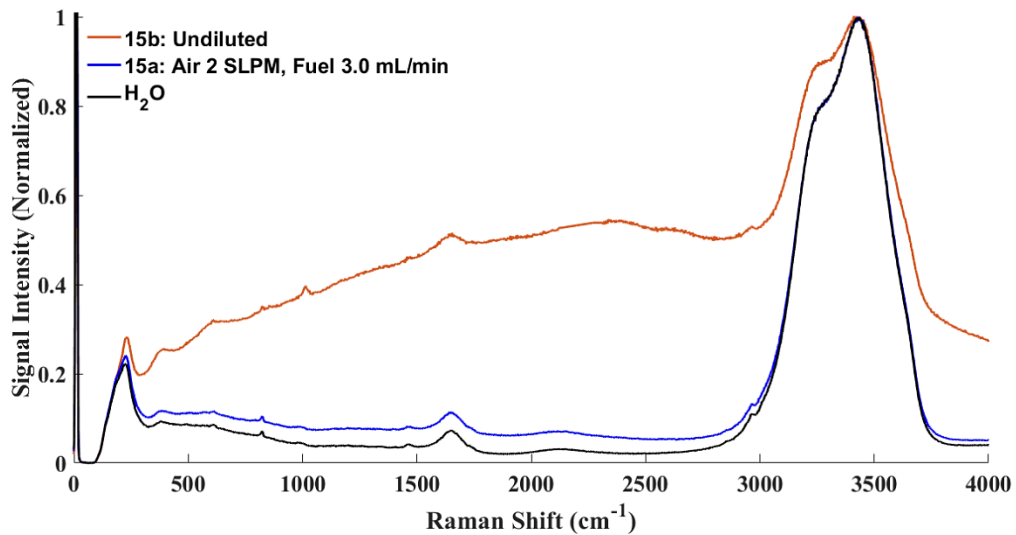


Figure 20: Normalized Raman shift comparisons to pure water and untreated undiluted EWW for Test.

Additionally, compared to the ethanol-treated tests, pH values trended downward with a transition from a weak base to a weak acid. Test 15's pretreated solution also presents similar TOC trends to the preliminary tests when measured in TC minus IC mode. IC to TC was almost double, with values of 2531 ppm IC to 1638 ppm of TC. With a 99% conversion of all TOC, the characteristics of the weak acidity presented by pH may be attributed to the number of inorganic salts redissolved into the post-treated solution after

reaching ambient conditions. Raman scans for all individual EWW tests can be observed in Appendix A.

### 1.16 Observation of Residence Time

As previously discussed, SCWO reaction kinetics are pseudo first order regarding waste concentration. Therefore, tubular reactors tend to be favorable since plug flow reactors can achieve high conversions in short residence times [5]. The values for residence time were calculated at average internal bulk temperatures and pressures. Residence time of the wastewater/air flow in the reactor varies with their flow rates but is computed within the order of tens of seconds for the flow rates used. Density is the relative thermophysical property needed for residence time calculations. Figure 21 presents the overall relation of TOC reduction percentage vs. residence time for all EWW tests.

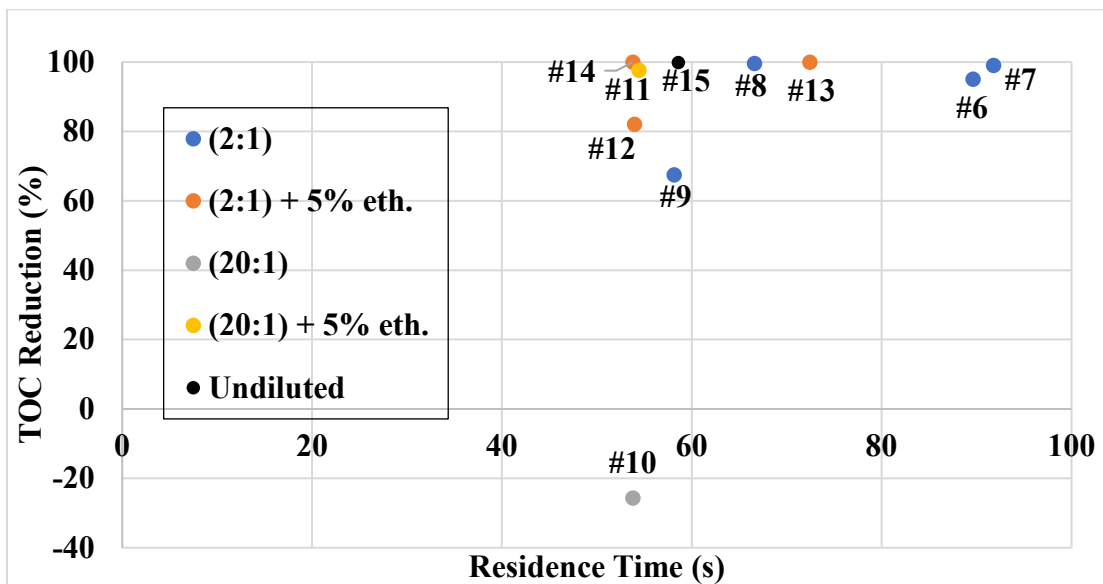


Figure 21: TOC Reduction vs. Residence Time for EWW SCWO Tests

In this study, all tests were performed within residence times of approximately 54s to 92s. The results suggest that a higher success of TOC reduction of 80% or higher could be achieved for all concentration types with and without addition of ethanol. As previously mentioned, Tests 7, 9, 10, and 11 TOC results were inconclusive, but from observing trends of the similar tests observed in this Figure, it has been concluded that all tests were able to achieve near 100% carbon conversion since they operated with equivalence ratios that favored more than adequate amounts of excess of air. More discussion of the measured TOC is discussed in the equivalence ratio results.

### **1.17 Influence of Operating Temperature**

Reaction temperature is another main operating parameter affecting conversion efficiency. Increasing the reaction temperature can directly increase the reaction efficiency and shorten the residence time [16]. Although complete oxidation is dependent on all operating parameters, the reaction temperature can limit the success of conversion of wastewater characteristics requiring specific operating temperatures. This is especially observed for nitrogen compounds, which require higher temperatures to convert to  $N_2$  gas. Figure 22 presents test comparisons of TOC reduction as a function of temperature.

Additionally, the data set is presented in groups of residence times that were less than 60s and more than 60s. In this data set, a conclusion is that most of the experiments were performed at internal bulk temperatures in the range of  $\sim 610^\circ\text{C}$  to  $\sim 680^\circ\text{C}$ . Additionally, in this temperature range, all tests that had residence time more than 60s also had near complete conversion of all organic material. As previously mentioned, TOC results for tests 7, 9, 10, and 11 were skewed, but they are assumed to have achieved similar conversion success.

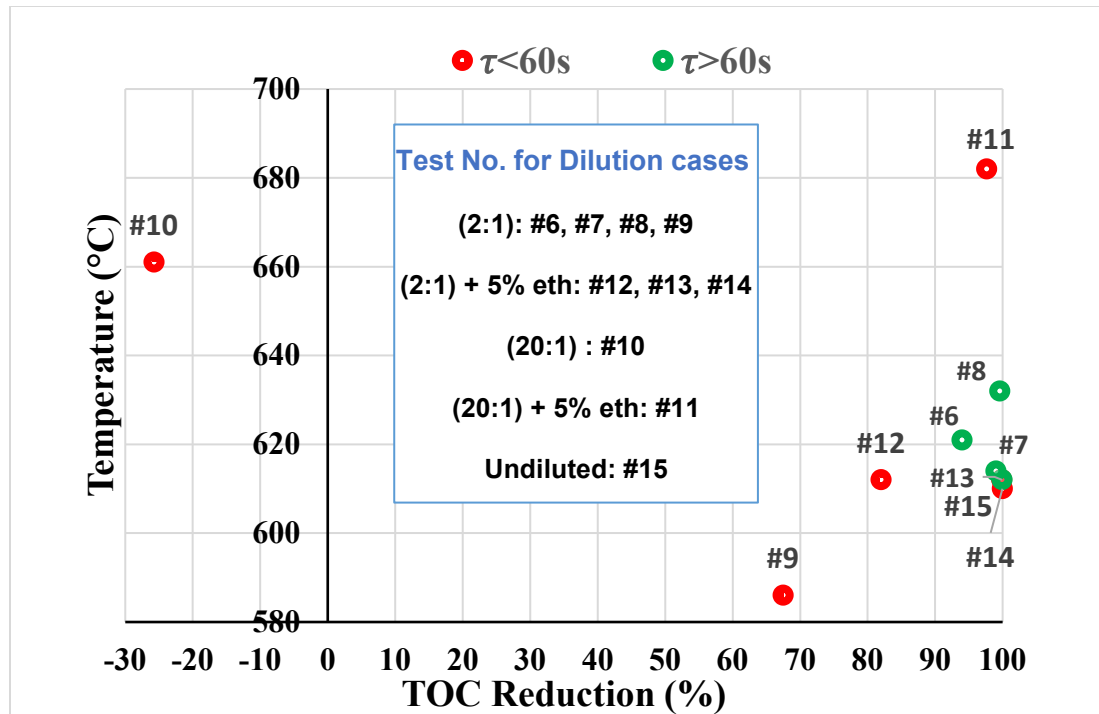


Figure 22: Influence of operating temperatures on residence time for EWW TOC success.

A fascinating observation within the tests at residence more than 60s, is the success of test 6 and 7. As discussed, tests 6 and 7 were preliminary tests performed with identical air/fuel flow rates of 0.75 SLPM air and 2.5 mL/min fuel with “stale” EWW solution. The “stale solution, which was likely composed of “organically prepped” reaction kinetics, may have caused the reaction process to advance quicker and easier, thus allowing success of TOC reduction.

The overall results for these tests are in accordance with other works that observed that TOC removal was enhanced by increasing temperature and that temperature is the most influential parameter for oxidation processes. [15,16].

## **1.18 Observation of Equivalence Ratio**

This section presents the results of equivalence ratio by three methods of calculation. Equivalency ratios were calculated in relation to the complete stoichiometric combustion of carbon. Uncertainties for TOC measurements included delay of measurement, uncontrolled pre-test conditions and uncontrolled time settings of lab measurements. Therefore, ratio calculations were performed separately for GRC, ARC, and theoretical inference. The impact of uncontrolled time lapses between refrigeration and testing as well as the difference in analysis equipment (i.e., TOC analysis) is unknown, therefore instead of comparing the measurements as they are, equivalence ratios will be presented separately for each case.

### **1.18.1 EWW Equivalence Ratios: NASA GRC**

Figure 23 presents TOC reduction in relation to equivalence ratios for SCWO tests performed at NASA GRC. TOC analysis at NASA GRC were taken for the following tests: 6,8,12,13,14,15. Since TOC analysis for the tests presented were taken at a much later time than post treatment, TOC values were much lower than expected. Regardless of uncontrolled parameters related to measurement time, 5 out of the 6 SCWO tests presented were able to achieve near 100% TOC reduction at equivalence ratios with high excess in air values, independent of initial concentration and solution type.

Test 12 was the only exception and is in direct relation to the Raman measurements in which only 82% of organic material was converted consisting of only ethanol. The stoichiometric air required for this test was approximately 1.28 SLPM, whereas the experiment was performed using 1.25 SLPM. These results correlate with the complete combustion of ethanol with an equivalence ratio of approximately 1.04. Therefore, to

improve this test, an equivalence ratio of less than 1 would favor increased conversion of the leftover organic material.

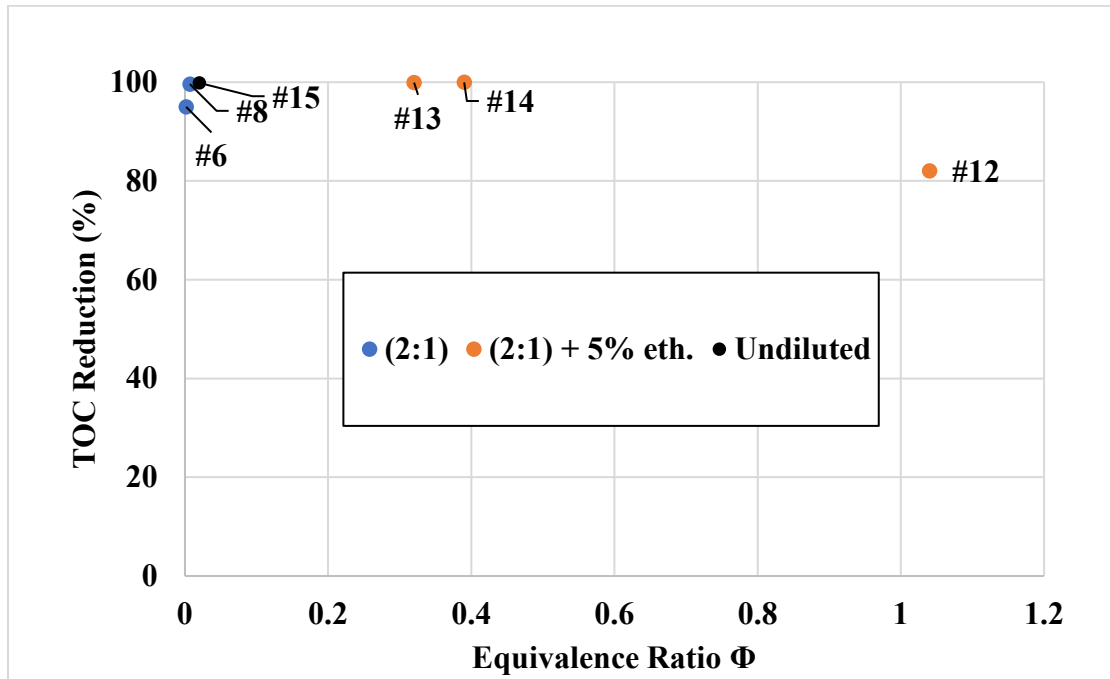


Figure 23: TOC vs. equivalence ratios for EWW SCWO tests at NASA GRC.

### 1.18.2 EWW Equivalency Ratios: NASA ARC

TOC analysis for the remaining tests: 7, 9, 10, and 11, were performed at NASA ARC. Figure 24 presents TOC reduction in relation to equivalence ratios for SCWO tests performed at NASA ARC. Calculated equivalency ratios in this data set present unexpected trends due to uncertainty of TOC values. Tests 7 and 11 follow accurate trends for equivalency ratio at their given post-treated TOC values, but Tests 9 and 10 do not. When observing the calculated flow equivalencies, both tests are expected to achieve near 100% carbon combustion. This is especially true for Test 10 which had an initial TOC of only 132 ppm. It has been suggested that the initial TOC content was too low for the effective

analysis of this test in terms of instrument detection capabilities at NASA ARC. Additionally, Test 9 should have also expected near 100% conversion success at the given flow equivalency. Though there was an inability to confirm the accuracy of the TOC measurements provided by NASA ARC, observation of trends suggests that these tests were also able to achieve successful carbon conversion.

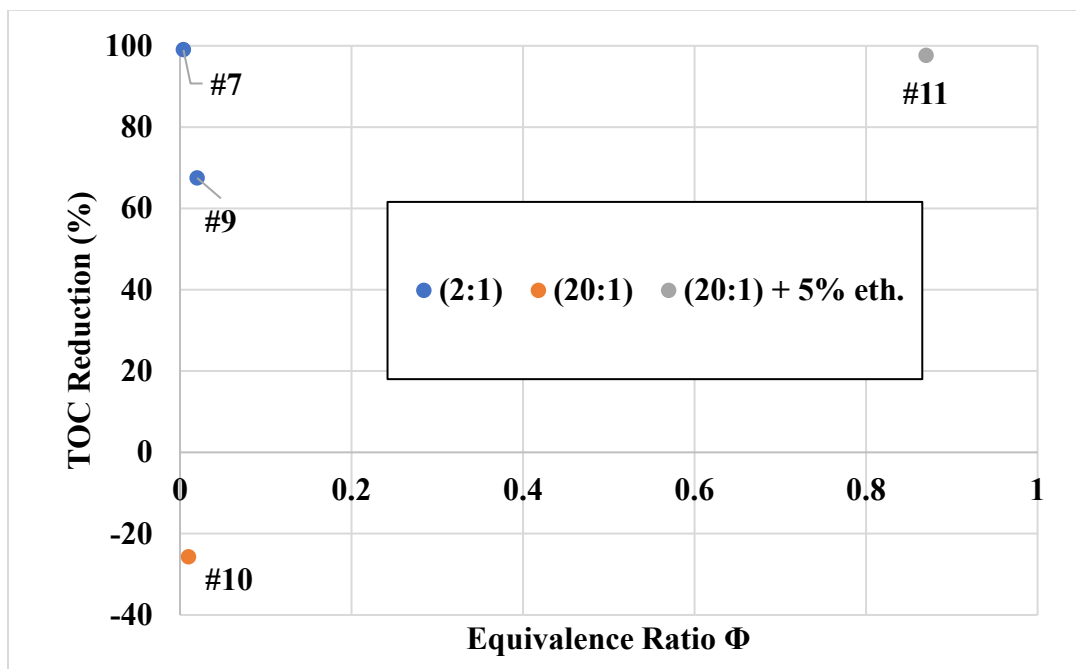


Figure 24: TOC vs. equivalence ratios for EWW SCWO tests at NASA ARC.

### 1.18.3 EWW Theoretical Equivalency Ratios

To provide a better understanding of the conversion tendencies related to flow equivalency independent of sample-shelf life and other undesirable factors, theoretical calculations were made. These calculations were generated with the assumption that all TOC analyses were taken at NASA Glenn GRC with no wait time between post-treatment

and TOC measurements. For reference, a fresh batch of undiluted EWW is approximately 1550 ppm. Therefore, (2:1), and (20:1) dilutions were assumed to be ~517 ppm and ~74 ppm, respectively. The ethanol batch solutions were assumed to be perfectly diluted for (2:1) + 5% Wt. ethanol and (20:1) + 5% Wt. ethanol at ~24,000 ppm and 12,000 ppm, respectively. In hindsight, the theoretical initial TOC values for the ethanol-treated tests did not vary much compared to the actual values presented above. Figure 25 shows the theoretically calculated equivalence ratios for all EWW tests based on initial TOC expectations.

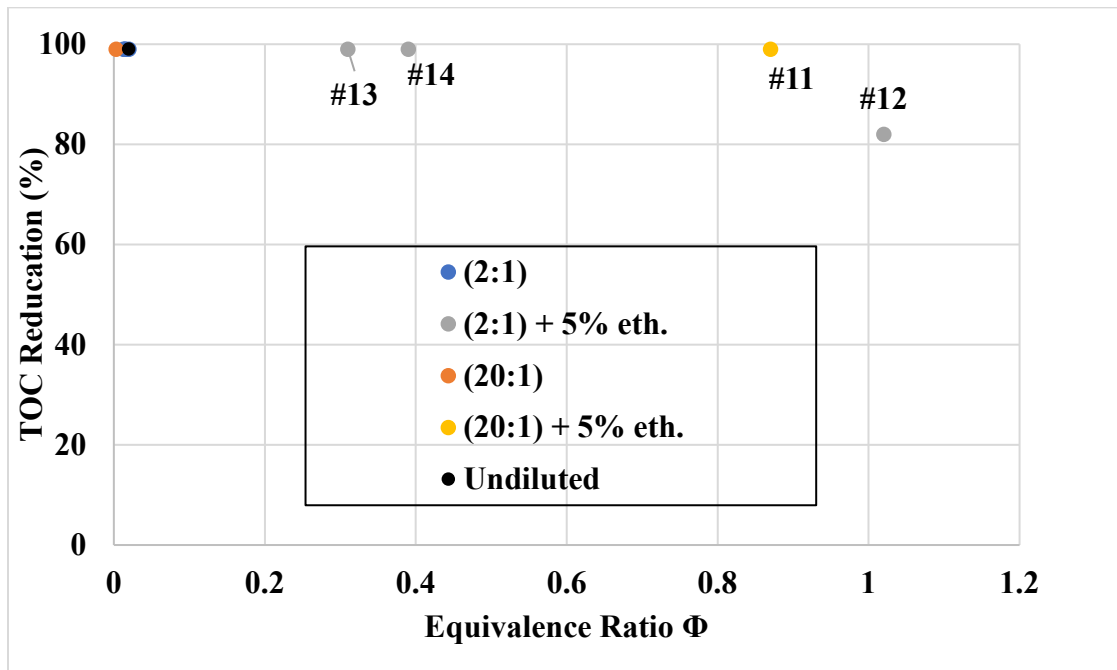


Figure 25: Theoretical calculations of TOC vs. equivalence ratios for all EWW tests.

With the expected theoretical values of TOC, equivalence ratios did not differ much due to the very miniscule amount of organic carbon present for initial concentrations. The main assumption that is made for this data is that at these lower equivalence ratios that

involve high amounts of excess air, TOC conversion should be near 100% for nearly all cases. The only test that was expected to not achieve these standards is Test 12.

In this Figure, only the ethanol treated tests are labeled, since all other concentrations experienced similar trends of equivalence and TOC reduction. Additionally, it is observed that ethanol treated cases require a larger amount of stoichiometric air supply. For reference, one mole of ethanol requires three moles of air for complete combustion. Therefore, the higher carbon content from addition of ethanol results in the higher equivalence ratio values presented for ethanol cases in this dataset.

### **1.19 Preliminary SCWO Tests for Urea-Aqueous Solutions**

As the main organic component of the EWW composition, aqueous urea was used for additional SCWO experimental tests. This preliminary study aimed to examine single and dual contaminant mixtures for correlation of Raman spectra to better visualize oxidation effects for less organically complex solutions. Table 9 presents the test matrix used for this preliminary study. The table features test dates, operating conditions, and fuel concentrations. The urea-aqueous solutions used in this study were made fresh for each test. The visual qualities and characteristics of the test solutions were clear, colorless, and without an odor. Therefore, the results presented in this section will only be quantitative due to the lack of qualitative observations that could be made from the characteristics of these tests. This study was performed to establish a basis for future single and dual-contaminant testing. Urea Tests 4 and 5 include multiple post treated samples and are characterized as “4A, 4B, 5A, and 5B. Subscript “b” is notated for “before treatment.” Taking multiple samples within the same test run allowed for efficient use of time as well as better observation of effects of operating conditions for each sample. Initial trial testing

was performed in Tests 1 and 2 with the purpose of establishing initial concentrations for testing. Raman results for the initial tests featured very minuscule quantities of scatter intensity for Urea at 5000 ppm and essentially non-detectable at 1000 ppm, with only a small conversion of urea and additions of other organics. Reference Raman scans for Tests 1 and 2 can be found in Appendix A.

Table 9: Test Matrix for Urea-Aqueous Solutions

Date	TEST #	Oxidizer flow rate	Fuel (C) flow rate (mL/min)	Reactor Set Point (°C)	Cell Pressure (psi)
11/16/2022	1	20% (2 SLPM)	1000 ppm 4	565	3900
11/17/2022	2	20% (2 SLPM)	5000 ppm 4	565	3900
11/22/2022	3	20% (2 SLPM)	50000 ppm 2	580	3900
11/23/2022	4 (A B)	20% 40% (1 2 SLPM)	50000 ppm + 5% eth. 2 2	570	3900
11/28/2022	5 (A B)	20% 40% (1 2 SLPM)	50000 ppm +10% eth. 2 4	570	3900
11/30/2022	6	75% (3.75 SLPM)	50000 ppm + 10% eth. 1.5	565	3900
12/01/2022	7	65% (3.25 SLPM)	50000 ppm + 5% eth. 2.5	565	3900

Table 10 presents the pH results for Tests 3-7 with urea-aqueous solutions. The pH values for the pretreated solutions were consistent across the duration of the testing matrix with values between 4.5 and 5.5. Like pH results for EWW, a color map of the pH is used

to show the trend of the pH values. The processed samples had extreme changes in pH associated with each test. The procedure of measurement for these pH values only involved the use of a standard litmus test in comparison to the procedure of the EWW tests which were measured by an external lab source. Evaluation for these pH tendencies will be discussed within the results to correlate the effects of operating conditions with changes in pH.

Table 10: pH Results for Urea-Aqueous Solutions

Test #	pH
3b	5.5
3a	8.5
4b	4.5
4 Sample A	8.5
4 Sample B	8.2
5b	4.5
5 Sample A	8.5
5 Sample B	8.5
6b	4.5
6a	3
7b	4.5
7a	1

### 1.20 Preliminary Quantitative Results for Urea-Aqueous Solutions

The results presented in this section include measurements from Raman spectroscopy and TOC analysis. Observations of conversion efficiency are correlated with

residence time, solution concentration, internal bulk temperatures, and patterns of reaction stoichiometry.

### 1.20.1 TOC Results for Urea-Aqueous Solutions

As with the EWW test, measurements were taken on the pretreated and post treated solutions to compare the percent TOC reduction relative to operating conditions. Table 11 shows the TOC measurements from this study with appropriate descriptions.

Table 11: TOC Results for Urea-Aqueous Solutions

TOC (ppm)			
C	Test #	TOC	% RD
50000 ppm	3b	6836.4	14.10%
	3a	5872.6	
50000 ppm + 5% eth.	4b	23099.4	X 96.24%
	4A	X	
	4B	868.3	
	7b	~23000	99%
	7a	58.3	
50000 ppm + 10% eth.	5b	36007.2	78%
	5A	7896.5	
	5B	5449.8	85%
	6b	33147.1	99.99%
	6a	64	

In comparison to EWW, the initial TOC value for a standard 50,000 ppm urea solution was higher than the standard fresh (2:1) EWW solution. Like the TOC procedure for EWW, measurements were taken in 3-5 replicates for accuracy, and the average TOC of the replicates is presented in ppm. Trends in TOC results are correlated through the

relationship between the respective fuel/air ratio, Raman scattering profile and other operating parameters such as solution concentration, bulk temperature, and residence time. TOC results for Test 4 Sample A (4A) and Test 7b were misplaced during data acquisition. An assumption was made for Test 7b TOC results to be like Test 4b since they were the exact same fresh dilution at ~23,000 ppm. A basic prediction of the TOC conversion value for Test 4 Sample A can be made by observing trends of other conversion successes. Also, for 10% Wt. of ethanol, the TOC values were lower than expected. The actual TOC range for this dilution should have been closer to 46,000 to 48,000 ppm and not 36,000 ppm. This may have been due to an instrument calibration issue for higher ethanol concentrations.

### **1.20.2 Preliminary Raman Results for Urea-Aqueous Solutions**

To establish a urea-baseline observation scatter, an arbitrary solution of 90,000 ppm urea-water was created. Figure 26 shows the acquired Raman results in arbitrary units of signal intensity for a 90,000 ppm solution. The main peaks that are specific to presence of urea are identified at 1006, 1155, 1460, 1590, and 1660  $\text{cm}^{-1}$ . Additional urea characteristic peaks can be observed overlapping water's O-H bend around 3200  $\text{cm}^{-1}$  [66]. Like the EWW tests, comparisons of the Raman scans for the pre and post treated solutions to pure water were made to observe conversion tendencies of the urea-aqueous solutions in relation to variation of operating conditions. The Raman results presented in this preliminary study were evaluated based on the reduction of the Urea peaks post treatment. A characteristic observation, made for the post-treated solutions in this preliminary study, is that the Raman broadband scatter presented higher intensities than the pre-treated solutions regardless of successful TOC conversion or operating conditions. This was the trend for all performed

Urea tests but was not observed for any of the EWW tests. A definitive reason for the increase in Raman intensity was not established, but a few hypotheses were made in lieu.

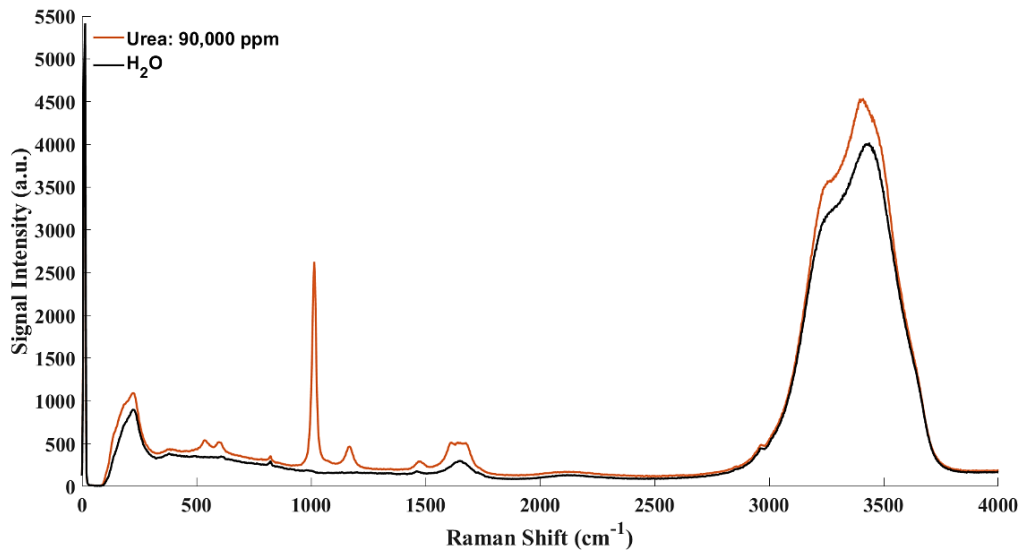


Figure 26: Raman scatter for 90,000 ppm Urea-water (non-normalized).

One theory is that the possible contamination occurred as fuel flowed into the reactor. The lifetime use of the reactor during this project was close to three years. Within this time, there was no maintenance performed for the reactor system. Possible contaminant buildup could have occurred within the reactor walls and inlet walls. The increase in contamination can cause additional fluorescence within the Raman scatter, thus increasing Raman intensity. Another possibility was that there was incomplete conversion of Urea leading to production of ammonia and its affiliates (nitrates and nitrites) without further conversion, thus presenting additional intensity scatter. Furthermore, the solutions created for this study contained only 50,000 ppm (5% Wt.) of Urea with and without the additions of ethanol. The lower concentration of organic material, as well as inadequate reactor

temperatures, may have created a negative effect on conversion efficiency. The greatest challenge of these preliminary tests was the kinetic limitation of the ammonia conversion. As previously mentioned, ammonia is known as the simplest refractory compound and is very chemically stable. The recalcitrant behavior is attributed to the nitrogen atom that forms strong triple bonds and thus there is a requirement for much higher temperatures to break those bonds for further decomposition. A focus of suggested future work should be to determine the reasons for the characteristics of these results through further Raman processing techniques, continued experimentation, and optimization of reactor design to sustain higher operating temperatures.

#### **1.20.2.1 Preliminary Raman Results for Various Urea-Aqueous Solutions**

After the urea-baseline test was performed, a standard was created for the proceeding urea solution concentrations. 50,000 ppm urea solutions were made as 5% Wt. of the total solution with the remaining 95% being pure deionized water. Additional concentrations contained 50,000 ppm urea with the addition of 5% and 10% Wt. ethanol. Figure 27 presents a normalized Raman shift comparison to pure water and a 50,000-ppm urea aqueous solution for Test 3 with a fuel flow of 2 mL/min and air flow of 1 SLPM. The average bulk temperature was 619°C with a residence time of approximately 97s.

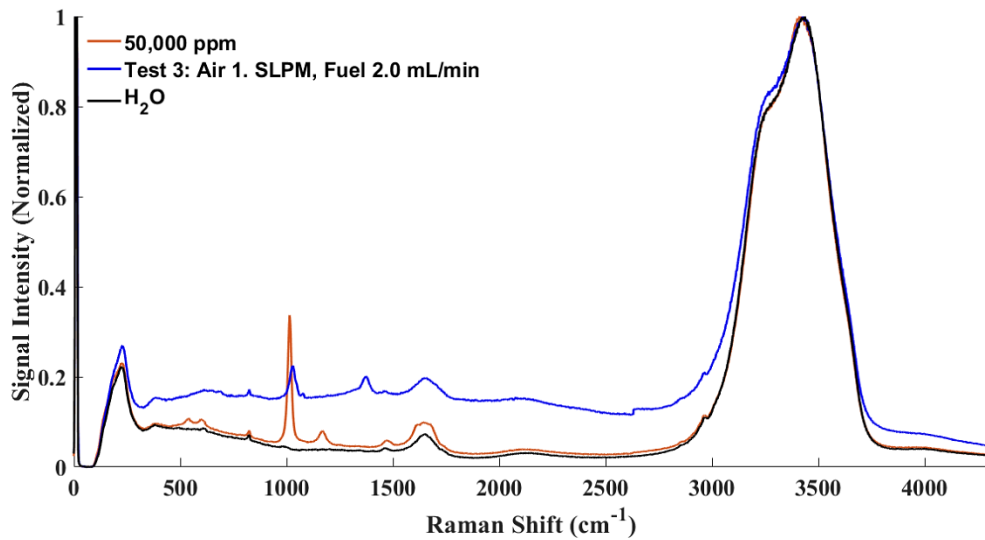


Figure 27: Normalized Raman comparisons to pure water and a 50,000-ppm urea Test 3.

As mentioned, the initial reaction that takes place is the hydrolysis of urea (eq. 4-5). Using a 10% urea aqueous solution, Timberlake et al. found that the conversion of ammonia was initiated at average reactor wall temperatures below 561°C, and at above 670°C, basically all nitrogen of the influent is oxidized into N<sub>2</sub> gas [37]. Additionally, it was observed that nitrous oxide peaks in concentration at temperatures between 587°C to 632°C [37]. The results for Test 3 suggest that at these conditions urea hydrolysis may have partially initiated. Overall reduction of the main urea peak for the post treated solution suggests that the reaction process-initiated urea decomposition without further conversion of ammonia.

Furthermore, modes of ammonia conversion are highly dependent upon temperature. The current reactor design is restricted to a maximum internal cell temperature of 630°C, therefore, the rate of conversion success is limited for ammonia under these conditions. Test 3 post-treated solution achieved only a 14% reduction of the initial TOC

content, and presented a pH value of 8.5, compared to the pre-treated pH of 5.5. The increase of base-like qualities supports the hypothesis of ammonia production from partial urea conversion since ammonia is typically characterized as a weak base. In this study, the inability to provide adequate temperatures for this reaction process will require additional support for reaction kinetics. Therefore, the use of ethanol as a co-fuel was established to increase internal bulk temperatures.

#### **1.20.2.2 Influence of Ethanol on Urea-Aqueous Solutions**

To enhance the conversion of urea as well as increase the amount of initial carbon concentration, ethanol was used as a co-fuel for oxidation. Killilea et al. [68] studied the potential of ethanol (as auxiliary fuel) to decompose ammonia in a tubular reactor. Results found that the presence of ethanol enhanced conversion of ammonia at lower temperatures. They reported that ammonia was converted at 690°C when ethanol was used compared to 41% for pure ammonia oxidation. Figure 28 presents normalized Raman scan comparisons for a 50,000-ppm urea plus 5% Wt. ethanol aqueous solution and treated samples from Tests 4 and 7. Two samples were taken for Test 4. Both samples operated under fuel flow of 2 mL/min but with varying air flows of 1 SLPM and 2 SLPM. Both tests were performed using a fresh batch solution. Residence times for these two samples were 99s and 77s, respectively. Observation of the Raman shifts for Test 4 samples suggests that there was complete conversion of ethanol, but there wasn't complete conversion of urea. Furthermore, reducing the amount of excess fuel relative to stoichiometric oxygen between Test 4 Sample A and Test 4 Sample B resulted in weaker signal intensities from the increased air supply, suggesting increased conversion of the second sample.

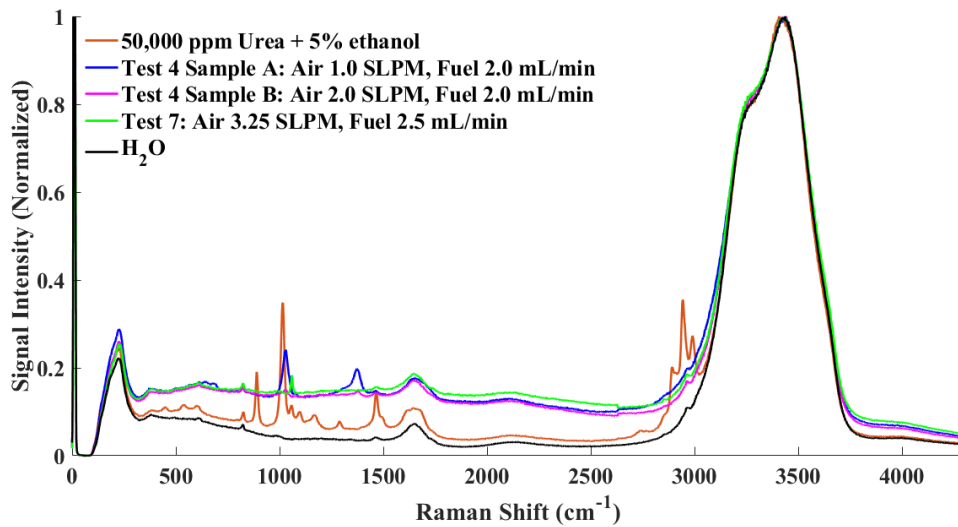


Figure 28: Normalized Raman comparisons for 50,000 ppm urea + 5% wt. ethanol.

The overall TOC reduction for Test 4 sample A was less than the 96% reduction for Sample B. It can be predicted that the TOC reduction for this sample was near 80-85% conversion. Additionally, Test 7 is presented as post-treated solution of a 50,000-ppm with 5% Wt. ethanol solution at varying flow rates of 3.25 SLPM air and 2.5 mL/min fuel. With an even lower fuel to stoichiometric oxygen ratio and residence time of 52s, Test 7 achieved an overall TOC reduction of 99%, with only approximately 58 ppm of TOC remaining. The operating bulk temperatures for the tests described in Figure 28 ranged between 595°C to 610°C. Since the temperature variances were not substantial between these tests, the noticeable differences in Raman scans can ultimately be attributed to fuel to air ratios. Another comparable measurement made between these three tests was the change in the pH values. Both samples for Test 4 resulted in similar changes in pH from 4.5 of the pre-treated solution to approximately 8.5 post-treatment indicating a change from a weak acid to a weak base, like Test 3. It has been found that increasing oxidant levels decreases

ammonia yield and there are fluctuating increases of nitrite and nitrate observed during oxidation [42, 62, 63]. Nitrate and nitrite are described as Lewis-base structures, thus could suggest why pH levels were higher for post treatment in this case, Additionally, Killilea et al. [68] observed that nitrate conversion success was higher (92% to 95%) at lower oxygen levels, and 75% conversion at moderate oxygen levels. Contrary to these results, Test 7 pH values changed from 4.5 of the pre-treated solution, to a pH value of 1 for the post-treated solution indicating transition from a weak acid to a strong acid. The increase in acidity at these conditions may suggest that ammonia was produced and highly oxidized down into its components of  $N_2$  and  $H_2$  in forms of nitric acid ( $HNO_3$ ), from thermal decomposition of nitrate, as its conjugate acid. Additionally, the presence of the hydrogen ions and highly ionic precipitated salts could have increased the acidity, hence the lower pH value presented.

To further observe trends for effects of ethanol as an additive, additional SCWO tests were performed for urea-aqueous solutions with 10% Wt. ethanol. Figure 29 shows a comparison of normalized Raman shifts for tests 5 and 6, where the flow rates of pure water and 50,000 ppm urea-ethanol pretreatment solution were varied. By adding an additional 5% Wt. ethanol, TOC content essentially doubled in concentration. As mentioned, actual TOC measurements measured for these tests measured at 36,000 ppm instead of the predicted 48,000 ppm. Unlike the tests featured in Figure 28, the tests presented in Figure 29 were performed two days apart using the same batch solution. Within this time, there was a slight reduction of overall TOC for the pre-treated solution by 8%, and Raman scatter comparisons for the two presented no differences. Therefore, only one representative of the pretreatment solution is shown in this figure.

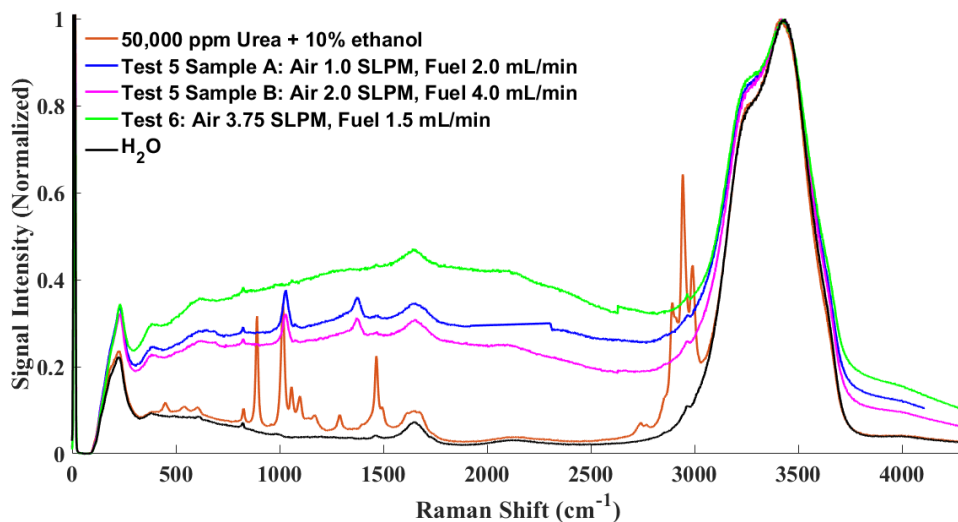


Figure 29: Normalized Raman comparisons for 50,000 ppm urea + 10% wt. ethanol.

With 10% WT. ethanol, there is additional reaction support through increased bulk temperatures. Test 5 Sample A had flow rates of 1 SPLM and 2 mL/min fuel, while Test 5 Sample B had flow rates of 2 SLPM and 4 mL/min fuel. The internal average bulk temperatures between these samples were 602°C and 611°C, respectively. At double the air and fuel flow rates, Test 5 Sample B achieves a slightly lower Raman intensity profile with a residence time of approximately 49 seconds. Although Test 5 Sample A had almost double the residence time, there was an insufficient supply of oxidizer per unit of fuel supplied. The overall TOC reduction for Test 5 Sample A was 78% reduction versus 85% reduction for Test 5 Sample B, which again suggests better conversion when oxidant is in excess. Both post-treated samples from Test 5 followed trends of pH of post-treated samples of Test 4, weak acid to weak base. Similarly, Test 6 shared comparable pH trends

to Test 7, weak acid to strong acid. The results for these ethanol tests give partial suggestion that the use of ethanol may not be needed to enhance overall conversion efficiency for urea. Instead, conversion success seemed to reflect flow rates and temperature. This was also observed by Okazaki et al., [40] in which urea was decomposed in sub- and supercritical water with and without the use of additives (NaCl, HCl, H<sub>2</sub>SO<sub>4</sub> and NaOH) or an oxidizer. Results obtained in this study showed that for a variation of additives used, there were positive effects for conversion of urea at 376°C. Although, it was also found that urea decomposed with almost the same slope without the addition of additives. This furthermore supports that efficacious conversion of urea as well as ammonia-based nitrogenous wastes is highly dependent on temperature for complete oxidation.

### **1.21 Observation of Residence Time**

Like the EWW residence time, the residence time of aqueous urea was also calculated for each test. The overall residence times were in a similar range to the EWW results, in the range of approximately 56 s to 98 s. Figure 30 presents these residence times in relation to the TOC reduction for each test. As previously mentioned, Test 4 sample A is without measurement of TOC, but an estimate of conversion is around 80-85% based on its equivalency ratio of  $\sim 0.6$  and the higher concentration sample 5A with only 78% conversion at the same flow rates.

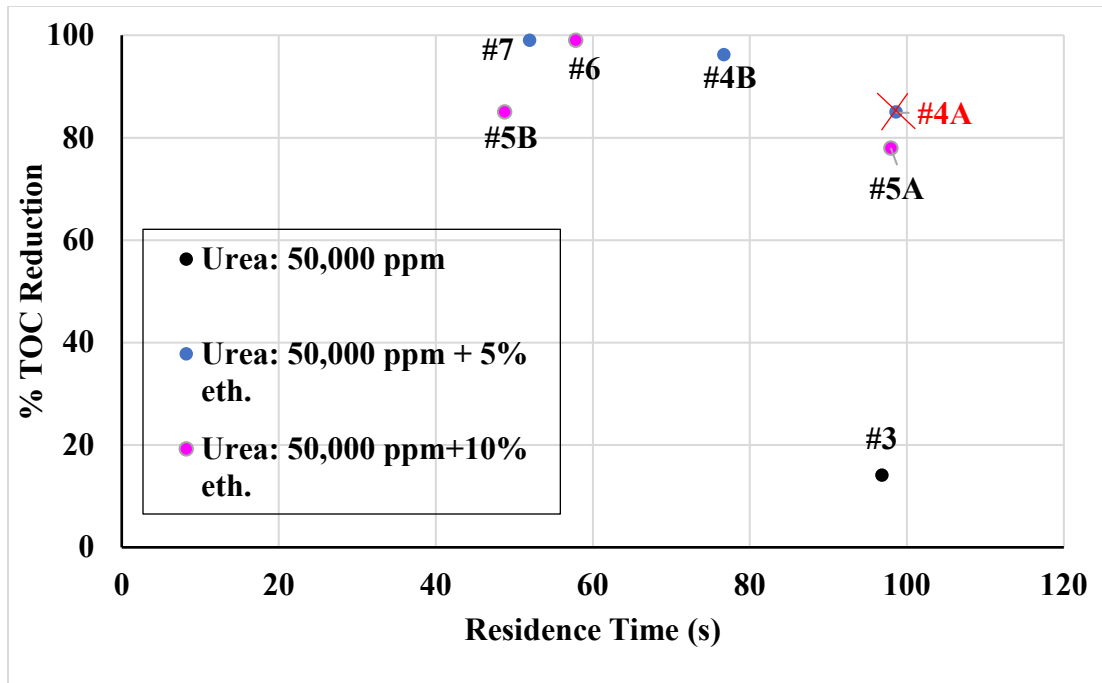


Figure 30: Observation of residence times for urea-aqueous solutions.

Results for Tests 6 and 7 suggest that there was successful oxidation of 99% of TOC presented. Test 3, without ethanol, only relied on temperature and oxidizer for conversion. At these lower internal temperatures and lower amounts of carbon content, there may not be enough initial concentration to drive the reaction, thus presenting only 14% conversion of TOC.

### 1.22 Influence of Operating Temperatures

Figure 31 presents the trends of operating temperature relating to TOC reduction for the urea tests. Additionally, the data points are grouped in relevance to residence times. As mentioned, operating temperature is of most importance since ammonia compound destruction relies on high reaction temperatures.

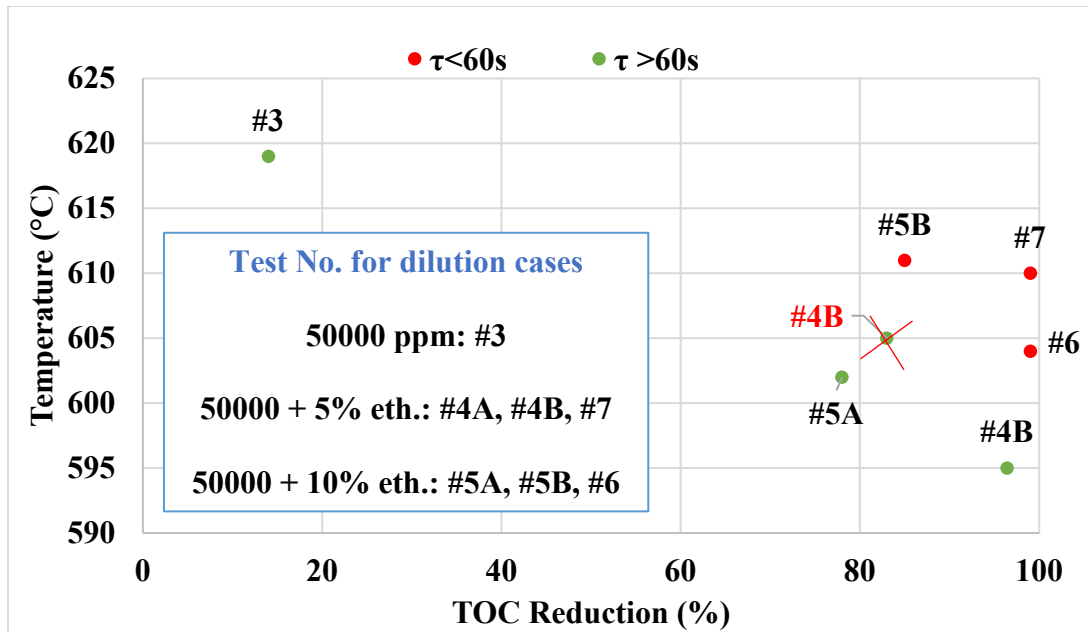


Figure 31: Influence of operating temperatures on residence time for Urea TOC.

It has been concluded that none of the tests performed operated with temperatures that were sufficient for complete oxidation of urea and ammonia. Rather, the TOC conversion success of tests like 6, 7 and 4B were directly a result of their relatively low fuel to air equivalency ratios. This will be further explained within the next section.

### 1.23 Urea- Aqueous Solutions Preliminary Equivalence Ratios

Equivalency ratios were calculated for the Urea- Ethanol case studies. These results are presented in Figure 32. The presented ratios follow a similar trend for the EWW equivalents, which supports complete oxidation of organics in favor of excess in stoichiometric air. As mentioned before, Test 4 sample A results for TOC are estimated and therefore can be disregarded but are shown for curiosity purposes.

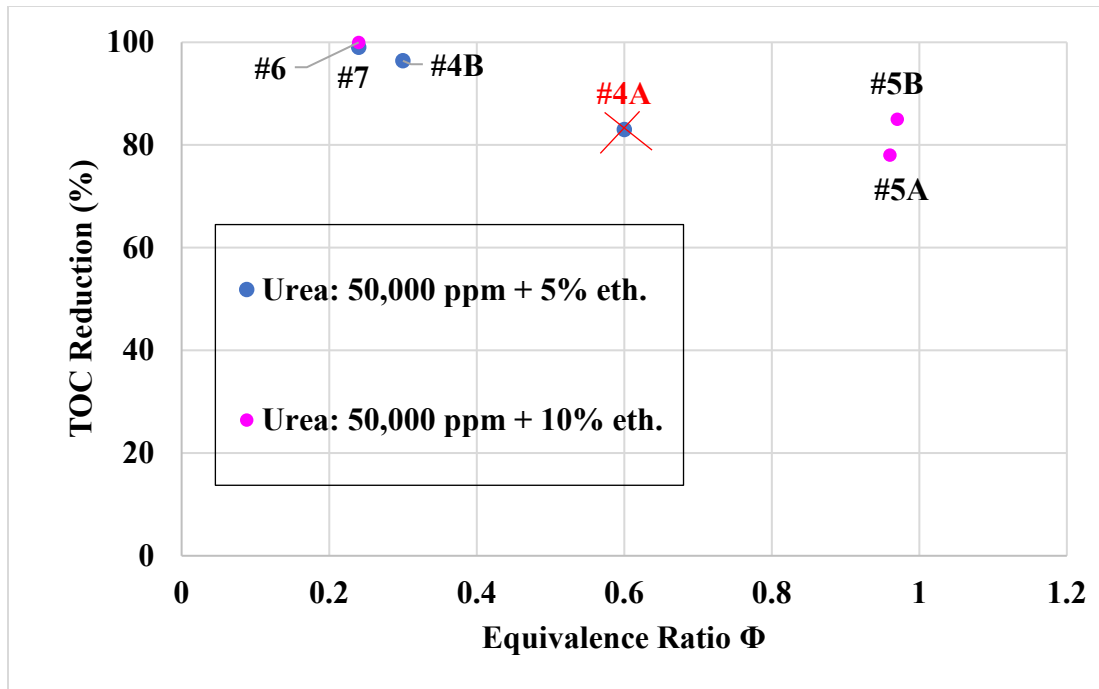


Figure 32: Equivalency ratios for urea-ethanol-treated tests.

Additionally, like the EWW equivalence ratios for ethanol-treated tests, at a ratio of 1, TOC is converted at approximately 80%, thus requiring a higher amount of oxidizer, lower equivalencies for complete oxidation. The most optimized tests for conversion were Tests 6, 7, and 4B. Although operating temperatures were inadequate, the addition of ethanol coupled with lower fuel equivalencies proved to overcompensate for the lack of required heat supply.

#### 1.24 Preliminary Gas Measurements for Urea-Ethanol Tests

Towards the end of this research timeline, the start of construction of a real-time gas measurement system was performed using a Horiba Gas Analyzer. Preliminary on-time measurements were taken for Urea Tests 6 and 7. Figure 33 shows preliminary gas measurements for Urea Test 6. Additionally, Figure 34 shows preliminary gas

measurements for Urea Test 7. Each Figure features time stamps according to when the image was taken using an iPhone. Results in both figures suggest that a level of combustion is occurring from the observance of CO<sub>2</sub>, NO, reduced levels of O<sub>2</sub>.



Figure 33: Preliminary gas measurements for Urea Test 6.

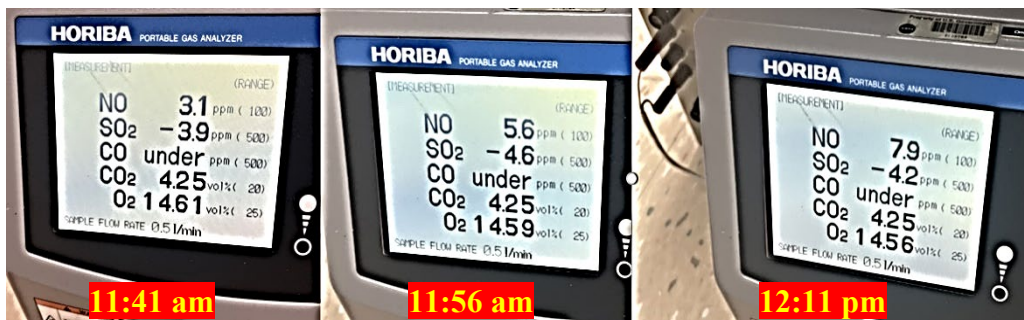


Figure 34: Preliminary gas measurements for Urea Test 7.

Both tests present the increase in detection of NO over some time. Regarding TOC conversion, both Test 6 and 7 achieved 99% conversion of TOC at an equivalency ratio of approximately .24. The values of SO<sub>2</sub>, observed for Test 6, are due to not replacing a SO<sub>2</sub> scrubber before measurements. An additional software interface is currently being established to enable a stable data acquisition procedure. Future testing will need to be

performed to confirm accurate levels of ppm and calibration for effluent gases, but from these results, detection of complete combustion gases gives positive insight regarding conversion success.

## CONCLUSION AND DISCUSSION

The focus of this chapter will be to consider the research and its findings for the purpose of determining if SCWO technologies can be proposed as a reliable option for treating wastewater during extended space missions.

To advance functionality of life-support systems for extended space missions, there needs to be technology that can allow the reclamation of resources from the air, water, and waste stream accumulation. Supercritical Water Oxidation experiments for an ISS waste representative, ersatz wastewater, were conducted using a 62 mL continuous tubular flow reactor designed and fabricated at NASA Glenn Research Center. Operating parameters for these tests operated within bulk temperatures of  $\sim 600^{\circ}\text{C}$  to  $680^{\circ}\text{C}$  and average pressures of 3900 MPa. Preliminary testing of (2:1) ersatz dilutions was performed to observe operation conditions for successful conversion efficiency and to verify proper experimental procedures for subsequent tests in accordance with a previous study by Hicks et al. [4]. Additional qualitative observation of treated wastewater, Raman spectral analysis, and TOC measurements suggest that organic material can and were reduced with relatively low “fuel” and oxidizer flow rates SCWO reaction processes are favored for flowrates with excess in oxidizer per unit of fuel, and calculated equivalency ratios favored effective conversion with lower amounts of excess in fuel. Additional tests were performed for “fresh” batch solutions at various concentrations of (2:1), (20:1) and undiluted solution with and without the addition of 5% Wt. ethanol mixtures. These tests followed similar trends of conversion success within literature with implications of shorter residence times from higher oxidizer values and lower excess in fuel. For EWW, an organically complex solution, it was found that conversion success followed trends within literature regarding

reaction stoichiometry. With proper equivalency ratios, 9 out of 10 EWW experiments presumed to achieve 99% of TOC conversion with and without ethanol as an auxiliary fuel. pH values trended mostly from an initial value of a weak base to weak acid for post-treatment. These values for pH suggest that complete combustion could be accomplished with oxidation of organic species into  $\text{NO}_2$ , thus inferring reduction of pH from reduced nitrogenous compounds with probable effluent quantities of inorganic salts.

Additionally, a preliminary study for conversion of single and dual contaminant mixtures for correlation of Raman spectra to better visualize oxidation effects for lesser complex solutions was performed using urea-aqueous solutions. These tests presented challenges related to reaction kinetics for effective conversion of ammonia. Within literature it has been found that there are many factors that can affect ammonia conversion, but temperature is the most important influencer for effective ammonia decomposition. SCWO tests were performed for urea-aqueous solutions with and without the addition of ethanol. Test solutions were made with 50,000 ppm urea with and without the addition of 5% and 10% Wt. ethanol. Preliminary results follow suit that ammonia, the most refractory compound for nitrogenous wastes, requires maximum optimization of reactor conditions with the most influential parameter being operating temperature. The addition of ethanol may have improved conversion success, but literature suggests that ammonia on its own can yield similar conversion success without an additive at appropriate temperatures. Conversion success was comparable to EWW tests which favor equivalence ratios that favor excess in oxidizer. The challenge presented for urea-aqueous solutions was the inability to sustain higher internal bulk temperatures needed for effective conversion of ammonia.

The SCWO of EWW and Urea testing in this project exercised the use of a “green technology” for waste treatment of in-space effluent waste streams. Although the reactor used in this project was gravity dependent, the overall observation for tendencies of SCWO technology provides additional understanding, confirmation, and suggestion of future experimental work. The continued advancement of SCWO technology will benefit waste processing techniques within terrestrial applications and furthermore for the benefit of future extended space exploration.

### **1.25 Recommendations for Future Work**

To better observe effects of operating parameters, in the future, tests for EWW compositions should be performed with more repetition of specific reactor conditions to increase the sample size of data sets to observe trend effects. Additional testing can also be performed to discover the equivalency ratio thresholds for EWW. Additionally, gas measurements should be performed to analyze and confirm success of conversion through observation of yield of combustion gases. Moreover, reactor and other apparatus configuration should be optimized to increase the maximum allowable cell temperature to 700°C. This will inherently allow the maximum allowable internal bulk temperatures to increase, thus allowing higher experimental success variability for urea-aqueous solutions, ammonia, and other desired wastewater subjects. Additionally, due to added Raman scatter for Urea testing, two recommendations are proposed. The first is to perform additional Raman process techniques to eliminate spectral background, if possible. The second recommendation is to incorporate a filtration technique for post treatment solutions to reduce potential contaminants such as salts or other hydrocarbon ions before Raman diagnostics to reduce fluorescence. Finally, the last recommendation for future study is to

incorporate a separate SCWO study for microgravity experimentation to compare the effects of reduced gravity effects in relation to the work presented in this thesis.

## REFERENCES

- [1] S. Xia, A. Morse, A. Jackson, T.F. Wiesner, Simulation of a closed loop wastewater treatment system for extended space flight, In Proceedings of the 2008 3rd IEEE Conference on Industrial Electronics and Applications. Singapore, 3–5 (2008) 1252–1257. doi:10.1109/ICIEA.2008.4582719.
- [2] M.C. Hicks, U.G. Hegde, C. Lecoutre, S. Marre, Y. Garrabos, Supercritical water (SCW) investigations in the DECLIC and DECLIC-Evo: Past, present and future, *Acta Astronautica*.176 (2020) 59-68. <https://doi.org/10.1016/j.actaastro.2020.06.006>.
- [3] M.S. Anderson, M.K. Ewert, J.F. Keener, and S.A. Wagner. Life support baseline values and assumptions document. Technical Report NASA/TP-2015-218570, NASA JSC, 2015. <https://ntrs.nasa.gov/citations/20180001338>.
- [4] M.C. Hicks, D.J. Gotti, R.E. Padilla, U.G. Hegde, J. Kojima, M.T. Flynn, Supercritical Water Oxidation: Testing of Ersatz Wastewater, 51<sup>st</sup> International Conference on Environmental Systems, St. Paul, MN, July 2022. <https://hdl.handle.net/2346/89823>.
- [5] A.M. Figueroa, M. Flynn, Supercritical Water Oxidation (SCWO) Trade Study and 2021 Final Report, NASA Ames Research Center, USA, October 2021. <https://ntrs.nasa.gov/citations/20210022923>.
- [6] I. Piore, Advanced Supercritical Fluids Technologies, University of Ontario Institute of Technology, Ontario, CAN, 2020.
- [7] M. Modell, Processing Methods for the Oxidation of Organics in Supercritical Water. U.S. Patent 4,338,199, June 1982. <https://patents.google.com/patent/US4338199A/en>.
- [8] A. Gidner, L. Stenmark, Supercritical Water Oxidation of Sewage Sludge: State of the Art, In Proceedings of the IBC's Conference, Chematur Engineering AB. 430 (2001). [http://news.caloosahatchee.org/docs/Sewage\\_Sludge\\_SWO\\_110530.pdf](http://news.caloosahatchee.org/docs/Sewage_Sludge_SWO_110530.pdf).
- [9] A.M. Figueroa, M. Flynn, M.C. Hicks, U.G. Hegde, R.E. Padilla, J. Kojima, D.J. Gotti, Supercritical Water Oxidation: A Promising Wastewater Treatment Technology, 51<sup>st</sup> International Conference on Environmental Systems, St. Paul, MN, July 2022.
- [10] S. Zhang, Z. Zhang, R. Zhao, J. Gu, J. Liu, B. Örmeci, J. Zhang, A Review of Challenges and Recent Progress in Supercritical Water Oxidation of Wastewater, *Chemical Engineering Communications*. 204 (2016) 265-282. 10.1080/00986445.2016.1262359.
- [11] Z. Jiang, S.; Y. Li, S. Wang, C. Cui, C. Yang, and J. Li. Review on Mechanisms and Kinetics for Supercritical Water Oxidation Processes, *Appl. Sci.* 10(14) (2020), 4937. <https://doi.org/10.3390/app10144937>.
- [12] M.B. García Jarana, J. Sánchez-Oneto, J.R. Portela, E. Nebot Sanz, E.J. Martínez de la Ossa, Supercritical Water Gasification of Industrial Organic Wastes, *J. Supercrit. Fluids*. 46 3 (2008) 329-334. <https://doi.org/10.1016/j.supflu.2008.03.002>.

- [13] V. Vadillo, J. Sanchez-Oneto, J.R. Portela, E.J. Martinez de la Ossa, Chapter 10-Supercritical water oxidation. *Advanced Oxidation Processes for Wastewater Treatment*, Academic Press. Elsevier, U.S.A (2018) 333-358. <https://doi.org/10.1016/B978-0-12-810499-6.00010-3>.
- [14] W.R. Killilea, G.T. Hong, K.C. Swallow, T.B. Thomason, 1988. Supercritical Water Oxidation: Microgravity Solids Separation, In *SAE Technical Papers*; 881038. <https://doi.org/10.4271/881038>.
- [15] M.D. Bermejo, M.J. Cocero, Supercritical water oxidation: A technical review, *AIChE Journal*. 52, 11 (2006) 3933-3951. <https://doi.org/10.1002/aic.10993>.
- [16] M. J. Cocero; E. Alonso, R. Torío, D. Vallelado, F. Fdz-Polanco. Supercritical water oxidation in a pilot plant of nitrogenous compounds: 2-propanol mixtures, *Ind. Eng. Chem. Res.* 39 10 (2000) 3707–3716. <https://doi.org/10.1080/19443994.2012.749196>.
- [17] V. Vadillo, J. Sanchez-Oneto, J. Ramon Portela, E.J. Martinez de la Ossa. Problems in supercritical water oxidation process and proposed solutions, *Ind. Eng. Chem. Res.* 52 23 (2013) 7617-7629. <https://doi.org/10.1021/ie400156c>.
- [18] H. Schmeider, J. Abeln, Supercritical water oxidation: State of the art, *Chem. Eng. Tech.* 22 11 (1999) .903-908. [https://doi.org/10.1002/\(SICI\)1521-4125\(199911\)22:11%3C903::AID-CEAT903%3E3.0.CO;2-E](https://doi.org/10.1002/(SICI)1521-4125(199911)22:11%3C903::AID-CEAT903%3E3.0.CO;2-E).
- [19] M. J. Cocero, D. Vallelado, R. Torio, E. Alonso, F. Fdez-Polanco, Optimization of the operation variables of a supercritical water oxidation process, *Water Sci Technol.* 42 5–6 (2000) 107-113. <https://doi.org/10.2166/wst.2000.0503>.
- [20] E. Asselin, A. Alfantazi, S. Rogak, Thermodynamics of the corrosion of alloy 625 supercritical water oxidation reactor tubing in ammoniacal sulfate solution. *Corrosion.* 64 4 (2008). <https://doi.org/10.5006/1.3278474>.
- [21] M.D. Bermejo, F. Fernández-Polanco, M.J. Cocero, Modeling of a transpiring wall reactor for the supercritical water oxidation using simple flow patterns: Comparison to experimental results, *Ind. & Eng. Chem. Res.* 44 (11) (2005) 3835–3845. <https://doi.org/10.1021/ie0487742>.
- [22] G.T. Hong, Process for the Oxidation of Materials in Water at Super- Critical Temperatures and Subcritical Pressures. 5 106 513, 1992. <https://patents.google.com/patent/US5106513A/en>.
- [23] M.J. Cocero, E. Alonso, M.T. Sanz, F. Fernandez-Polanco, Supercritical water oxidation process under energetically self-sufficient operation, *J. Supercrit. Fluids.* 24 1 (2002). [https://doi.org/10.1016/S0896-8446\(02\)00011-6](https://doi.org/10.1016/S0896-8446(02)00011-6).
- [24] D.D. Macdonald, S.N. Lvov, Development of advanced in-situ techniques for chemistry monitoring and corrosion mitigation in SCWO environments, USDOE Office of Energy Research (ER) (US) 2000. <https://doi.org/10.2172/781020>.

- [25] L.B. Kriksunov, D.D. Macdonald, Corrosion in supercritical water oxidation systems: A phenomenological analysis, *Journal of The Electrochemical Society*. 142 12 (1995). <https://doi.org/10.1149/1.2048464>.
- [26] B.R. Pinkard, D.J. Gorman, K. Tiwari, E.G. Rasmussen, J.C. Kramlich, P.G. Reinhall, I.V. Novosselov, Supercritical water gasification: practical design strategies and operational challenges for lab-scale, continuous flow reactors, *Heliyon*. 5 2 (2019). <https://doi.org/10.1016/j.heliyon.2019.e01269->.
- [27] P.A. Marrone, G.T. Hong, Corrosion control methods in supercritical water oxidation and gasification processes, *J. Supercrit. Fluids*. 51 2 (2009) 83-103. <https://doi.org/10.1016/j.supflu.2009.08.001>.
- [28] B.P. Somerday, K.T. Wiggans, R.W. Bradshaw, Environment-assisted failure of alloy C-276 burst disks in a batch supercritical water oxidation reactor, *engineering failure analysis*. 13 1 (2006) 80-5, <https://doi.org/10.1016/j.engfailanal.2004.10.017>.
- [29] B. Veriansyaha , T.J. Parka, J.S. Limb, Y.W. Lee. Supercritical water oxidation of wastewater from LCD manufacturing process: Kinetic and formation of chromium oxide nanoparticles, *J Supercrit Fluids*. 34 (2005) 51-61. <https://doi.org/10.1016/j.supflu.2004.10.001>.
- [30] H.C. Lee, J.H. Kim, J.H. In, C.H. Lee. NaFeEDTA decomposition and hematite nanoparticle formation in supercritical water oxidation, *Ind Eng Chem Res*. 44 17 (2005) 6615-6621. <https://doi.org/10.1021/ie050115h>.
- [31] L. Stenmark, Supercritical fluid technologies within chematur engineering AB, In *Proceedings from the Third International Disposal Conference*. Karlskoga, Sweden, November 10-11 2003.
- [32] <https://epiccleantec.com>
- [33] G. Brunner, Near and supercritical water. part II: Oxidative processes, *J. Supercritical Fluid*. 47 (2009) 382-390. <http://dx.doi.org/10.1016/j.supflu.2008.09.001>.
- [34] X. Tang, S. Wang, D. Xu, Y. Gong, J. Zhang, Y. Wang, Corrosion behavior of Ni-based alloys in supercritical water containing high concentrations of salt and oxygen, *Ind. & Eng. Chem. Res.* 52 51 (2013), 18241-18250. <https://doi.org/10.1021/ie401258k>.
- [35] P. Kritzer, E. Dinjus, An assessment of supercritical water oxidation (SCWO). Existing problems, possible solutions and new reactor concepts. *Chem, Eng. J.* 83 3 (2001) 207-214. [https://doi.org/10.1016/S1385-8947\(00\)00255-2](https://doi.org/10.1016/S1385-8947(00)00255-2).
- [36] G.T. Hong, W.R. Killilea, A.L. Bourhis, Method for treating halogenated hydrocarbons prior to hydrothermal treatment, U.S. Patent No. 5,492,634, <https://patents.google.com/patent/US5492634A/en>
- [37] L. Li, P. Chen, E.F. Gloyna, Generalized kinetic model for wet oxidation of organic compounds, *AIChE J.* 37 11 (1991) 1687-1697. <https://doi.org/10.1002/aic.690371112>.

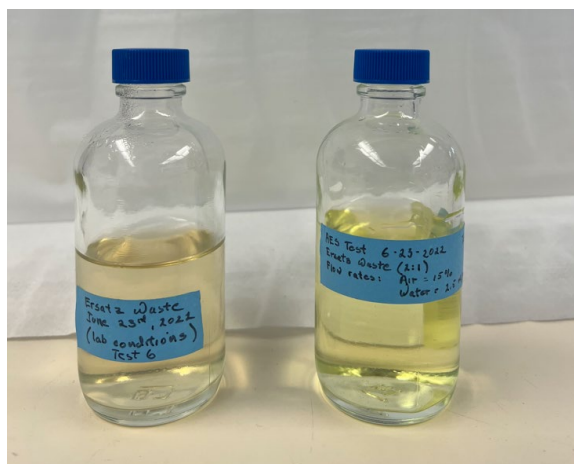
- [38] P.A. Marrone, Supercritical water oxidation- Current status of full-scaled commercial activity for waste destruction, *J. Supercrit. Fluids.* 79 (2013) 283-288. <https://doi.org/10.1016/j.supflu.2012.12.020>.
- [39] S.H. Timberlake, G.T. Hong, M. Simon, M. Modell, Supercritical water oxidation for wastewater treatment: Preliminary study of urea destruction, *Intersociety Conference on Environmental Systems.* 820872 (1982). <https://doi.org/10.4271/820872>.
- [40] M. Okazaki, T. Funazukuri, Decomposition of urea in sub- and supercritical water with/without additives, *J Mater Sci.* 43 (2008) 2316-2322. <https://doi.org/10.1007/s10853-007-2027-6>
- [41] S.V. Prasad Mylapilli, S.N. Reddy, Supercritical water oxidation of recalcitrant acetaminophen with methanol, ethanol, n-propanol, isopropanol and glycerol as co-fuels, *Chemical Engineering Journal Advances* 3 100028 (2020). <https://doi.org/10.1016/j.cej.2020.100028>
- [42] T. Oe, H. Suzugaki, I. Naruse, A.T. Quitain, H. Daimon, K. Fujie, Role of Methanol in Supercritical Water Oxidation of Ammonia, *Ind, & Eng. Chem. Res.* 46 (2007) 3566-3573. <https://doi.org/10.1021/ie070168u>.
- [43] J. Li, S. Wang, Y. Li, Z. Jiang, T. Xu, Y. Zhang, Supercritical water oxidation and process enhancement of nitrogen-containing organics and ammonia, *Water Research.* 185 15 (2020) 116222. <https://doi.org/10.1016/j.watres.2020.116222>.
- [44] B. Al-Duri, F. Alsoqyani, Supercritical water oxidation (SCWO) for the removal of N— containing heterocyclic hydrocarbon wastes; Part II: System kinetics, *J. Supercrit. Fluids.* 128 (2017) 412-418. <http://dx.doi.org/10.1016/j.supflu.2017.05.010>
- [45] R.K. Helling, J.W. Tester, Oxidation of simple compounds and mixtures in supercritical water: Carbon monoxide, ammonia, and ethanol. *Environ. Sci. Technol.* 22 11 (1988) 1319-1324. <https://doi.org/10.1021/es00176a012>.
- [46] M.D. Bermejo, F. Cantero, M.J. Cocero, Supercritical water oxidation of feeds with high ammonia concentrations: Pilot plant experimental results and modeling, *Chemical Engineering Journal.* 137 3 (2008) 542-549. <https://doi.org/10.1016/j.cej.2007.05.010>.
- [47] F.S. Alysoqyani, Supercritical water oxidation of nitrogen-containing organic compounds: Process enhancement using isopropyl alcohol [Published Doctoral Thesis]. University of Birmingham, (2017).
- [48] Y. Aviezer, O. Lahav, Determining the kinetic constants leading to mineralization of dilute carbamazepine and estradiol-containing solutions under continuous supercritical water oxidation conditions, *Journal of Hazardous Materials.* 422 126797 (2022). <https://doi.org/10.1016/j.jhazmat.2021.126797>.
- [49] C.J. Martino, P.E. Savage, Total organic carbon disappearance kinetics for the supercritical water oxidation of monosubstituted phenols, *Environ. Sci. Technol.* 33 11 (1999) 1911-1915. <https://doi.org/10.1021/es981201u>.

- [50] R. Doty, New brine processor increases water recycling on international space station, NASA Johnson Space Center (2021). doi:<https://www.nasa.gov/feature/new-brine-processor-increases-water-recycling-on-international-space-station>.
- [51] Committee, S. NASA Space Technology Roadmaps and Priorities: Restoring NASA's Technological Edge and Paving the Way for a New Era in Space, The National Academies Press. (2012).
- [52] L. K. Kelsey, S. P. Boyce, G. Speight, P. Pasadilla, P. Tewes, E. Rabel, and C. Meyer, Closing the water loop for exploration: 2020-2021 Status of the brine processor assembly, 50th International Conference on Environmental Systems, Albuquerque, NM, July 2021. <https://hdl.handle.net/2346/87310>.
- [53] C. Zhan, L. Zhang, W. Ai, and W. Dong, Green and sustainable treatment of urine wastewater with a membrane-aerated biofilm reactor for space applications, *Water*. 14 22 (2022) 3704. <https://doi.org/10.3390/w14223704>.
- [54] L. Carter, J. Pruitt, A.B. Christopher, R. Schaezler, L. Bankers, Status of ISS Water Management and Recovery. In Proceedings of the 45th International Conference on Environmental Systems, Albuquerque, NM, USA, 8–12 July 2015. <https://arc.aiaa.org/doi/pdf/10.2514/6.2013-3509>.
- [55] G. Gotti, Supercritical Water Oxidation Investigation: Operating Procedures, Universities Space Research Association, Cleveland, OH (2011).
- [56] <https://www.slideshare.net/RohanJagadale2/raman-spectroscopy-243143879>
- [57] E. Smith, G. Dent, Modern raman spectroscopy: A practical approach, Wiley. Germany (2013).
- [58] G.R. Medders and F. Paesani, Infrared and Raman Spectroscopy of Liquid Water through “First-Principles” Many-Body Molecular Dynamics. *Molecules. Journal of Chemical Theory and Computation* 11 (2015) 1145–1154.
- [59] S. Liu, M. Zhang, B. Huang, N. Wu, S. Ouyang, Raman Spectroscopy for the Competition of Hydrogen Bonds in Ternary (H<sub>2</sub>O-THF-DMSO) Aqueous Solutions, *Molecules*. 24 20 (2019) 3666. <https://doi.org/10.3390/molecules24203666>
- [60] Teledyne Technologies Incorporated. (2019). Lotix: User Manual. Mason, OH 45040 U.S.A: Teledyne Tekmar.
- [61] B. Shrestha, R. Hernandez, D.B. Fortela, W. Sharp, A. Christoserdov, D. Gang, E. Revellame, W.E. Holmes, and M.E. Zappi, Formulation of a simulated wastewater influent composition for use in the research of technologies for managing wastewaters generated during manned long-term space exploration and other similar situations—literature-Based composition development, *BioTech*. 12 8 (2023). <https://doi.org/10.3390/biotech12010008>
- [62] C. Verostko, Development of ersatz formulations of wastewater streams generated in spacecraft closed life support systems." *Wyle Astronautics*, 1-50, (2009).

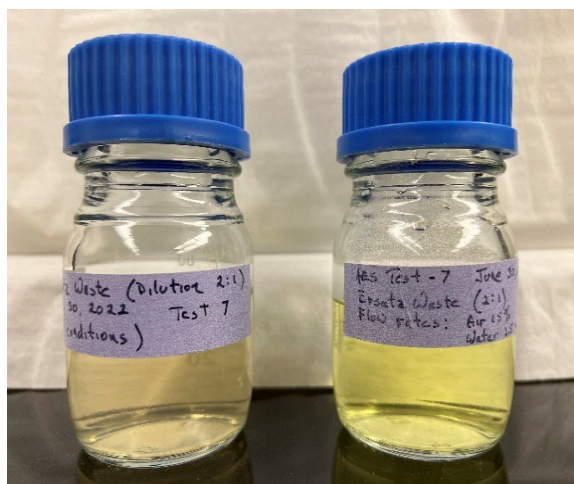
- [63] J.T. James, Spacecraft water exposure guidelines for selected contaminants: Volume 2 (2007) National Academies of Sciences, Engineering, and Medicine. 2007. Spacecraft Water Exposure Guidelines for Selected Contaminants: Volume 2. Washington, DC: The National Academies Press.
- [64] N.L. Bentley, E.A. Thomas, M. Van Wie, C. Morrison, and R.G. Stinson, Second generation international space station (ISS) total organic carbon analyzer (TOCA) verification testing and on-orbit performance results, International Conference on Environmental Systems, 2010. <https://ntrs.nasa.gov/citations/20100015492>.
- [65] A. Emin, A. Hushur, T. Mamtamin, Raman study of mixed solutions of methanol and ethanol, AIP Advances. 10 065330 (2020) <https://doi.org/10.1063/1.5140722>
- [66] I. Durickovic, Laura Thiebaud, P. Bourson, T.H. Kauffmann, M. Marchetti. Spectroscopic characterization of urea aqueous solutions: Experimental phase diagram of the urea-water binary system, Appl. Spectrosc. 67 10 (2013) 1205-1209, <https://hal.archives-ouvertes.fr/hal-01280736>.
- [67] P. Cabeza, M.D. Bermejo, C. Jimenez, M.J. Cocero, Experimental study of the supercritical water oxidation of recalcitrant compounds under hydrothermal flames using tubular reactors. Water Research. 45 (2011) 2485-2495. <https://doi.org/10.1016/j.watres.2011.01.029>.
- [68] W.R. Killilea, K.C. Swallow, G.T. Hong, The fate of nitrogen in supercritical-water oxidation, J. Supercrit. Fluids. 5 1 (1992) 72-78. [https://doi.org/10.1016/0896-8446\(92\)90044-K](https://doi.org/10.1016/0896-8446(92)90044-K).

## APPENDIX A: Raw data

Raw data in this section will include raw individual Raman spectral scans, TC-IC and turbidity images taken and collected during this study.



Sample Date	Ersatz Waste Water (2:1)	pH	Turbidity (NTU)
6/23/22	Lab Conditions	9.15	9.99
6/23/22	AES Test 6 Air 15% Water 2.5 mL/min	3.16	3.55



Sample Date	AES Test #7 Ersatz Waste Water (2:1)	pH	Turbidity (NTU)
6/30/22	Lab Conditions	9.14	13.9
6/30/22	Flow Rate Air 15% Fuel 2.5 mL/min	2.85	2.0



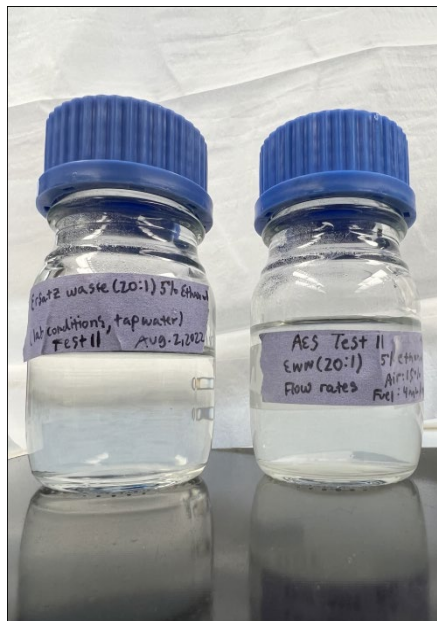
Sample Date	AES Test #8 Ersatz Waste Water (2:1)	pH	Turbidity (NTU)
7/5/22	Fresh sample from fridge	7.67	9.99
7/5/22	Air 20% Water 3.0 mL/min	7.72	3.56



Sample Date	AES Test #9 Ersatz Waste Water (2:1)	pH	Turbidity (NTU)
7/7/22	Lab Sample	8.13	18.3
7/7/22	Flow Rate Air 20% Fuel 4.0 mL/min	8.10	5.4



Sample Date	AES Test #10 Ersatz Waste Water (20:1)	pH	Turbidity (NTU)
7/12/22	Lab Conditions Tap Water	9.05	3.1
7/12/22	Flow Rate Air 20% Fuel 4.0 mL/min	8.25	2.1



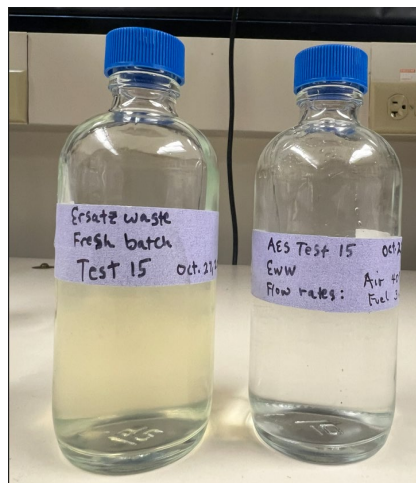
Sample Date	AES Test #11 Ersatz Waste Water (20:1)	pH	Turbidity (NTU)
8/2/22	Lab Conditions 5% Ethanol	8.82	4.14
8/2/22	Flow Rate 5% Ethanol Air 15% Fuel 4.0 mL/min	7.20	26.3



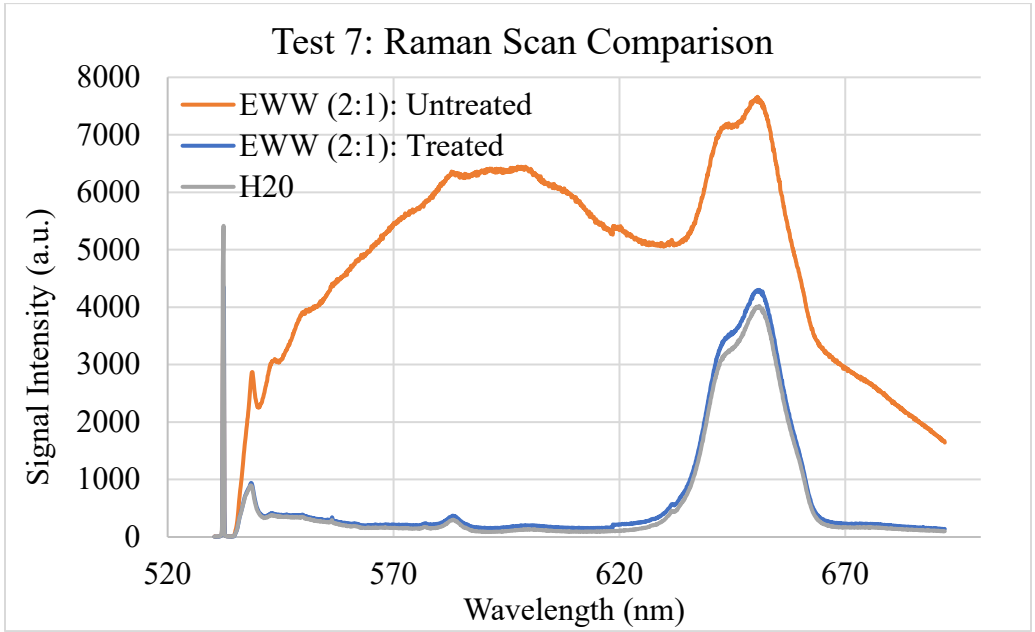
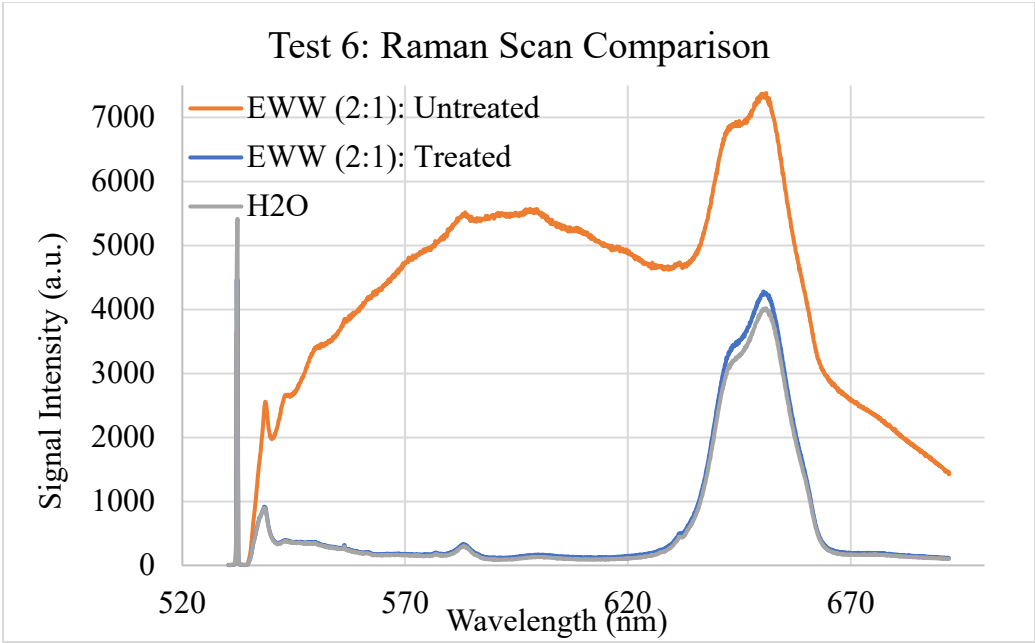
Sample Date	AES Test #12 Ersatz Waste Water (2:1)	pH	Turbidity (NTU)
8/11/22	5% Ethanol	6.91	3.70
8/11/22	5% Ethanol Flow Rate: Air: 25% Fuel: 4.0 mL/min	4.89	2.31

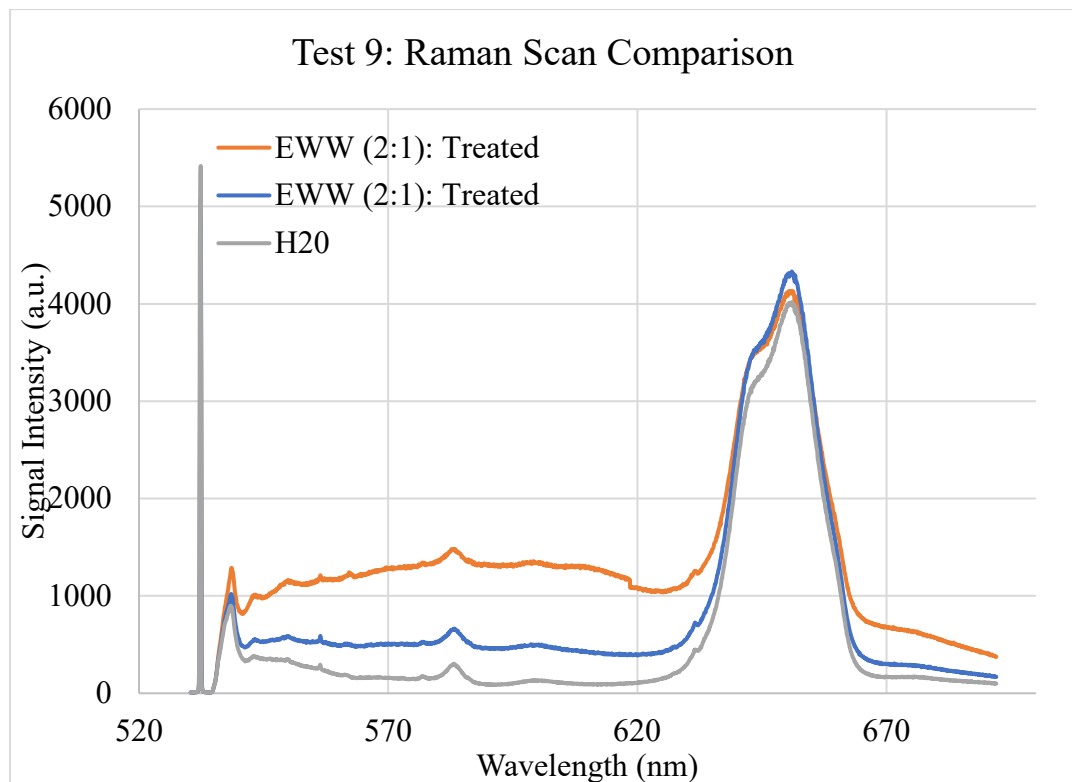
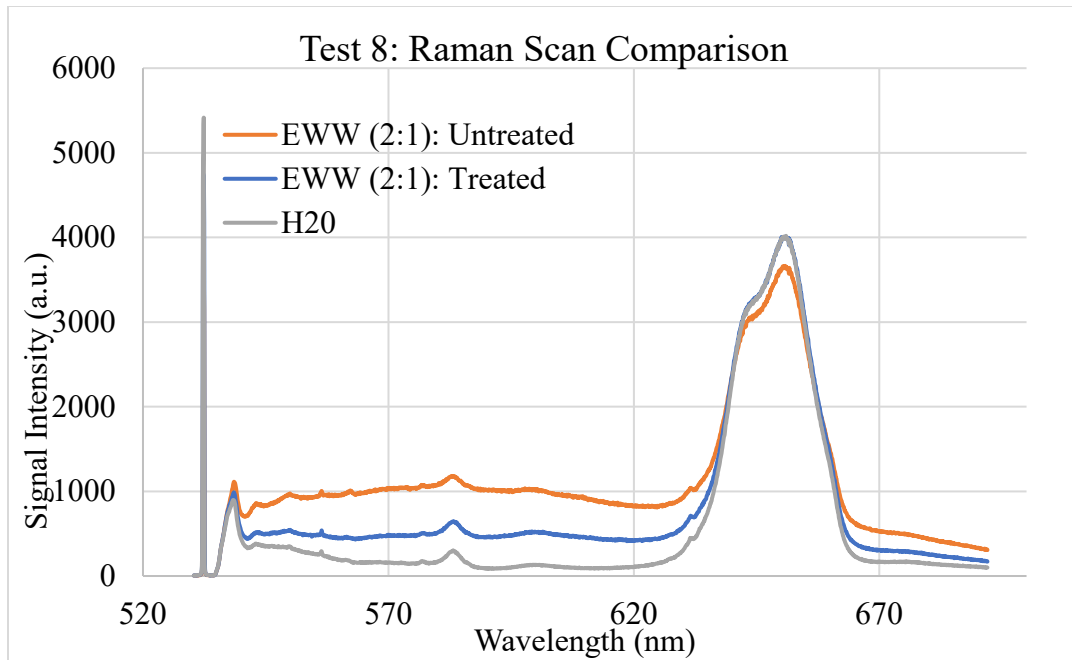


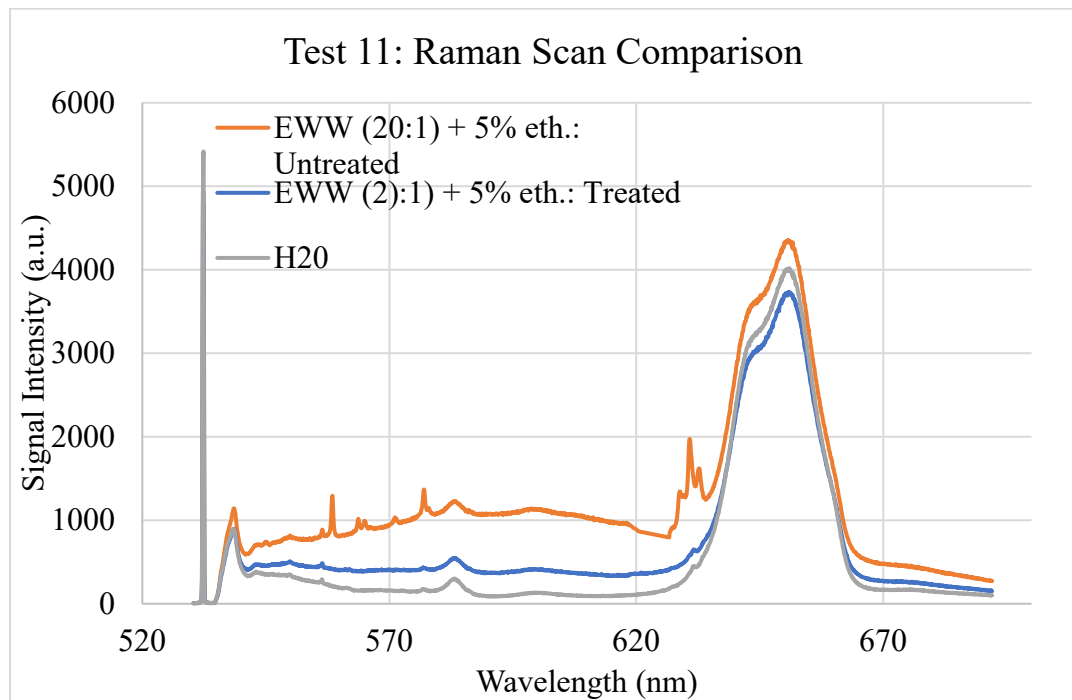
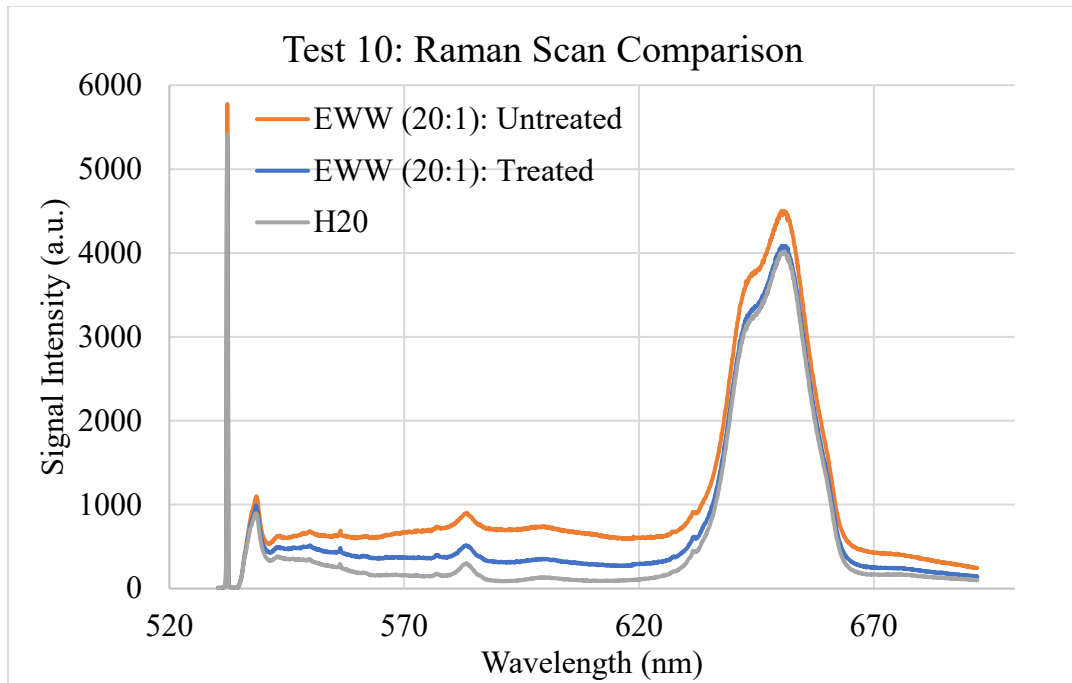
Sample Date	AES Test #13 Ersatz Waste Water (2:1)	pH	Turbidity (NTU)
8/17/22	5% Ethanol Approx. 6 days old Lab Conditions	7.37	4.67
8/17/22	5% Ethanol Flow Rate: Air: 40% Fuel: 2.0 mL/min	3.24	4.85

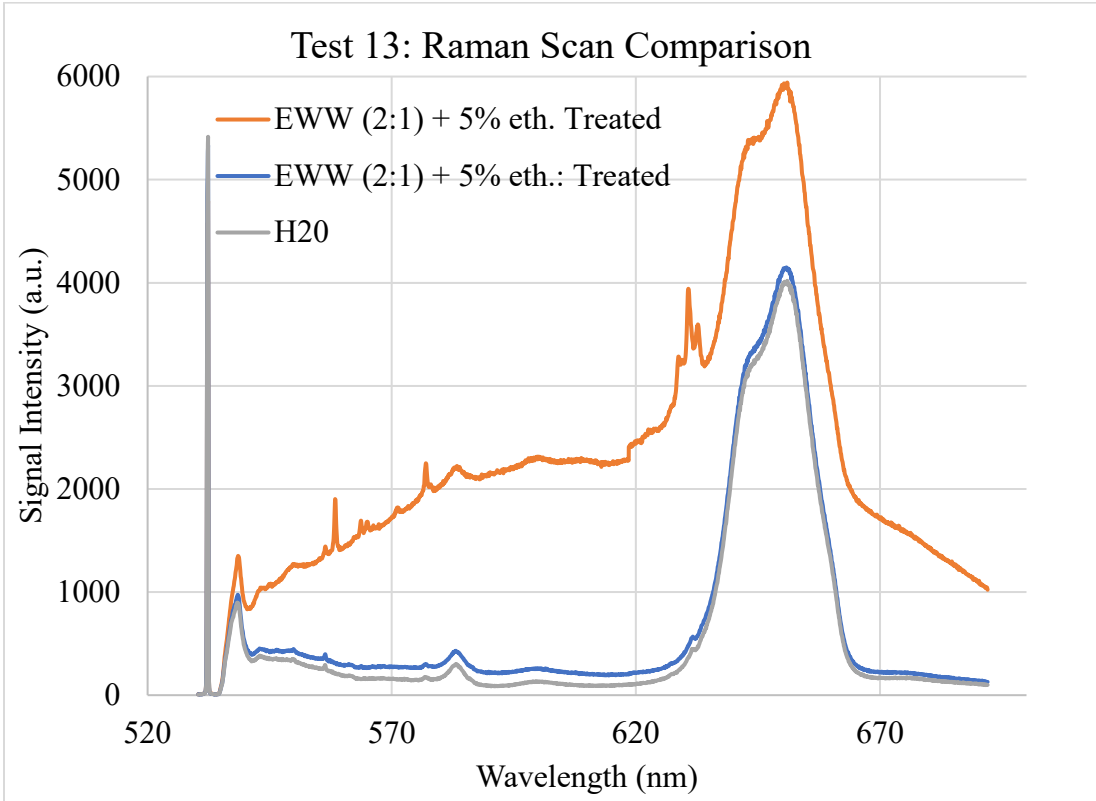
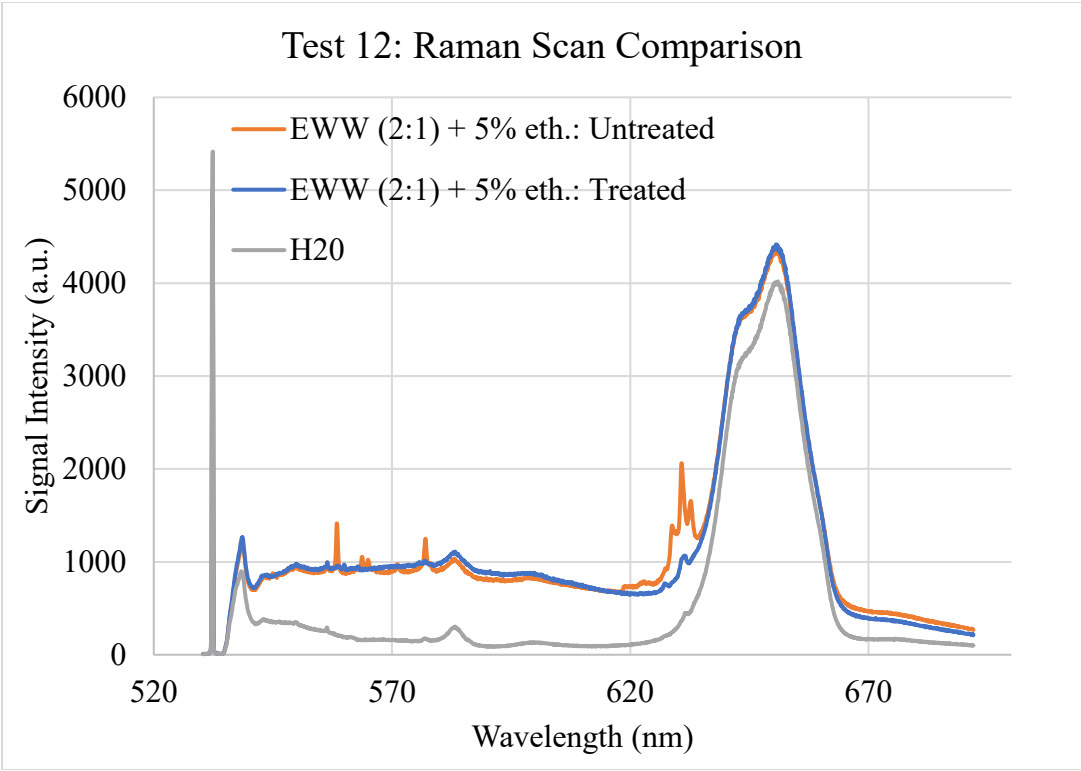


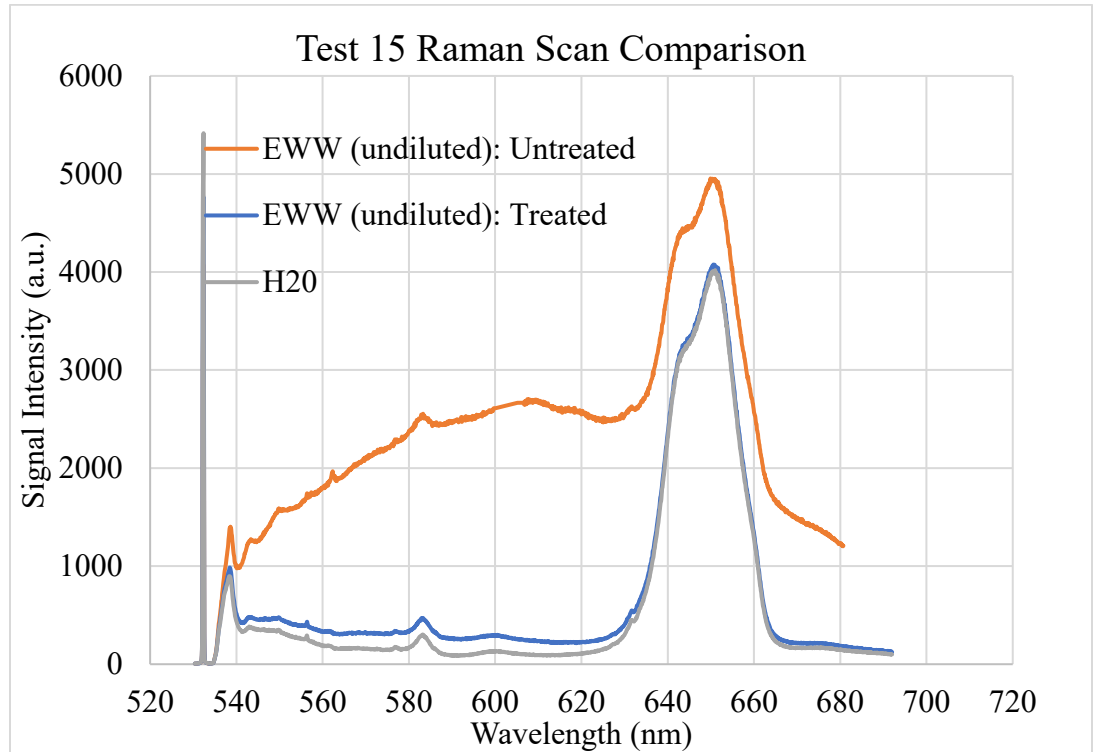
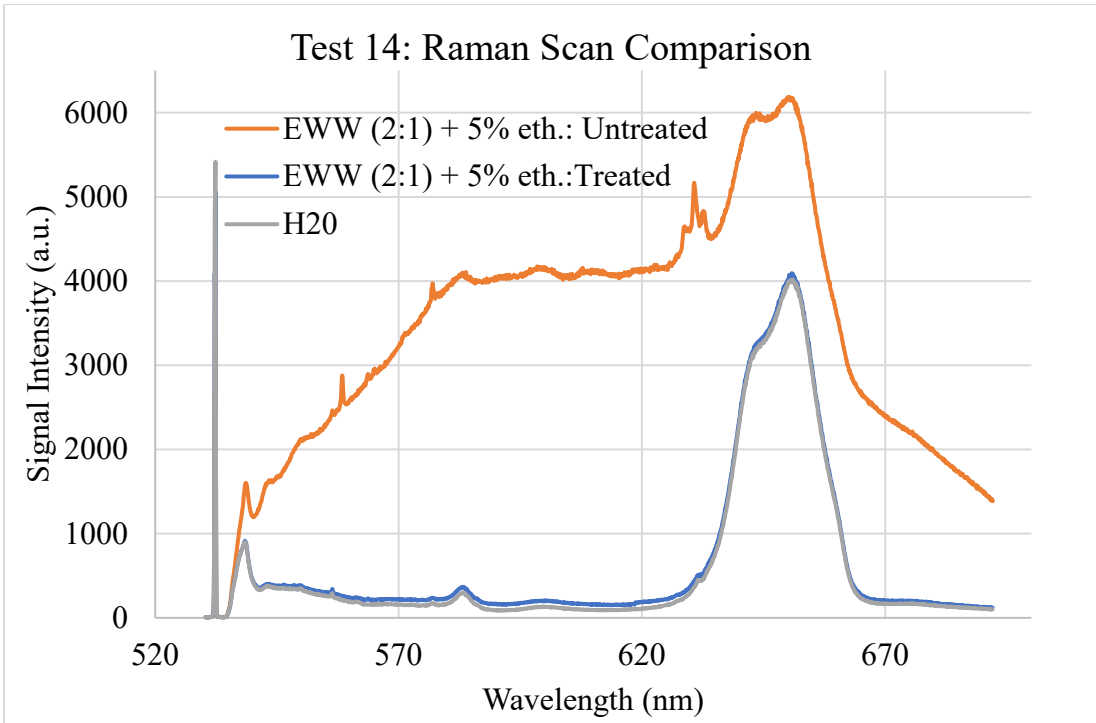
Sample Date	AES Test #15 Ersatz Waste Water	pH	Turbidity (NTU)
10/27/22	Fresh Sample	9.06	62.1
10/27/22	Flow Rate: Air: 40% Fuel: 3.0 mL/min	3.02	2.22

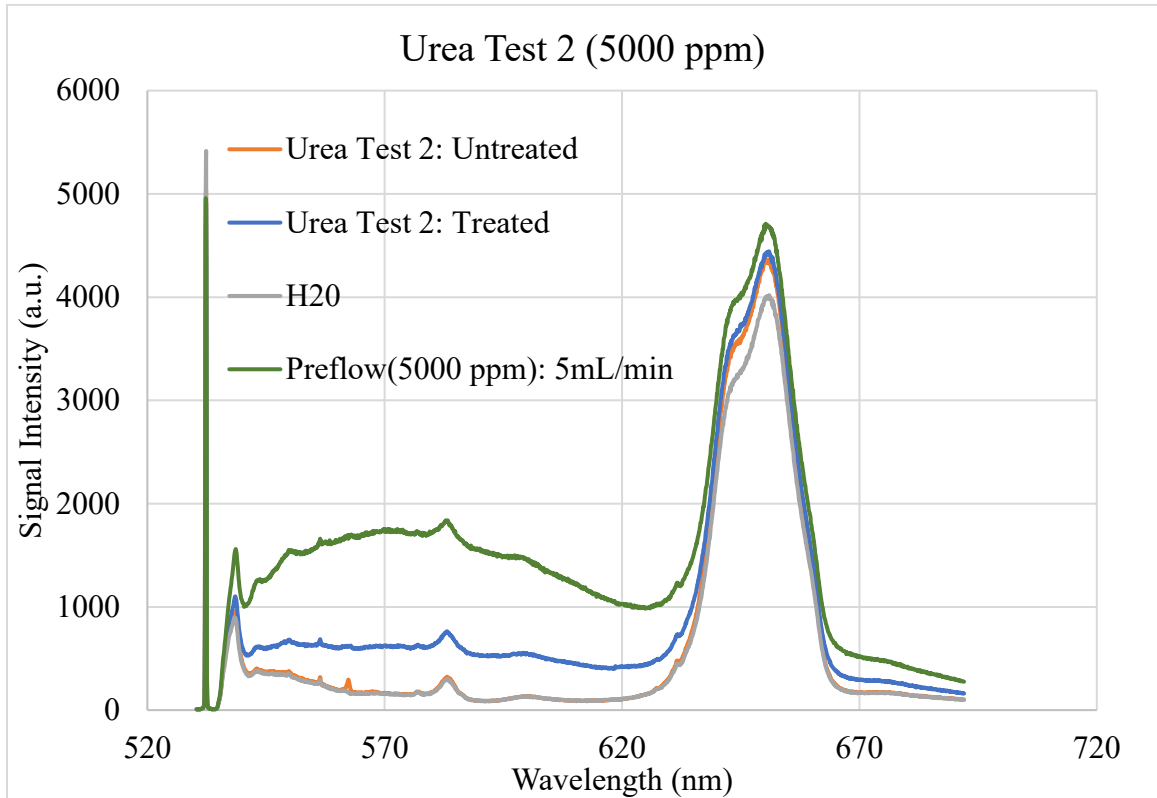
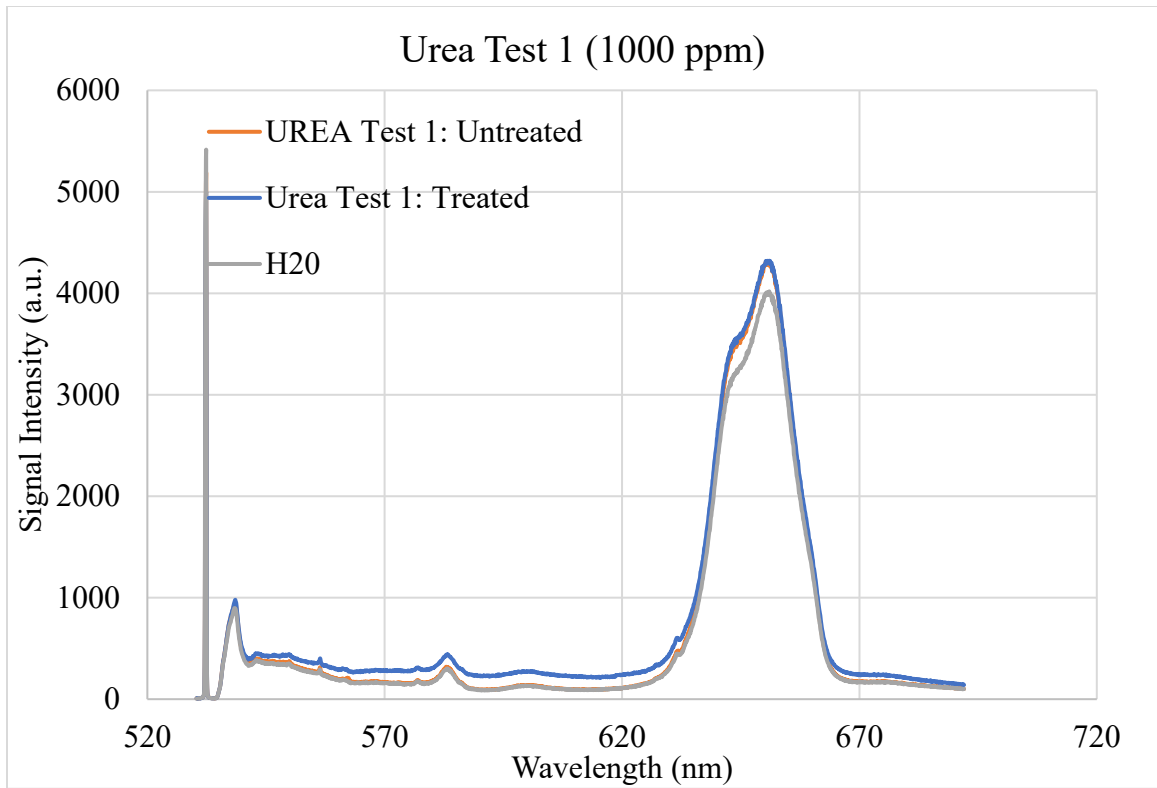


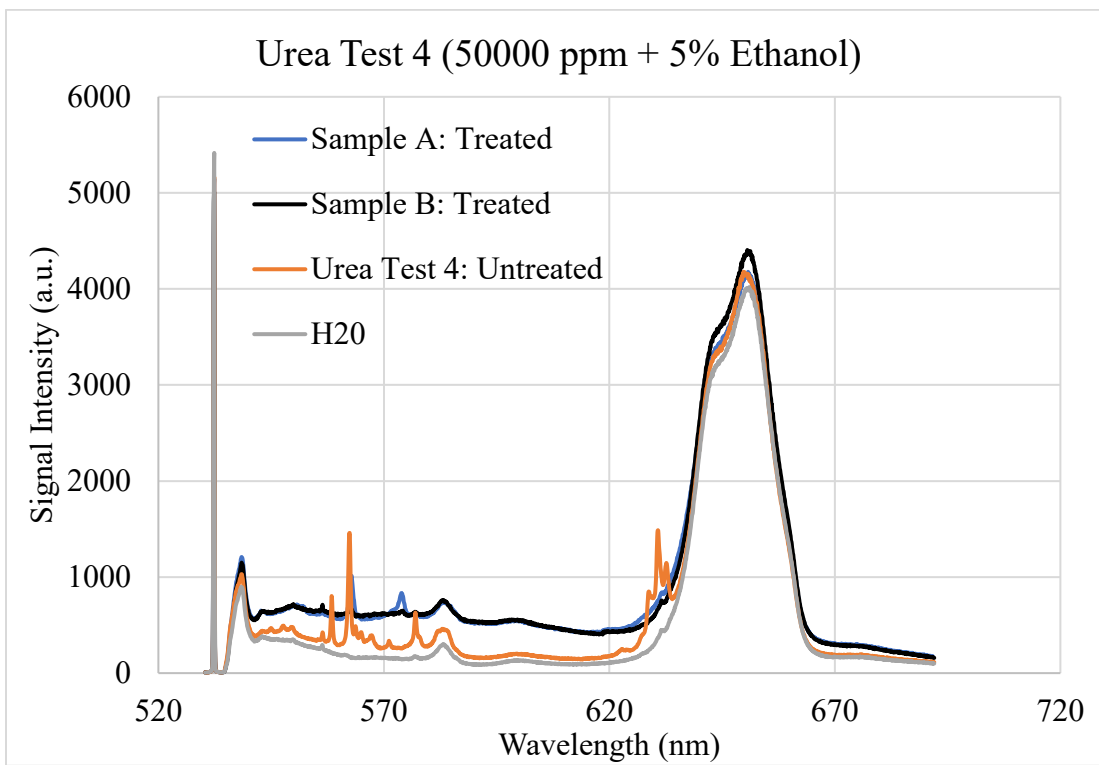
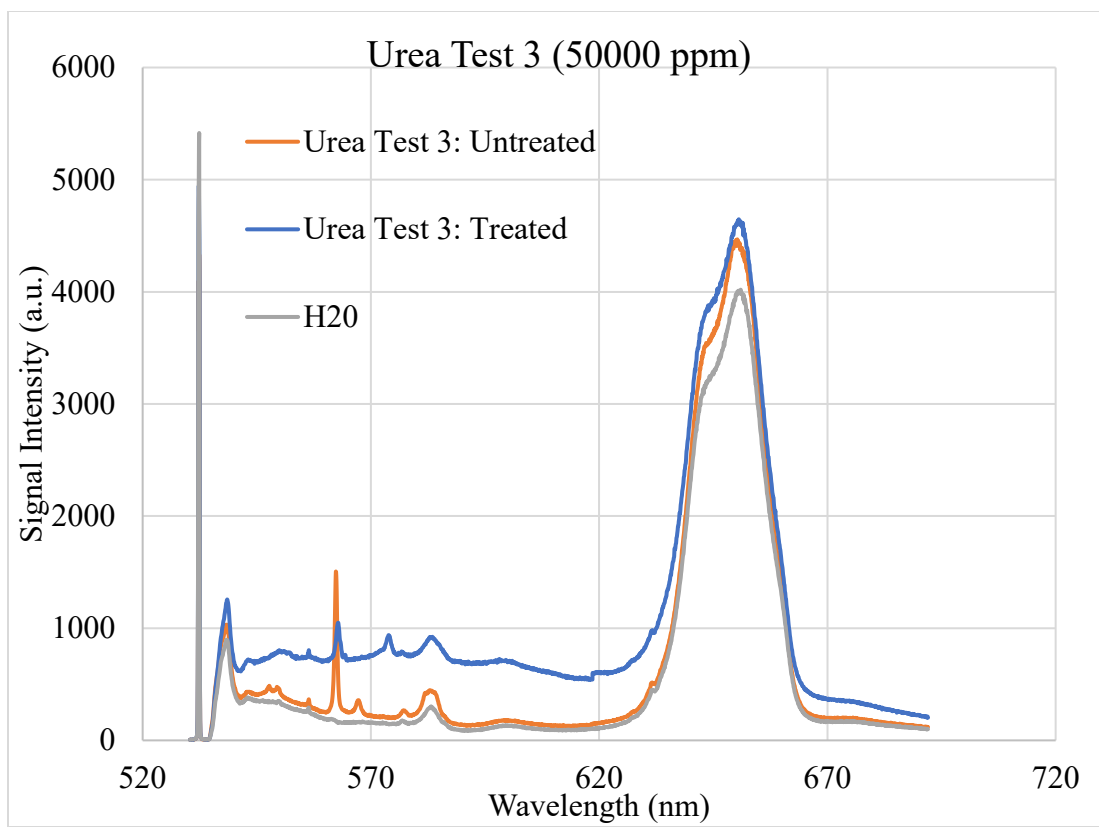


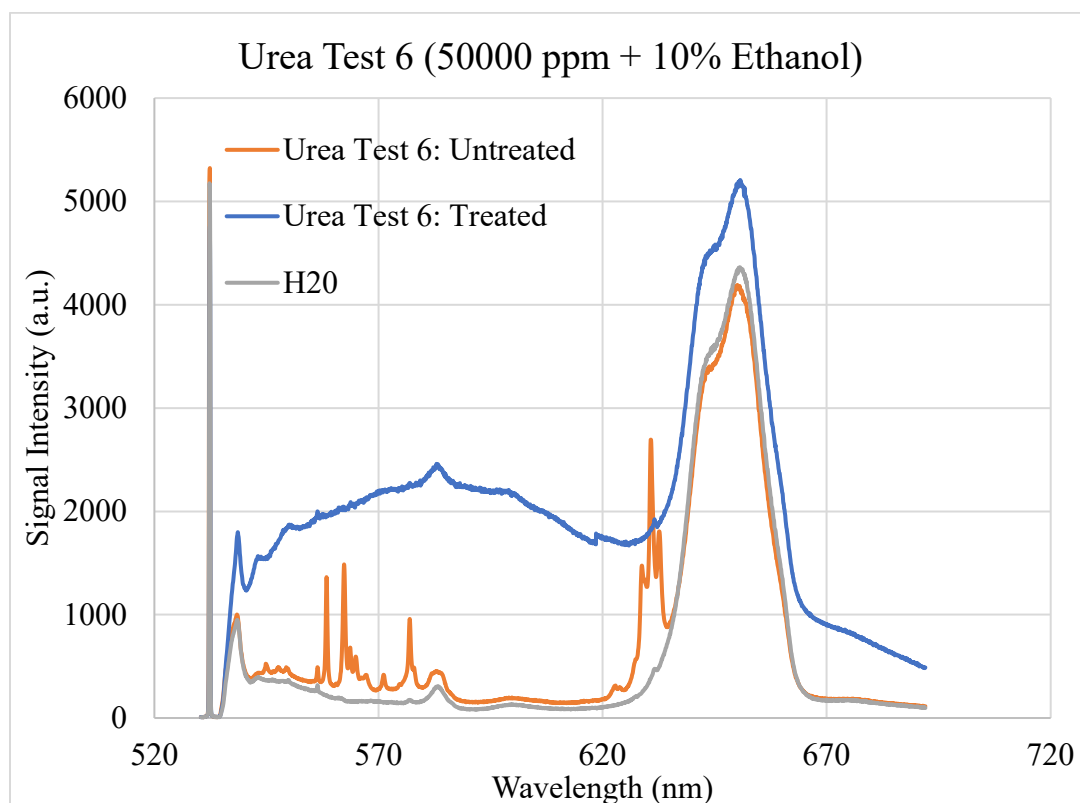
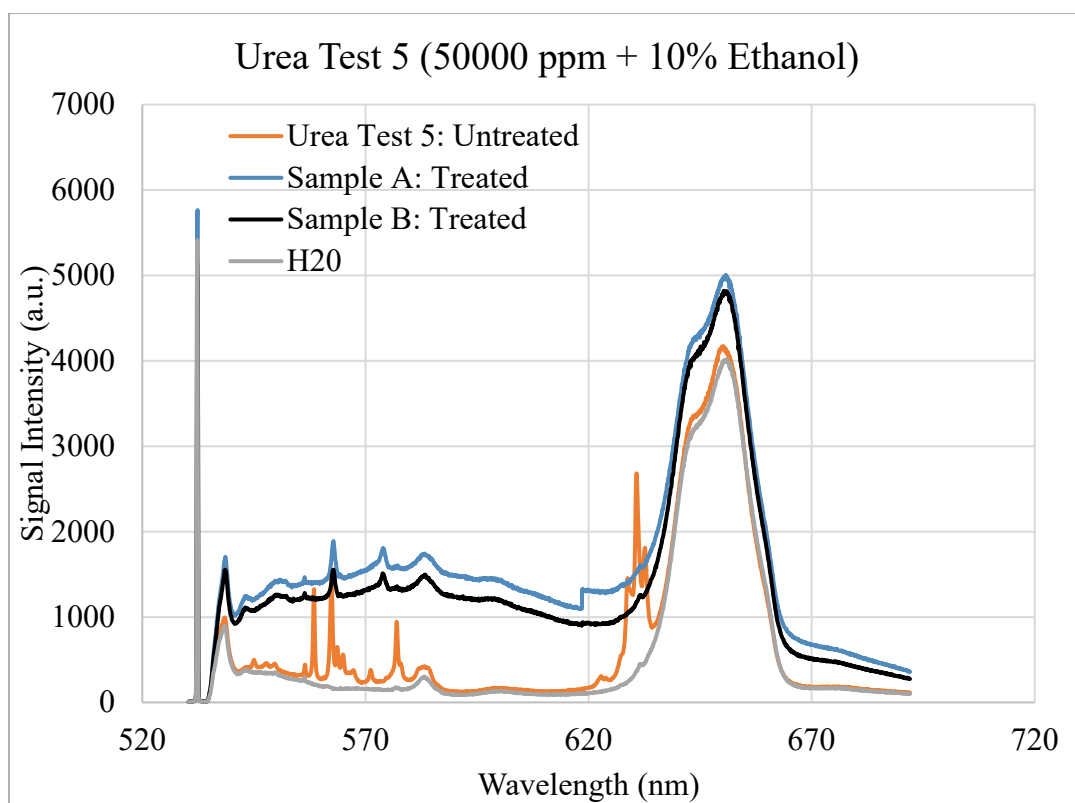


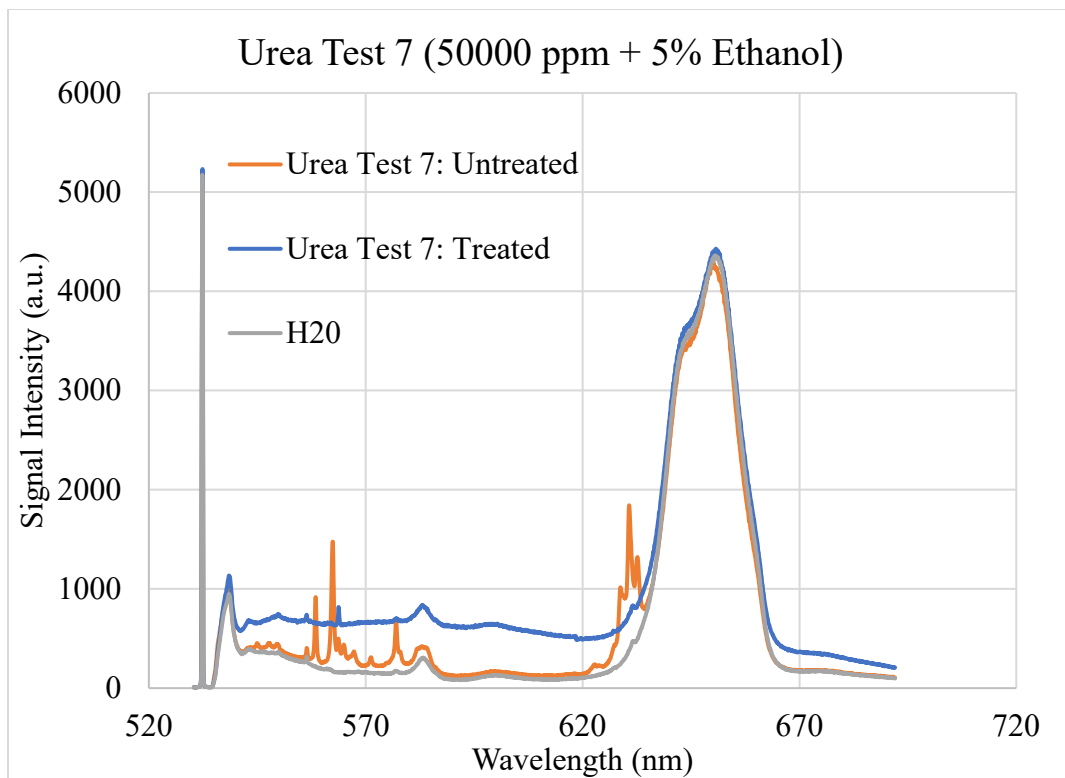












TOC (TC-IC) (ppm)						TC (ppm)		
C	Test #	TC	IC	TOC	% RD	TC	% RD	
(2:1)	1b	444.5	858.3	413.8	99.00%	56.8	94.54%	
	1a	1.85	0	1.85				
	2b	*	*	139.8	99.00%	*	*	
	2a	*	*	0				
	3b	473.1	444.3	28.8	99.00%	270.1	99.60%	
	3a	23.6	42	18.41				
	4	*	*	591	67.50%	*	*	
	4B	*	*	192.3				
	(20:1)	5b	*	*	132	-25.75%	*	*
		5a	*	*	166			
6b		*	*	12575	97.65%	*	*	
6a		*	*	295.2				
(2:1) + 5% ethanol		7b	23764.4	4186	19578.4	79.67%	23768.5	82.01%
	7a	4007	24.6	3982.4				
	8b	25132.6	420.6	24711.4	98.81%	24310	99.92%	
	8a	13.7	8.5	5.2				
	9b	21338.1	974.7	20363.4	99.00%	22732.9	99.97%	
	9a	10.1	10.3	0.2				
EWW	10b	1638	2531.4	893.4	99.00%	1552.7	99.86%	
	10a	2.2	1.8	0.4				

TC- IC Results

## APPENDIX B: Experimental Apparatus

Additional apparatus references can be observed in this section.



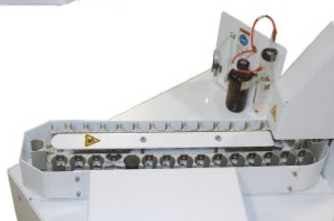
(a)



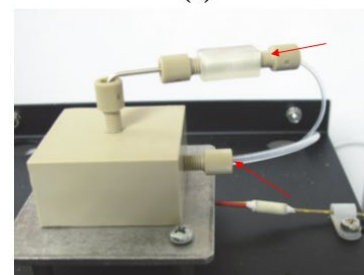
(c)



(d)

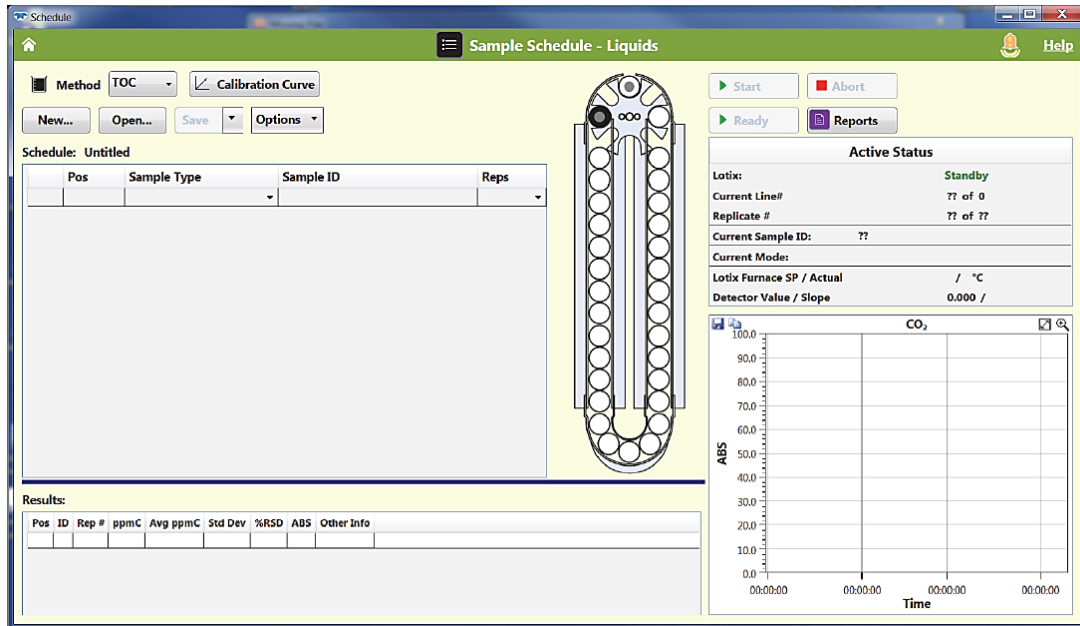


(b)



(e)

Overview of major components: (a) Lotix System, (b) sample conveyor, (c) glass ware panel with halogen scrubber and IC sparge components, (d) furnace, and (e) injection block assembly with injection needle (top) and carrier gas injector (bottom)[58].



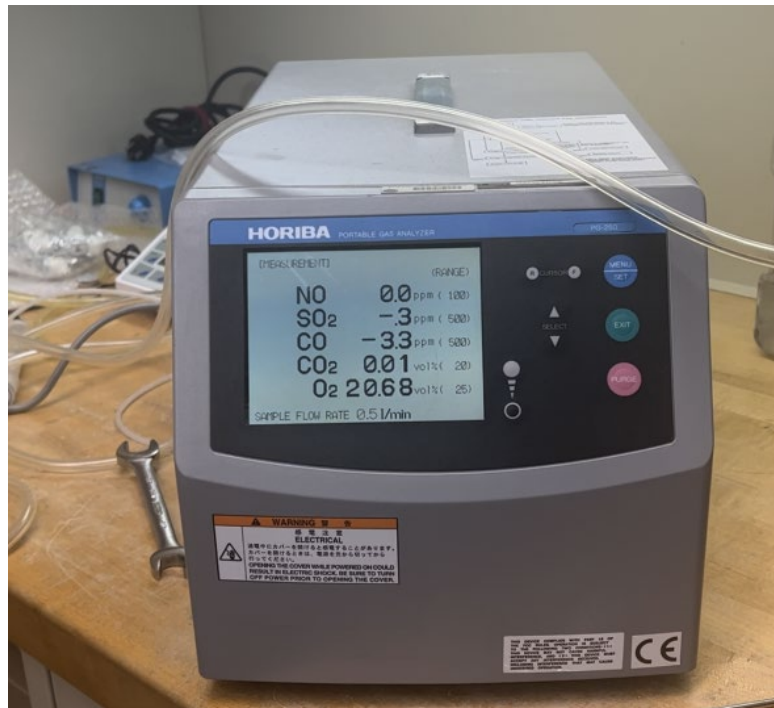
Software interface for TOC measurements [60].



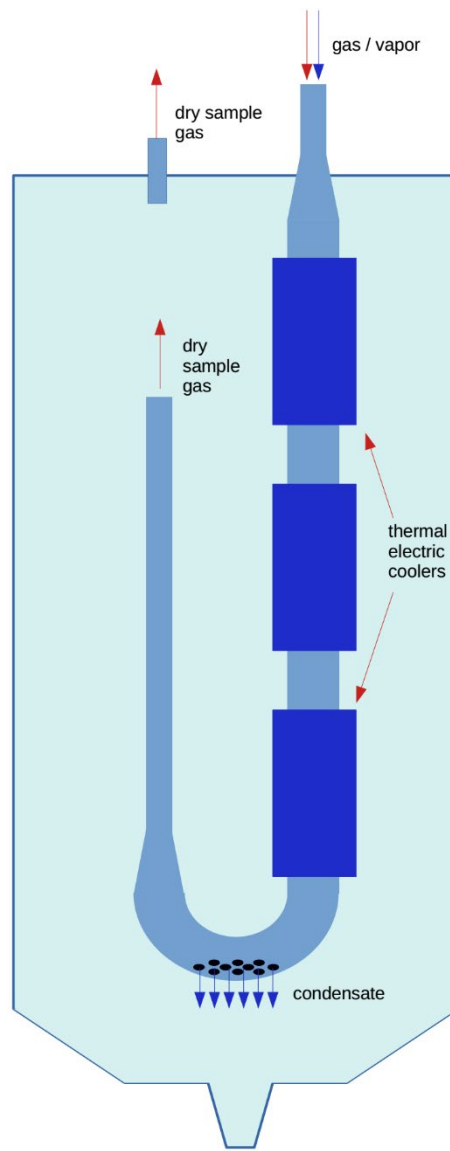
LabVIEW and mass flow controller setup



Oakton pH/CON 510 Benchtop Meter[ <https://www.ijstech.com/wd-35610-10.html>]



Horiba Gas Analyzer



Sample Gas Separator

## APPENDIX C: Additional Supplemental References

**RAMAN Band Correlation Table**

Approximate Wavenumber Range (cm <sup>-1</sup> )	Group	Intensity
100–210	Lattice vibrations	Strong
150–430	Xmetal-O	Strong
250–400	C-C aliphatic chain	Strong
295–340	Se-Se	Strong
425–550	S-S	Strong
460–550	Si-O-Si	Strong
490–660	C-I	Strong
505–700	C-Br	Strong
550–790	C-Cl	Strong
580–680	C=S	Strong
630–1250	C-C aliphatic chains	Moderate
670–780	C-S	Strong
720–800	C-F	Strong
800–950	C-O-C	Weak
910–960	Carboxylic acid dimer	Weak
990–1100	Aromatic rings	Strong
1010–1095	Si-O-C	Weak
1010–1095	Si-O-Si	Weak
1020–1225	C=S	Strong
1025–1060	Sulfonic acid	Very weak
1050–1210	Sulfonamide	Moderate
1050–1210	Sulfone	Moderate
1120–1190	Si-O-C	Weak
1145–1240	Sulfonic acid	Very weak
1315–1435	Carboxylate salt	Moderate
1320–1350	Nitro	Very strong
1355–1385	C-CH <sub>3</sub>	Weak
1365–1450	Aromatic azo	Very strong
1405–1455	CH <sub>2</sub>	Weak
1405–1455	CH <sub>3</sub>	Weak
1450–1505	Aromatic ring	Moderate
1535–1600	Nitro	Moderate
1540–1590	Aliphatic azo	Moderate
1550–1610	Aromatic/hetero ring	Strong
1550–1700	Amide	Strong
1600–1710	Ketone	Moderate
1610–1740	Carboxylic acid	Moderate
1625–1680	C=C	Very strong
1630–1665	C=N	Very strong
1690–1720	Urethane	Moderate
1710–1725	Aldehyde	Moderate
1710–1745	Ester	Moderate
1730–1750	Aliphatic ester	Moderate

1735–1790	Lactone	Moderate
1740–1830	Anhydride	Moderate
1745–1780	Acid chloride	Moderate
2020–2100	Isothiocyanate	Moderate
2070–2250	Alkyne	Strong
2080–2150	Si-H	Moderate
2090–2170	Isonitrile	Moderate
2100–2170	Thiocyanate	Very weak
2110–2160	Azide	Moderate
2200–2230	Aromatic nitrile	Moderate
2200–2280	Diazonium salt	Moderate
2220–2260	Nitrile	Moderate
2230–2270	Isocyanate	Very weak
2290–2420	P-H	Very weak
2530–2610	Thiol	Strong
2680–2740	Aldehyde	Weak
2750–2800	N-CH <sub>3</sub>	Weak
2770–2830	CH <sub>2</sub>	Strong
2780–2830	Aldehyde	Weak
2790–2850	O-CH <sub>3</sub>	Weak
2810–2960	C-CH <sub>3</sub>	Strong
2870–3100	Aromatic C-H	Strong
2880–3530	OH	Weak
2900–2940	CH <sub>2</sub>	Strong
2980–3020	CH=CH	Strong
3010–3080	=CH <sub>2</sub>	Strong
3150–3480	Amide	Moderate
3150–3480	Amine	Moderate
3200–3400	Phenol	Weak
3210–3250	Alcohol	Weak
3250–3300	Alkyne	Very weak

Chemistry Department, University of California, Irvine

<https://www.chem.uci.edu/~dmitryf/manuals/Raman%20correlations.pdf>



**APPENDIX D: Thermophysical Properties and Test Parameters**

<b>AES TEST #</b>	<b>Density @ Reactor Conditions</b>	<b>Average Bulk Temp. (°C)</b>	<b>STDEV</b>	<b>Avg. Cell Pressure(psi)</b>
6	Air Density: .11059 g/cm <sup>3</sup> , H2O Density: .07646 g/cm <sup>3</sup>	621	4.37	4018
7	Air Density: .11197 g/cm <sup>3</sup> , H2O Density: .07793 g/cm <sup>3</sup>	614	6.28	4039
8	Air Density: .10224 g/cm <sup>3</sup> , H2O Density: .06911 g/cm <sup>3</sup>	632	6.63	3739
9	Air Density: .10903 g/cm <sup>3</sup> , H2O Density: .07662 g/cm <sup>3</sup>	586	9.74	3795
10	Air Density: .10482 g/cm <sup>3</sup> , H2O Density: .07036 g/cm <sup>3</sup>	661	6.74	3969
11	Air Density: .10240 g/cm <sup>3</sup> , H2O Density: .06792 g/cm <sup>3</sup>	682	7.14	3961
12	Air Density: .10820 g/cm <sup>3</sup> , H2O Density: .07477 g/cm <sup>3</sup>	612	68.9	3883
13	Air Density: .10629 g/cm <sup>3</sup> , H2O Density: .07315 g/cm <sup>3</sup>	612	16.6	3809
14	Air Density: .10908 g/cm <sup>3</sup> , H2O Density: .07561 g/cm <sup>3</sup>	610	8.24	3908

15	<b>Air Density: .10869 g/cm3 , H2O Density: .07519 g/cm3</b>	612	7.9	3902
UREA #1	<b>Air Density: .10777 g/cm3 , H2O Density: .07465 g/cm3</b>	606	1.94	3839
UREA #2	<b>Air Density: .10744 g/cm3 , H2O Density: .07425 g/cm3</b>	609	2.75	3840
UR EA #3	<b>Air Density: .10815 g/cm3 , H2O Density: .07459 g/cm3</b>	619	2.24	3913
UR EA #4 (A/B)	<b>Air Density: .10948/.11125, H2O Density: .07616/.07816</b>	605/ 595	2.25/3 .48	3899/39 21
UR EA #5	<b>Air Density: .11023/.10948, H2O Density: .07694/.07591</b>	602/ 611	2.84/3 .97	3915/39 28
UR EA #6	<b>Air Density: .10850 g/cm3 , H2O Density: .07536 g/cm3</b>	604	6.45	3858
UR EA #7	<b>Air Density: .10901 g/cm3 , H2O Density: .07554 g/cm3</b>	610	5.63	3905

<b>AES TEST #</b>	<b>Average Air (SLPM)</b>	<b>Fuel/flow rate(mL/min)</b>	<b>Residence time(sec)</b>
6	Air 15% ,0.696 SLPM	EWV(2:1)/2.5	89.64
7	Air/15% .694 SLPM	EWV(2:1)/2.5	91.79
8	Air/20%, .944 SLPM	EWV(2:1)/3.0	66.62
9	Air/20% .944 SLPM	EWV(2:1)/4.0	58.14
10	Air/20% .944 SLPM	EWV(20:1)/4.0	53.81
11	Air 15%,.695 SLMP	EWV(20:1)5% ethanol/4.0	54.46
12	Air 25% ,1.24 SLPM	EWV(2:1)5% ethanol/4.0	53.97
13	Air 40%, 1.94 SLPM	EWV(2:1)5%ethanol/2.0	72.45
14	Air 50%, 2.44 SLPM	EWV(2:1)5% ethanol/3	53.8
15	Air 40%, 1.94 SLPM	EWV(undiluted)/3	58.58
UREA #1	Air 20%, .944 SLPM	1000 ppm Urea 4ml/min	56.79
UREA #2	Air 20%, .944 SLPM	5000 ppm Urea 4 ml/min	56.51
UREA #3	Air 20%,.944 SLPM	50000 ppm Urea 2ml/min	96.81
UREA #4 (A/B)	Air 20%/Air 40% .944/1.94 SLPM	50000 + 5% eth (2ml/min+2ml/min)	98.60/76.69
UREA #5	Air 20%/Air 40% 2.944/1.94 SLPM	50000 + 10% eth (2ml/min+4ml/min)	97.96/48.78
UREA #6	Air 75%,3.69 slpm	50000 + 10% eth 1.5 ml/min	57.8
UREA #7	Air 65%	50000 + 5% eth 2.5 ml/min	51.96

## CURRICULUM VITAE

### CALEB A. RIGGINS

13406 Greenwood Manor Drive Cypress, TX 77429  
346-491-6097 \* [Cariggins96@gmail.com](mailto:Cariggins96@gmail.com) \* [linkedin.com/in/caleb-riggins-1566501a9](https://www.linkedin.com/in/caleb-riggins-1566501a9)

#### SUMMARY OF QUALIFICATIONS

---

- Excellent communication skills, able to build and maintain positive working relationships.
- Exceptional critical thinker with time management and multi-tasking abilities
- Productive, efficient, and easily adaptable to new environments
- Ability to learn new skills quickly and accurately.

#### EDUCATION

---

##### **Prairie View A&M University**

**Prairie View, TX**

*Candidate for Master of Science in Mechanical Engineering, May 2023*

GPA: 3.66/4.00

##### **Prairie View A&M University**

*Bachelor of Science in Mechanical Engineering, May 2021*

**Prairie View, TX**

Engineering GPA: 3.46/4.00

Cumulative GPA: 3.33/4.00

#### EXPERIENCE

---

##### **NASA (GRC) - Graduate Student Intern, June 2022- March 2023**

**Cleveland, OH**

- High-pressure combustion work involving exploration and testing of supercritical water oxidation technologies for wastewater reclamation during extended space missions (Artemis Program)
- Performed advanced diagnostics and data analysis (i.e., Spectroscopy, TOC/Gas Analyzer)
- MATLAB/Cantera utilized to analyze, simulate, and present data for mentors and project leaders
- Collaborative work with senior combustion engineers to plan, design, and conduct experiments in concurrent efforts to successfully create a graduate thesis and credible publication
- Held the position as a peer leader for the Fall 2022 internship session

##### **HGE Consulting – MEP Systems Engineer Intern, Feb. 2022-June 2022**

**Houston, TX**

- Directly involved in planning and design of mechanical, electrical, and plumbing (MEP) systems, including developing policies, standards, inspection procedures, and evaluation for new construction of multi-family apartment complexes. Projects in (TX, FL, TN, CO, SC, GA, NV)

- Coordination of MEP design and energy code compliance with various engineering teams
- Utilized CAD software to review design plans and generate compliance certifications for submittal
- Experience with the full life cycles of engineering project production from design to construction

**Prairie View A&M University- Research Assistant, Fall 2020- Spring 2022**

**Prairie View, TX**

- Conducted research based on NASA’s Flame Extinguishment Experiment (FLEX) program
- Research focused on improving fuel efficiency through the study of heptane droplet combustion under microgravity conditions. MATLAB coding performed for image data processing and analysis

**The University of Texas in Austin- NASCENT REU Intern, Summer 2020  
Austin, TX**

- Procured knowledge and examined current advances within Nanomanufacturing, materials, and nanodevices through extensive research and professional seminars

**H-E-B Grocery Company - Assistant Service Manager, Nov. 2015- Feb. 2022  
Cypress, TX**

- Delegated service tasks and delivered excellent customer service experiences by offering knowledge and providing quality information while maintaining a healthy work environment

**ACTIVITIES AND HONORS**

- 
- Dean’s List, Prairie View A&M Fall 2018- Present
  - Tau Beta Pi, Engineering Honor Society Active member
  - Pi Tau Sigma, Mechanical Engineering Honor Society Active member
  - NASA Peer Mentor Fall 2022
  - 2023 Most Outstanding Mechanical Engineering Master’s Student Award Recipient

**ADDITIONAL SKILLS**

- 
- Applications: Word, Excel, PowerPoint, AUTOCAD, NX Graphic Design, CREO, Python, Solidworks, C++, EES, MATLAB, Mathematica, LabVIEW, ANSYS, Raman Spectroscopy